Symmetrical Windowing for Quantum States in Quasi-Classical Trajectory Simulations

by

Stephen Joshua Cotton

A dissertation submitted in partial satisfaction
of the requirements for the degree of

Doctor of Philosophy

in

Chemistry

in the

Graduate Division

of the

University of California, Berkeley

Committee in Charge:
Professor William H. Miller, Chair
Professor Birgitta Whaley
Professor Robert G. Littlejohn

Fall 2014

ProQuest LLC.
789 East Eisenhower Parkway
P.O. Box 1346
Ann Arbor, MI 48106 - 1346

Abstract

Symmetrical Windowing for Quantum States in Quasi-Classical Trajectory Simulations

by

Stephen Joshua Cotton

Doctor of Philosophy in Chemistry

University of California, Berkeley

Professor William H. Miller, Chair

An approach has been developed for extracting approximate quantum state-to-state information from classical trajectory simulations which "quantizes" symmetrically both the initial and final classical actions associated with the degrees of freedom of interest using quantum number bins (or "window functions") which are significantly narrower than unit-width. This approach thus imposes a more stringent quantization condition on classical trajectory simulations than has been traditionally employed, while doing so in a manner that is time-symmetric and microscopically reversible.

To demonstrate this "symmetric quasi-classical" (SQC) approach for a simple real system, collinear $H + H_2$ reactive scattering calculations were performed [1] with SQC-quantization applied to the H_2 vibrational degree of freedom (DOF). It was seen that the use of window functions of approximately $\frac{1}{2}$-unit width led to calculated reaction probabilities in very good agreement with quantum mechanical results over the threshold energy region, representing a significant improvement over what is obtained using the traditional quasi-classical procedure.

The SQC approach was then applied [2] to the much more interesting and challenging problem of incorporating non-adiabatic effects into what would otherwise be standard classical trajectory simulations. To do this, the classical Meyer-Miller (MM) Hamiltonian was used to model the electronic DOFs, with SQC-quantization applied to the classical "electronic" actions of the MM model—representing the occupations of the electronic states—in order to extract the electronic state population dynamics. It was demonstrated that if one ties the zero-point energy (ZPE) of the electronic DOFs to the SQC windowing

function's width parameter this very simple SQC/MM approach is capable of quantitatively reproducing quantum mechanical results for a range of standard benchmark models of electronically non-adiabatic processes, including applications where "quantum" coherence effects are significant. Notably, among these benchmarks was the well-studied "spin-boson" model of condensed phase non-adiabatic dynamics, in both its symmetric and asymmetric forms—the latter of which many classical approaches fail to treat successfully.

The SQC/MM approach to the treatment of non-adiabatic dynamics was next applied [3] to several recently proposed models of condensed phase electron transfer (ET) processes. For these problems, a flux-side correlation function framework modified for consistency with the SQC approach was developed for the calculation of thermal ET rate constants, and excellent accuracy was seen over wide ranges of non-adiabatic coupling strength and energetic bias/exothermicity. Significantly, the "inverted regime" in thermal rate constants (with increasing bias) known from Marcus Theory was reproduced quantitatively for these models—representing the successful treatment of another regime that classical approaches generally have difficulty in correctly describing. Relatedly, a model of photoinduced proton coupled electron transfer (PCET) was also addressed, and it was shown that the SQC/MM approach could reasonably model the explicit population dynamics of the photoexcited electron donor and acceptor states over the four parameter regimes considered.

The potential utility of the SQC/MM technique lies in its stunning simplicity and the ease by which it may readily be incorporated into "ordinary" molecular dynamics (MD) simulations. In short, a typical MD simulation may be augmented to take non-adiabatic effects into account simply by introducing an auxiliary pair of classical "electronic" action-angle variables for each energetically viable Born-Oppenheimer surface, and time-evolving these auxiliary variables via Hamiltons equations (using the MM electronic Hamiltonian) in the same manner that the other classical variables—i.e., the coordinates of all the nuclei—are evolved forward in time. In a complex molecular system involving many hundreds or thousands of nuclear DOFs, the propagation of these extra "electronic" variables represents a modest increase in computational effort, and yet, the examples presented herein suggest that in many instances the SQC/MM approach will describe the true non-adiabatic quantum dynamics to a reasonable and useful degree of quantitative accuracy.

Acknowledgment

It has been quite interesting and wonderful to come back to Berkeley and finish the Ph.D. that I began so very many years ago. Lawyer work has its benefits and drawbacks, interesting bits and bits of tedium, but I always seemed to have harbored a deep-rooted fascination with the field of theoretical chemical dynamics and its manifest correspondences between the classical and quantum theories of mechanics. Professor Miller has spent a career pursuing these ideas and developing these theories—more than anything, I am very grateful for having had the opportunity to return to Berkeley and make a small contribution to that intellectual endeavor and to its practical application. The work described here in this dissertation reflects that bit of contribution, and moreover, hopefully reflects my great appreciation to Professor Miller personally, my appreciation for all his scientific achievements, and also more generally reflects my great fondness for quantitive physical science, mathematics, algorithm development, simulation, and theory.

Pushing forward with the research necessary to complete the Ph.D. degree while simultaneously practicing law in what I would characterize as the very demanding role of a patent attorney has not always been easy, and nor did I expect it to be. Nevertheless, when I understood that returning to Berkeley and working under Professor Miller was actually viable, I never questioned that it was something that simply must be done. Professor Miller was game from the beginning, never seeming to doubt that I could do both these things and make it work, always pushing just enough, always encouraging (always famously creative and brilliant—and inspirational) and, truth be told, as we have said to each other on numerous occasions, this has all been great fun, so much fun that we will continue this work with the conclusion of this degree. Yet another source of my appreciation to him.

Of course, there are many others I'm thankful to as well. First and foremost, my wife Abigail has provided me with constant support and encouragement through this process (while she herself manages to work full-time as a patent agent and simultaneously complete her J.D.). I am thankful for her patience, understanding, hard work, and also for seeing that rekindling the Ph.D. work would be a worthwhile endeavor.

I'm also appreciative to the many past members of the Miller Research Group with whom I have overlapped including David Skinner from my original stint as a graduate student, Bin Li and Kirill Igumenshchev from my current tenure, and Michael Thoss who happened to be a member of the group for a

time during both periods.

Also, steadfastly supporting Professor Miller and his students during both of my tenures with the Miller Research Group has been Cheryn Gliebe. I certainly thank Cheryn for keeping us all tracked and organized on the administrative front, but more than that, I am thankful to Cheryn for her moral support and good cheer. My readmission to the graduate program after many years away created an unusual situation requiring special attention, and I am particularly grateful to Cheryn for her perseverance and handling of that situation. Lynn Keithlin, the Department of Chemistry's Graduate Student Services Advisor, was also instrumental in this regard, and I am grateful to having had her special attention and care as well.

I also thank Jeff Weaver and Jim Austin of Weaver Austin Villeneuve & Sampson Intellectual Property Law for giving me the flexibility to work part-time while completing this Ph.D. as well as for their guidance in the practice of patent law. I have learned a great deal over the last two years from them as well.

Finally, I think of my undergraduate advisors at Pomona College: Professors Fred Grieman and Wayne Steinmetz in Chemistry, and Karen Barad in Physics (now Professor of Feminist Studies at U.C. Santa Cruz). I have often thought of them while refreshing—in the course of this research—many of the things I learned from them in my undergrad days. I truly feel a deep gratitude to each of them for sparking my interest in all of this so many years ago.

To Abigail

Contents

List of Figures

List of Tables

Part I

Symmetric Quantization of Nuclear Motion and Calculation of Reaction Probabilities

Chapter 1

Introduction, Background, and Theory

1.1 The Traditional Quasi-Classical Approach

The quasi-classical (QC) approach embodies a simple methodology, based purely on classical mechanics, for modeling transitions between quantum states in atomic and molecular dynamics (MD) simulation. In the standard quasi-classical trajectory (QCT) simulation [4], molecular vibrational and/or rotational degrees of freedom (DOFs) are expressed in terms of classical action-angle variables, the action variables being classical generalized momenta serving as the classical analogues of the vibrational and/or rotational quantum numbers. "Quantization" is then accomplished by initializing classical trajectories with integer values of the action variables—i.e., at the quantum energy level of the initial state—and the final distribution of quantum states is obtained by accumulating the values of the classical action variables in "bins" (or histograms) of unit-width centered about the integer quantum values corresponding to the accessible quantum states.

For instance, in a typical collinear atom-diatom scattering process:

$$A + BC(N_1) \rightarrow A + BC(N_2) \qquad \text{(inelastic)}$$

or

$$A + BC(N_1) \rightarrow AB(N_2) + C \qquad \text{(reactive)}$$

where N is the vibrational quantum number of the diatomic molecule (and there are no rotational DOFs), vibrational quantum state-to-state scattering processes may be described by beginning trajectories with the vibrational en-

ergy of the diatom $BC(N_1)$ being equal to the quantum mechanical energy level of the initial vibrational state N_1, and then "assigning" the trajectory to the final quantum state N_2 whose energy level is closest to that of the actual final classical vibrational energy. Repeating the process over an ensemble of trajectories—i.e., as a phase space average over initial conditions—allows one to map out the transition probabilities from the initial to all accessible final vibrational quantum states. Rotational DOFs may be treated similarly.

Because this QCT approach is arguably the simplest (and least computationally demanding) way possible to extract quantum state specific information from a classical MD simulation—and because it has been widely applied to the treatment of complex molecular systems over the past 50 years—it is worthwhile to explore how it can be improved and expanded upon, as it would seem that any discernible improvement that one could come up with would potentially have immediate practical utility.

1.2 Tightening the Quantization Condition: Bonnet's and Rayez's "Gaussian Windowing" Approach

In this spirit of improving the QCT approach, several groups have recently presented modifications to the traditional quasi-classical model which have been seen to give improved results in particular applications. For instance, Bonnet and Rayez [5], as well as Czäko and Bowman [6], have shown that considerably improved quasi-classical results for product state distributions in inelastic and reactive scattering processes can be obtained by using "Gaussian binning" rather than the tradition box-shaped histogram bins (or "windowing" functions) of the standard model. Significantly, the width parameter of these Gaussian bins/windows is typically chosen to be something substantially less than the unit-width used in the standard quasi-classical model, and in this manner the approach forces the final conditions of the DOFs of interest to be more narrowly restricted about their quantum values.

Furthermore, it is noted that in much of this work the restriction on the final conditions of the trajectories can be quite severe, in many instances employing Gaussian windowing functions having widths of about 10% of the full unit-width used in the traditional scheme. See Ref. [6]. This does then of course raise efficiency concerns if more than a few relevant DOFs are "quantized" via such narrow binning. For example, quantizing vibrational motion in a polyatomic involves binning the classical action variable associated with

each of the polyatomic's $3n-6$ normal modes (where n is the number of atoms) and thus, fractionally, only $\left(\frac{1}{10}\right)^{3n-6}$ of the trajectories are "counted"[1] in such an approach. Thus, despite the simplicity of such techniques, it is still key for efficiency's sake to identify the interesting DOFs where state-to-state quantization is desired.

1.3 Concept of a Symmetrical Quasi-Classical (SQC) Approach

Another potential modification to the traditional QCT technique stems from the traditional approach's inconsistent treatment of initial and final conditions. In the case of a vibrational DOF, for example, a molecule's initial vibrational energy is equal to the true energy of the selected initial quantum state, but a molecule's final vibrational energy (as computed in the classical trajectory simulation) does not generally come out equal to the true quantum energy associated with the vibrational quantum state to which the molecule is assigned.[2]

However, this does not have to be the case. It has been pointed out [7] that the quasi-classical description may be made more self-consistent—and made to obey microscopic reversibility—by *averaging* the initial values of the classical action variables using the same window functions which are used to *bin* the final action variables, thus enforcing quantization of the initial and final classical action variables generally to the same extent.

One formal justification for such an approach may be shown based on semiclassical principles by beginning with the "primitive" semiclassical expression for the state-to-state transition probability [8]:

$$P_{N_2 \leftarrow N_1} = \sum_{\substack{n_1=N_1, \\ q_1 \in \{\text{roots of Eq. (1.1b)}\}}} \frac{1}{2\pi} \left| \frac{\partial n_2(n_1, q_1)}{\partial q_1} \right|^{-1} \tag{1.1a}$$

$$n_2(N_1, q_1) = N_2 \tag{1.1b}$$

[1] To be precise, all trajectories contribute to some extent if Gaussian windows are employed since the tails go to $\pm\infty$, however, while requiring the same level of computation, trajectories landing in the tails have little effect on the outcome.

[2] In the traditional QCT approach, the final quantum state to which a trajectory is assigned is simply that which is closest in energy to the final energy computed via the classical trajectory simulation.

where (n, q) are the classical action-angle variables for the quantized DOF in question; (n_1, q_1) being their initial conditions and n_2 being the final value of the action variable (the final angle q_2 is not needed). The final action n_2—which corresponds[3] to the final quantum number for this DOF—is thus a function of the initial action-angle variables n_1 and q_1 and also of the initial values of any other variables corresponding to system's other DOFs (translations, vibrations, rotations) which are not explicitly indicated in Eq. (1.1). Because, in Eq. (1.1), the initial action n_1 is initialized to N_1 and the final action n_2 is *made* equal to N_2 by finding the roots of $n_2(N_1, q_1) = N_2$, the Jacobian $\left|\frac{\partial n_2(N_1,q_1)}{\partial q_1}\right|$ in Eq. (1.1) is evaluated over trajectories which begin and end with their correct quantum values. In other words, the initial and final classical actions in the primitive semiclassical expression for the $N_1 \to N_2$ transition probability are constrained exactly to their quantum values.

Finding the roots q_1 of Eq. (1.1b) constitutes a double-ended boundary value problem and hence, while feasible in simple cases, is generally impractical for complex systems of many interacting DOFs. Accordingly, the QCT approach avoids the root search problem by simply assigning trajectories to the closest final quantum state, and one can find the relationship of this approach to the primitive semiclassical expression of Eq. (1.1) simply by averaging Eq. (1.1) over the final action n_2 by unit-width about the final quantum value of the action N_2:

$$P^{QC}_{N_2 \leftarrow N_1} = \sum_{\substack{n_1=N_1,\\ q_1 \in \{\text{roots of}\\ \text{Eq. (1.1b)}\}}} \int_{N_2-\frac{1}{2}}^{N_2+\frac{1}{2}} dn_2 \; \frac{1}{2\pi} \left|\frac{\partial n_2(n_1, q_1)}{\partial q_1}\right|^{-1} . \tag{1.2}$$

A change of integration variables from n_2 to q_1 then gives the standard QCT state-to-state expression:

$$P^{QC}_{N_2 \leftarrow N_1} = \frac{1}{2\pi} \int_0^{2\pi} dq_1 \; h\left(\tfrac{1}{2} - |n_2(N_1, q_1) - N_2|\right) \tag{1.3}$$

where

$$h(x) = \begin{cases} 0 & x < 0 \\ 1 & x \geq 0 \end{cases}$$

is the usual Heaviside step-function. This is similar to the change of variables

[3]For a vibrational DOF, the classical action is actually $n + \frac{1}{2}$, so that with $\hbar = 1$, n is the classical counterpart to the vibrational quantum number; i.e., the vibrational energy levels are the energies for which $n = 0, 1, 2, \ldots$.

which leads to the initial value representation of semiclassical theory—the SC-IVR [9]—and Eq. (1.3) is also now expressed as an integral over only the initial values of the angle variable q_1, with the initial value of the action variable still fixed at N_1.

In view of the relationship of the QCT approach to the primitive semiclassical expression of Eq. (1.1), it is clear that a symmetrical quasi-classical (SQC) approach (which treats quantization of initial and final states in equal fashion) may be accomplished simply by averaging Eq. (1.1) over both the initial and final action variables over a unit-width about their respective quantum values, i.e. averaging n_1 over $N_1 \pm \frac{1}{2}$ and n_2 over $N_2 \pm \frac{1}{2}$:

$$P^{SQC}_{N_2 \leftarrow N_1} = \sum_{\substack{n_1=N_1, \\ q_1 \in \{\text{roots of} \\ \text{Eq. (1.1b)}\}}} \int_{N_1-\frac{1}{2}}^{N_1+\frac{1}{2}} dn_1 \int_{N_2-\frac{1}{2}}^{N_2+\frac{1}{2}} dn_2 \, \frac{1}{2\pi} \left| \frac{\partial n_2(n_1, q_1)}{\partial q_1} \right|^{-1}; \qquad (1.4)$$

which after changing integration variables as above gives

$$P^{SQC}_{N_2 \leftarrow N_1} = \frac{1}{2\pi} \int_{-\frac{1}{2}}^{\infty} dn_1 \int_0^{2\pi} dq_1 \; h\left(\tfrac{1}{2} - |n_1 - N_1|\right) h\left(\tfrac{1}{2} - |n_2(n_1, q_1) - N_2|\right). \qquad (1.5)$$

Thus, the basic SQC expression of Eq. (1.5) is just an average over the initial phase space[4] of the DOF being "quantized," with the integrand being the product of normalized window functions for this DOF's initial and final states. And, moreover, since phase space averages are invariant to canonical transformations, Eq. (1.5) may be equivalently evaluated by averaging the integrand over any canonical set of generalized momentum p and conjugate coordinate q.

The basic SQC expression of Eq. (1.5) has the desired property of microscopic reversibility, but for reasons that will become more apparent below, it is appealing (and quite useful) to go another step further beyond the standard QCT procedure and to symmetrically tighten the quantization conditions imposed by Eq. (1.5) in the same spirit that Bonnet and Rayez applied narrowed Gaussian windows to final product states. This may be done, of course, simply by replacing the unit-width "bins" in equation Eq. (1.5) with normalized window functions having reduced widths, whether Gaussians, histogram "boxes," or of some other functional form. The usefulness of this approach has been demonstrated through the treatment of various examples which are described herein, beginning with quantization of molecular vibrational degrees

[4]It has been assumed throughout that $\hbar = 1$, so 2π is the volume of phase space for one degree of freedom. Also recall that the actual classical action is $n + \frac{1}{2}$.

of freedom in a simple reactive scattering scenario.

Chapter 2

Reactive Scattering: $H + H_2 \rightarrow H_2 + H$

2.1 Motivation

To demonstrate the SQC approach in perhaps the simplest non-trivial context, reactive scattering of $H + H_2$ (in the collinear geometry) was first considered. [1] One goal of this work was simply to ascertain the extent to which

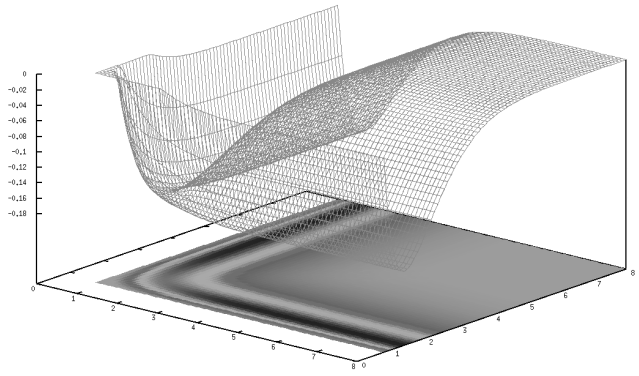

Figure 2.1: View of the $H + H_2$ BKMP2 [10] PES in Cartesian coordinates (collinear geometry)

symmetrically varying the windowing functions (using different classes of window functions, narrowing the window functions, etc.) effected the calculated results, and generally to gauge the sensitivity of such results to the variations. However, another perhaps more useful goal was to determine the extent to which symmetrically "tuning" the windowing functions could be used to yield an optimal imitation of the true quantum mechanical (QM) state-to-state reaction probabilities.

It turns out, to give a little historical perspective, that the latter goal (in

addition to the pedagogical advantage of microscopic reversibility) motivated perhaps the original attempt to use a symmetrical approach to QCT simulation. In particular, it was pointed out at a Faraday Discussion in 1973 [7] that symmetrically averaging over initial and final vibrational actions might—just as a practical matter—smooth out the sharp reaction thresholds often seen in QCT simulations of reactive scattering events which, due to the smoothing effects of quantum tunneling, were often not seen in the true results. However, the results presented at this meeting for collinear $H + H_2$ reactive scattering [7, see the "General Discussion" following the published papers] revealed that the additional smoothing provided by the symmetric approach vastly over-smoothed the reaction probabilities in the threshold energy region. Hence, despite any inherent pedagogical advantage, the symmetric approach was dismissed as not particularly useful.

Fig. 2.2 shows an updated version of essentially the same result from 1973 for the ground vibrational state to ground vibrational state reaction probability, $P_{0\leftarrow 0}$, recalculated using the current state of the art BKMP2 H_3 potential energy surface (PES) [10]. The standard QCT result shows a sharp reaction threshold, the QM result[1] shows a smoothed threshold because of tunneling, and the symmetrical version of the quasi-classical result significantly over-smooths the classical reaction threshold, as just described.

While symmetrical windowing of vibrational states was considered back in 1973, what was not considered was the notion of narrowing the quantization condition in the spirit of "Gaussian binning," but to do so symmetrically with respect to initial and final vibrational states. It is seen below that this simple modification fixes the over-smoothing problem noted in this early work and can be used to very closely mimic (for this particular problem) the correct quantum result in the threshold energy region.

[1]Note that over this threshold energy region, $P_{0\leftarrow 0}(E)$ is equal to $N(E)$, the cumulative reaction probability, since the only open reactive channel is between ground vibrational states. Thus, the QM curve displayed in Fig. 2.2 was generated via a direct calculation of $N(E)$ using a discrete variable representation (DVR) of the QM Green's function with absorbing boundary conditions (ABC). [11, 12, 13, These papers provide details of the DVR-ABC Green's function method. In particular, see Eq. 2.9(d) of Ref. [11] for the expression used to directly calculate $N(E)$. Eq. 3.2 of Ref. [13] was used as the analytical form of the reactant and product adsorbing potentials.]

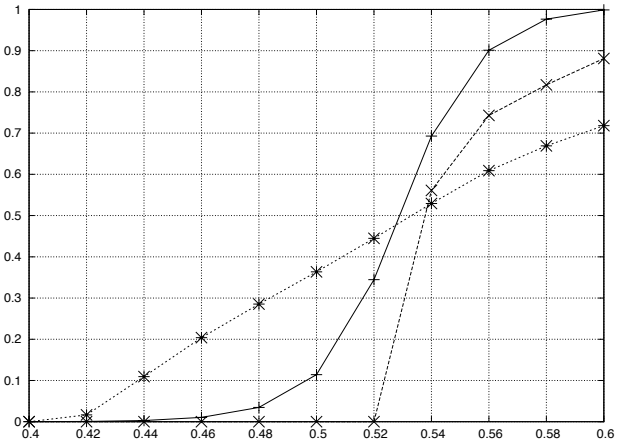

Figure 2.2: Analogue of the 1973 result: Reaction probability $P_{0\leftarrow 0}$ for $H + H_2$ (collinear) versus total energy in eV; QCT ($\times$), QM ($+$), and symmetrical QCT ($*$, $\Delta n = 1$)

2.2 SQC Results

Thus, in order to investigate the SQC approach, considered first was the use of square histogram window functions, as in the early work, but here varying the widths Δn about the quantum value N. The normalized histogram window function for state N with width Δn is thus

$$W_N(n) = \frac{1}{\Delta n}\, h\left(\frac{\Delta n}{2} - |n - N|\right) \tag{2.1}$$

Replacing the unit-width histograms of Eq. (1.5) with these variable width window functions gives, for the $N_1 \rightarrow N_2$ transition probability,

$$P^{SQC}_{N_2\leftarrow N_1} = \frac{1}{2\pi}\int_0^{2\pi} dq_1 \int_{\frac{1}{2}}^{\infty} dn_1 \cdot W_{N_1}(n_1) \cdot W_{N_2}(n_2(n_1, q_1)). \tag{2.2}$$

The 40-year old symmetric treatment recalculated in Fig. 2.2 corresponds to using the windowing function of Eq. (2.1) with $\Delta n = 1$, the maximum possible value, which in 1973 was seen to be too large. Fig. 2.3 shows results for smaller values of Δn (again calculated using the BKMP2 PES [10]), and one sees that a value of $\Delta n = \frac{1}{2}$ gives quite reasonable results over the threshold energy region shown in Fig. 2.3a: the maximum reaction probability is in reasonable agreement with the quantum result, as is the general shape of the reaction probability curve over the threshold region.

The reaction probabilities shown in Fig. 2.3a for various choices of Δn are shown over a wider energy range in Fig. 2.3b. More precisely, Fig. 2.3b plots the cumulative reaction probability $N(E)$—which is just equal to the sum of all

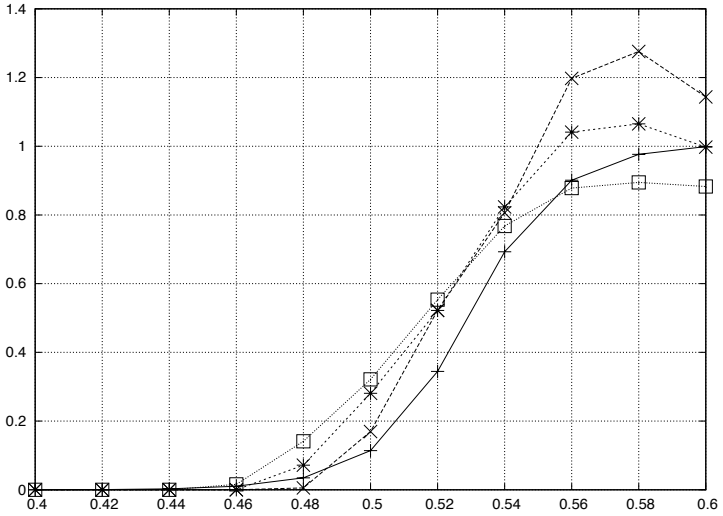

(a) Reaction threshold energy region ($P_{0\leftarrow 0}(E) = N(E)$

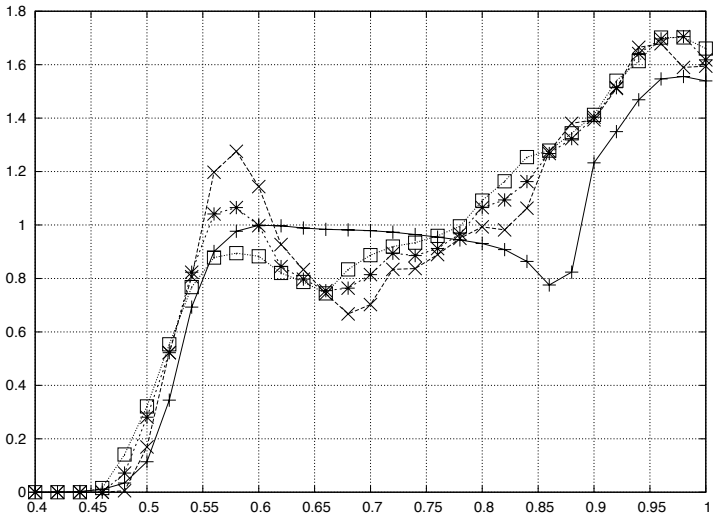

(b) Expanded energy range ($P_{0\leftarrow 0}(E) \neq N(E)$)

Figure 2.3: Cummulative reaction probability $N(E)$ for $H + H_2$ (collinear) calculated via the SQC approach using histogram "box" window functions of various widths: exact QM result (+); SQC with $\Delta n = 0.4$ ($\times$), $\Delta n = 0.5$ ($*$), and $\Delta n = 0.6$ ($\Box$); energies are in electron volts (eVs)

state-to-state reaction probabilities $P_{p \leftarrow r}(E)$ (reactants (r) to products (p)) which are non-zero over the higher energies of this expanded range. Here, one sees that the results given by the symmetric binning procedure using various width parameters exhibit a bit of an oscillation about the plateau region of the QM $N(E)$ curve before climbing in the high-energy region where additional reactive channels open up.

Next, to investigate the effect of altering the functional form of the windowing function, employed (in Eq. (2.2)) were normalized Gaussian window functions:

$$W_N(n) = \frac{1}{\sqrt{\pi}\,\Delta n/2}\, e^{-\left(\frac{n-N}{\Delta n/2}\right)^2} \tag{2.3}$$

The result for $\Delta n = \frac{1}{2}$ is shown in Fig. 2.4 and compared to the result obtained by using histogram windows, also with $\Delta n = \frac{1}{2}$. While the use of Gaussian windows does seem to give somewhat smoother results than the use of histogram windows, choice of the optimal width parameter Δn—see, e.g., the variation in Fig. 2.3b (for histogram windows, but also see Fig. 2.5b for Gaussian windows)—is seen to have a significantly more pronounced effect on the results than the particular choice of the functional form of the window, suggesting that in most cases, a simple adjustment of Δn will likely provide the greatest opportunity for tuning SQC calculations to the true quantum results in most cases.

Nevertheless, despite the more significant effect of varying the width parameter, reaction probabilities for $H + H_2$ calculated using Gaussian window functions (Eq. (2.3)) of various widths Δn are shown in Fig. 2.5, and it is seen that the best overall SQC approximation is obtained by choosing a Gaussian window of width $\Delta n = \frac{1}{2}$. Over the reaction threshold energy region shown in Fig. 2.5a, results for $P_{0 \leftarrow 0}(E)$ computed using the SQC approach with this window function show excellent agreement with the true QM result: in terms of the onset of the tunneling region, the location and value of maximum reaction probability, as well as the overall curve shape $P_{0 \leftarrow 0}(E)$. Fig. 2.6a overlays this result for $\Delta n = \frac{1}{2}$ with the analogue of the 1973 (also shown in Fig. 2.2).

Finally, since it is well-known from semiclassical theory[2], also considered was the use of the Wigner distribution for the initial and final action window functions. The Wigner distribution (in Cartesian variables) for a given

[2]See, for example, Ref. [14] regarding the linearized semiclassical initial value representation (LSC-IVR).

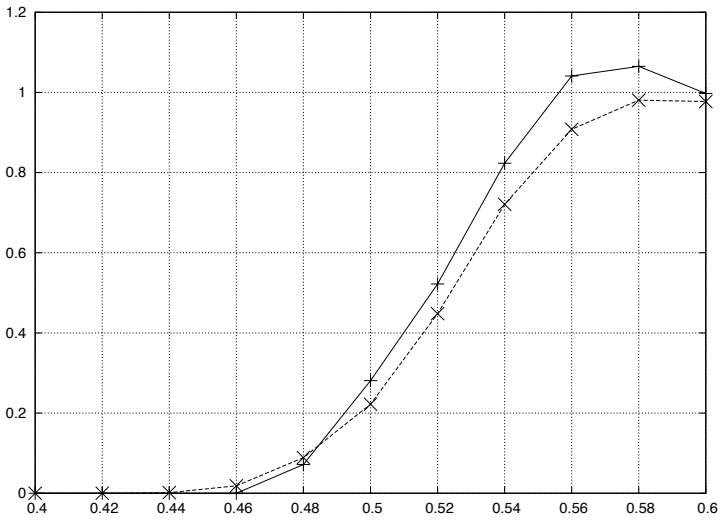

(a) Reaction threshold energy region ($P_{0\leftarrow 0}(E) = N(E)$)

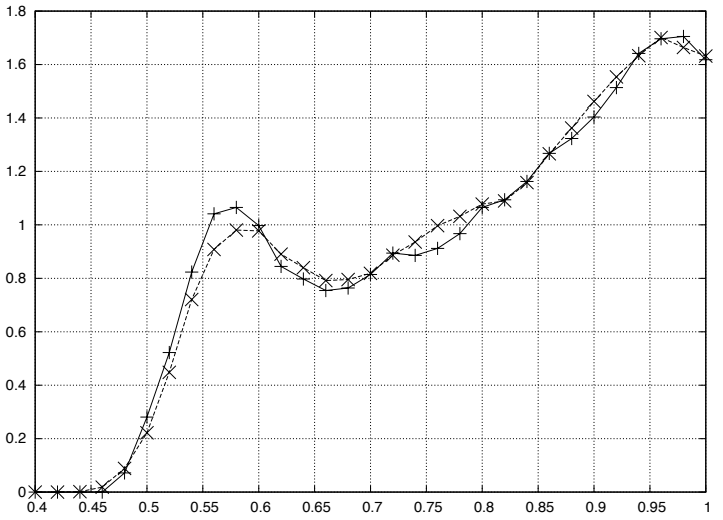

(b) Expanded energy range ($P_{0\leftarrow 0}(E) \neq N(E)$)

Figure 2.4: Comparison of Gaussian ($\times$) versus histogram "box" ($+$) window functions (of width $\Delta n = \frac{1}{2}$) used to calculate $N(E)$ for $H + H_2$ (collinear); note the significant similarity, particularly over the full energy range in (b)

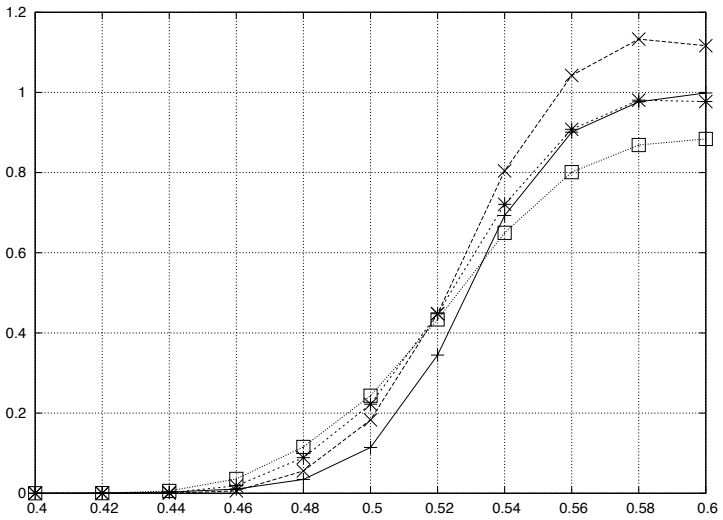

(a) Reaction threshold energy region ($P_{0\leftarrow 0}(E) = N(E)$)

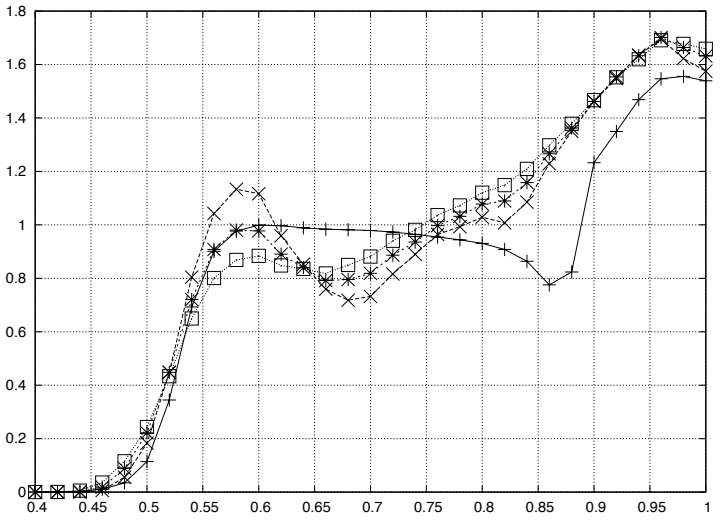

(b) Expanded energy range ($P_{0\leftarrow 0}(E) \neq N(E)$)

Figure 2.5: Analogue of Fig. 2.3, but here using Gaussian window functions of various widths Δn versus the exact QM result (+): SQC with $\Delta n = 0.4$ ($\times$), $\Delta n = 0.5$ ($\ast$), and $\Delta n = 0.6$ ($\square$)

vibrational quantum state N is

$$W_N(p,x) = \int_{-\infty}^{+\infty} d\Delta x \; e^{ip\Delta x} \; \phi_N(x + \tfrac{\Delta x}{2}) \; \phi_N(x - \tfrac{\Delta x}{2}) \tag{2.4}$$

where $\phi_N(x)$ is the wavefunction corresponding to quantum state N. Evaluating Eq. (2.4) using the ground state 1D-harmonic oscillator wavefunction and expressing the result in terms of action-angle variables gives

$$W_0(n) = 2\, e^{-2\left(n+\frac{1}{2}\right)} \tag{2.5}$$

as the window function for the ground vibrational state. This expression was then used in Eq. (2.2) and the results are shown in Fig. 2.6b. Since Eq. (2.5) gives a very broad distribution for the action variable n, and one weighted heavily at small values, it does a poor job of localizing the action variable n about the integer quantum value versus using Gaussian or histogram window functions with Δn set to $\frac{1}{2}$. Thus, reaction probabilities generated with Eq. (2.5) provide very poor estimates of the correct quantum transition probabilities as shown in Fig. 2.6b.

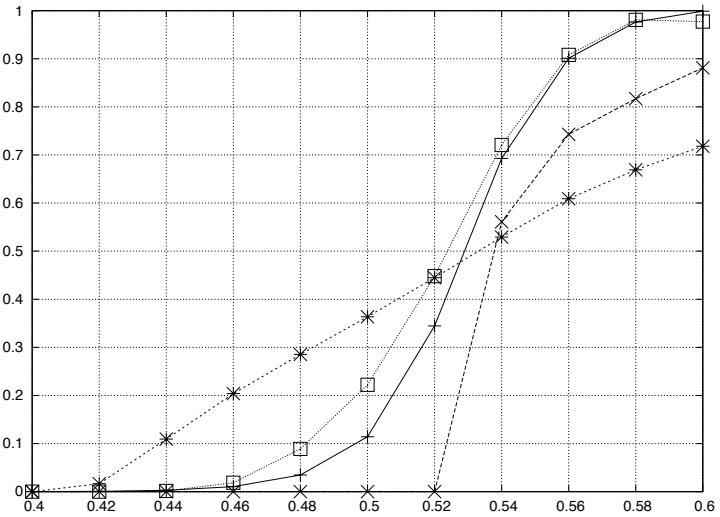

(a) Summary of improvement: exact QM (+); traditional (asymmetric) QCT (×); analogue of the 1973 result (∗) (i.e., SQC using histogram windows with $\Delta n = 1$); SQC using Gaussian windows with $\Delta n = \frac{1}{2}$ (□).

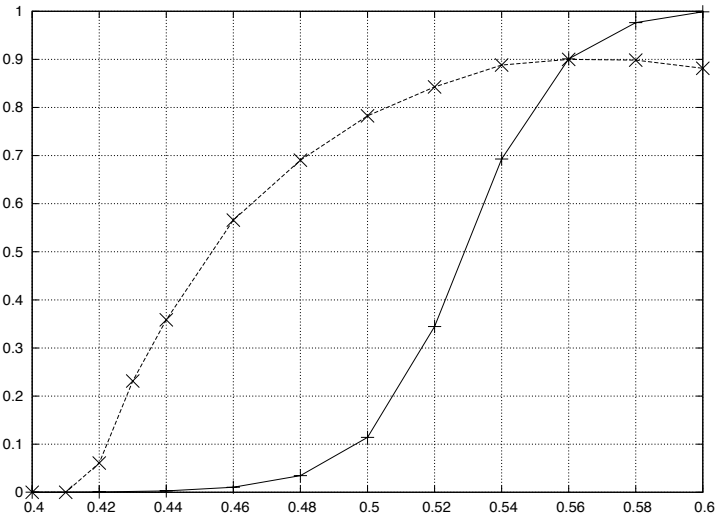

(b) Poor result seen using the Wigner distribution function in the SQC approach (×) versus the QM result (+)

Figure 2.6: Improvements in the calculation of the threshold reaction probability ($P_{0\leftarrow 0}(E) = N(E)$) for $H + H_2$ (collinear) seen using the SQC approach

Chapter 3

Conclusion

Presented here in Part I has been the development of an extremely simple, microscopically reversible, symmetric quasi-classical (SQC) procedure, and its application to the quantization of nuclear DOFs in the reactive scattering context.

In particular, it was demonstrated that vibrational state-to-state reaction probabilities for collinear $H + H_2$ computed via the SQC approach using window functions of about $\frac{1}{2}$ unit-width are in very good agreement with quantum mechanical results over the threshold energy region (doing a reasonable job of mimicking the onset of tunneling) and, moreover, it was shown that these results represent a significant improvement over what is obtained from the traditional QCT approach. In addition, while for this particular scattering problem Gaussian window functions were found to give the best results, it was demonstrated that the value chosen for the window function's width parameter, much more so than its functional form, was a far more significant factor affecting the results.

As far as efficiency, there is a performance penalty associated with applying the SQC approach with less than unit-width window functions because some trajectories finishing with intermediate actions will be thrown out. However, though this results in a scaling of computational cost by

$$\left(\frac{1}{\Delta n}\right)^G \tag{3.1}$$

where Δn is the width parameter and G is the number of DOF which are being "quantized," typically one only wishes to quantize a small number of key DOFs, and so this additional expense is likely of minor concern in many cases; and, of course, this is offset by the fact that the "inputs" to the SQC

procedure are just ordinary classical trajectories computed in the typical fashion without any additional auxiliary computations (such as, e.g., semiclassical phase information).

It is also interesting to contrast the SQC approach with the linearized version of the semiclassical IVR (initial value representation), the LSC-IVR. The relationship between the two is essentially that the LSC-IVR *is* the SQC approach if the functions used for the symmetric windowing are chosen to be the classical Wigner distribution functions corresponding to the initial and final quantum states. However, it was shown in Fig. 2.6b that the Wigner function gives extremely poor results in the context of $H+H_2$ reactive scattering relative to the SQC approach implemented with simple, narrowed $\frac{1}{2}$-width histogram window functions. Thus, although the LSC-IVR has been used successfully in a variety of circumstances [9, 14, 15], the foregoing work demonstrates that the SQC approach has the potential to lead to substantial and easily achievable improvements over this and other simple trajectory-based methods.

As stated, this Part I has involved developing and applying the SQC approach to the quantization of nuclear DOF in the context of state-to-state reactive scattering. In Part II, the SQC approach will be applied to the much more interesting, challenging, and important problem of accurately treating electronically non-adiabatic phenomena where the chemical dynamics is oftentimes dominated by the purely quantum effect of coherent nuclear motion on multiple Born-Oppenheimer PESs.

Part II

Symmetric Quantization of Electronic States and Treatment of Non-Adiabatic Processes

Chapter 4

Background

Within the standard picture provided by the Born-Oppenheimer approximation, chemical dynamics is generally envisioned as many interacting nuclear degrees of freedom (DOFs)—e.g., intermolecular separations, intramolecular vibrations, rotations, etc.—moving classically on effective electronic potential energy surfaces (PESs) generated by the mean electric field of the electrons and neighboring nuclei—as typically determined by approximately solving the electronic Schrödinger equation. However, when solutions to the electronic Schrödinger equation over some range of nuclear geometries yield two or more PESs which are close in energy, coupling between the PESs generally leads to so-called non-adiabatic effects such as quantum coherences between nuclear motion on the multiple PESs, and ultimately transitions between the electronic states which are represented by the PESs. While, it is, of course, in principle always possible to evaluate non-adiabatic effects through a complete solution to the coupled-channel Schrödinger equation with respect to all the intersecting PESs, in practice this will only be computationally feasible for simple chemical systems with only a few relevant DOFs.

Accordingly, a variety of quasi-classical and semiclassical approaches have been proposed and tested for modeling non-adiabatic dynamics in lieu of directly solving the full Schrödinger equation, all having the goal of capturing the essential features of the true quantum dynamics, but at an acceptable computational cost. These approaches include, for example, the traditional Ehrenfest model (described, for instance, in Ref. [9, see p. 1406]), as well as approaches based on the fewest switches surface-hopping (FSSH) methodology first introduced by Tully and coworkers [16].

The approach taken by Miller and coworkers [9] was to apply a semiclassical treatment [17] and a linearized semiclassical treatment [14] to a classical analogue model of the complete multi-state electronic system which was devel-

oped in the much earlier work of Meyer and Miller [18, 19, 20] (and relatedly of Miller and McCurdy [21]). The classical electronic Meyer-Miller (MM) Hamiltonian embodying this model is a function of the quantum mechanical electronic Hamiltonian matrix elements—which depend on the nuclear coordinates $\{R_i\}$—and also on pairs of classical action-angle variables $\{n_i, q_i\}$—one pair associated with each energetically accessible electronic state. These semi-classical treatments based on the MM Hamiltonian were shown [17, 14, 22] to yield quite reasonable results for a variety of model non-adiabatic problems, including the benchmark problems Tully and co-workers used initially to test the FSSH technique.

In the work presented here, a new and even simpler model has been explored which is based on the symmetric quasi-classical (SQC) approach presented in Part I. It may, in fact, be the simplest and least computationally-intensive (but still reasonable) approach that one can envision for dealing with this type of intrinsically quantum mechanical phenomena. In brief, one begins by using the Meyer-Miller (MM) classical electronic Hamiltonian to represent the electronic states in terms of classical action-angle variables, and then applies the SQC protocol in order to symmetrically "quantize" the initial and final classical "electronic action" variables within some specified bounds of the allowed quantum values. It is noted (as has been noted many times before) that by mapping electronic DOF onto pairs of classical canonical variables, the MM Hamiltonian treats nuclear and electronic DOFs in a dynamically consistent classical framework. Likewise, the SQC approach places quantization of initial and final states on equal footing.

After formally describing the theory behind the SQC/MM methodology, the results of the approach applied to several problems of interest is presented. The first set of applications are the three benchmark problems of Tully and co-workers, and it is described how various important "tweaks" to the basic approach were developed in the context of these models. Next presented are the results of applying the approach to the well-studied spin-boson model of condensed phase non-adiabatic processes, in both its symmetric and asymmetric variants, and then to various recently proposed models of electron transfer (ET) processes including a model of photo-induced proton coupled electron transfer (PCET). This work then concludes with several examples of treating systems of three non-adiabatically coupled electronic states (using two different approaches). It is seen that the SQC/MM approach provides very reasonable results in all cases and quite excellent results in most cases. It is of particular note that this simple approach describes the asymmetric spin-boson problem so well, for many approximate treatments which work well for the symmetric spin-boson system have been seen to fail for the asymmetric version. It is

also significant that the SQC/MM approach is able to accurately handle the Marcus inversion in ET rates (with increasing exothermicity), because this is another regime where many simple methods are seen to fail.

Chapter 5

Theory

5.1 The Meyer-Miller Classical Electronic Hamiltonian

For any system of electrons in an electric field generated by fixed nearby nuclei, the time-dependent electronic wavefunction can be expanded in a complete (possibly orthogonal) set of time-independent basis functions as

$$|\psi_{el}(t)\rangle = \sum_{k=1}^{F} c_k(t)\,|k\rangle \tag{5.1}$$

where the time-dependence is captured by the complex coefficients $c_k(t)$. If one rewrites each $c_k(t)$ in terms of real functions $n_k(t)$ and $q_k(t)$ as

$$c_k(t) = \sqrt{n_k(t)}\; e^{-iq_k(t)}, \tag{5.2}$$

then it can be shown that $n_k(t)$ and $q_k(t)$ are canonically conjugate action-angle variables (with the action $n_k(t)$ acting as the momentum conjugate to the coordinate angle $q_k(t)$), and that these "electronic" action-angle variables evolve in time according to Hamilton's equations,

$$\dot{n}_k(t) = -\frac{\partial H_{el}(\mathbf{n},\mathbf{q};\mathbf{R})}{\partial q_k} \tag{5.3a}$$

$$\dot{q}_k(t) = \frac{\partial H_{el}(\mathbf{n},\mathbf{q};\mathbf{R})}{\partial n_k}, \tag{5.3b}$$

provided that the classical Hamiltonian used in Eq. (5.3) is identified as the expectation value of the electronic quantum Hamiltonian operator written in terms of the $|k\rangle$ basis functions:

$$\begin{aligned} H_{el}(\mathbf{R}) &= \langle\psi_{el}(t)|\,\hat{H}_{el}\,|\psi_{el}(t)\rangle = \sum_{k,k'=1}^{F} c_{k'}^{*}\,\langle k'|\,\hat{H}_{el}\,|k\rangle\,c_k \\ &= \sum_{k,k'=1}^{F} c_{k'}^{*} c_k H_{k,k'}(\mathbf{R}). \end{aligned} \tag{5.4}$$

With substitution of $\sqrt{n_k(t)}\,e^{-iq_k(t)}$ for the $c_k(t)$'s (i.e., using Eq. (5.2)), this becomes

$$H_{el}(\mathbf{R},\mathbf{n},\mathbf{q}) = \sum_{k,k'=1}^{F} \sqrt{n_k\,n_{k'}}\;\cos(q_k - q_{k'})\;H_{k,k'}(\mathbf{R}), \tag{5.5a}$$

which upon rewriting the summation gives

$$H_{el}(\mathbf{R},\mathbf{n},\mathbf{q}) = \sum_{k=1}^{F} n_k\;H_{k,k}(\mathbf{R}) + 2\sum_{k<k'=1}^{F} \sqrt{n_k\,n_{k'}}\;\cos(q_k - q_{k'})\;H_{k,k'}(\mathbf{R}), \tag{5.5b}$$

the basic form of the classical analogue expression given in Ref. [18]. It is straightforward to show that the "classical" time-evolution of the $n_k(t)$'s and $q_k(t)$'s provided by this Hamiltonian when used in Hamilton's equations for $\dot{n}_k(t)$ and $\dot{q}_k(t)$ (i.e., Eq. (5.3)) is exactly equivalent to the time-evolution of the $c_k(t)$'s provided by the time-dependent Schrödinger Equation,

$$\dot{\mathbf{c}}(t) = -i\,\mathbf{H}(\mathbf{R})\cdot\mathbf{c}(t), \tag{5.6}$$

provided that the Hamiltonian only depends parametrically on the nuclear coordinates $\mathbf{R}$—e.g., if there is a pre-determined nuclear trajectory $\mathbf{R}(t)$. It is therefore noted that the trajectories generated with Eq. (5.5) are equivalent to the classical trajectories of the Ehrenfest approach generated by time-evolving the quantum amplitudes $\{c_k\}$ according to Eq. (5.6). [23] It is also noted that if the initial values of the $n_k(t)$'s are chosen such that

$$\sum_{k=1}^{F} n_k(t=0) = 1,$$

then the $n_k(t)$'s may be interpreted as the probability of finding the electronic system in quantum state $|k\rangle$ at time t—i.e., the $n_k(t)$'s are the occupation numbers of the electronic states (and one can easily show that $\sum_{k=1}^{F} n_k(t)$ is a constant of the motion as the system evolves according to Eqs. (5.3) and (5.5), or equivalently according to Eq. (5.6)).

While it is true that Eq. (5.5) is equivalent to solving the time-dependent electronic Schrödinger equation along a fixed (pre-determined) nuclear trajectory, it is not an exact representation of the full coupled nuclear-electronic quantum system. One defect in Eq. (5.5) noted in the original paper [18] (which also carries over to the Ehrenfest approach as noted in Ref. [23]) is that when the system begins in a pure quantum state—i.e., $n_i = 1$ for the initial state i and $n_k = 0, \forall\, k \neq i$—the Hamiltonian of Eq. (5.5) is independent of the angle variables $\{q_k\}$ (i.e., the coupling term depending on $H_{k,k'}$ vanishes), which means that if the system starts in a pure state i, there is only a single trajectory generated from Eqs. (5.3) and (5.5) rather than an ensemble of trajectories which may be associated with a given $n_i \rightarrow n_f$ transition.

Thus, when Eq. (5.5) was first proposed [18], Meyer and Miller added $\frac{1}{2}$ to the n_k's in Eq. (5.5) (i.e., $n_k \rightarrow n_k + \frac{1}{2}$), and at the same time subtracted $\frac{1}{2}\sum_{k=1}^{F} H_{k,k}$ from the diagonal terms, so that the effect of the $n_k \rightarrow n_k + \frac{1}{2}$ transformation was only to modify the off-diagonal coupling terms of H_{el}:

$$\begin{aligned} H_{el}(\mathbf{R},\mathbf{n},\mathbf{q}) = &\sum_{k=1}^{F} n_k H_{k,k}(\mathbf{R}) \\ &+ 2\sum_{k<k'=1}^{F} \sqrt{(n_k+\tfrac{1}{2})(n_{k'}+\tfrac{1}{2})}\cos(q_k - q_{k'})H_{k,k'}(\mathbf{R}). \end{aligned} \tag{5.7}$$

Since only the coupling terms are affected, it remains true that $n_i = 1$ (and $n_k = 0, \forall\, k \neq i$) still corresponds to initial electronic state i characterized by electronic Hamiltonian matrix element $H_{i,i}$, however, the fact that the coupling terms no longer vanish in this configuration results in the generation of an ensemble of trajectories through variation of the initial angle variables $\{q_k\}$.

The value of $\frac{1}{2}$ in the $n_k \rightarrow n_k + \frac{1}{2}$ transformation was chosen in the spirit of various Langer-type modifications well-known in semiclassical theory. However, for reasons explained in detail below, it is advantageous within the context of the SQC model to choose this value to be something less than $\frac{1}{2}$, and it thus becomes a parameter of the SQC model henceforth labeled as γ. Stock, in Refs. [24] and [25], also found reducing the $\frac{1}{2}$ to be a useful modification.

The full nuclear-electronic MM Hamiltonian written in terms of action-angle variables $\{n_i, q_i\}$ and γ is then given by:

$$H(\mathbf{P},\mathbf{R},\mathbf{n},\mathbf{q}) = \frac{|\mathbf{P}|^2}{2\mu} \; + \; \sum_{k=1}^{F} n_k \; H_{kk}(\mathbf{R}) \\ + \; 2 \sum_{k<k'=1}^{F} \sqrt{(n_k+\gamma)(n_{k'}+\gamma)}\cos(q_k - q_{k'}) \; H_{kk'}(\mathbf{R}). \tag{5.8}$$

where the first term is the kinetic energy of the nuclear DOFs and γ is a parameter chosen from the interval $\left(0, \frac{1}{2}\right]$.

The Hamiltonian of Eq. (5.8) embodies the essential physics of the Meyer-Miller model, but there are additional modifications which are generally made to it in order to improve its practical implementation. For instance, the equations of motion generated from Eq. (5.8) via Hamilton's equations, such as

$$\dot{q}_k(t) = \frac{\partial H}{\partial n_k} = H_{kk}(\mathbf{R}) + \sum_{k'=1}^{F} \sqrt{\frac{n_{k'}+\gamma}{n_k+\gamma}} \; \cos(q_k - q_{k'}) \; H_{kk'}(\mathbf{R}), \tag{5.9}$$

become numerically ill-behaved when n_k takes on values near its minimum value $(-\gamma)$. However, such singular behavior may be eliminated by transforming the Hamiltonian of Eq. (5.8) to Cartesian oscillator variables $\{p_i, x_i\}$ via the canonical transformation

$$x_k = \; \sqrt{2(n_k+\gamma)} \; \cos(q_k), \tag{5.10a}$$

$$p_k = -\sqrt{2(n_k+\gamma)} \; \sin(q_k) \tag{5.10b}$$

having inverse transformation

$$n_k = \frac{1}{2}p_k^2 + \frac{1}{2}x_k^2 - \gamma, \tag{5.11a}$$

$$q_k = -\tan^{-1}\left(\frac{p_k}{x_k}\right) \tag{5.11b}$$

which gives

$$H(\mathbf{P},\mathbf{R},\mathbf{p},\mathbf{x}) = \frac{|\mathbf{P}|^2}{2\mu} + \sum_{k=1}^{F}\left(\frac{1}{2}p_k^2+\frac{1}{2}x_k^2-\gamma\right) H_{kk}(\mathbf{R}) + \sum_{k<k'=1}^{F}\left(p_k p_{k'}+x_k x_{k'}\right) H_{kk'}(\mathbf{R}). \tag{5.12}$$

Not only do no singularities arise in the equations of motion generated from the Cartesian representation of the MM Hamiltonian of Eq. (5.12) but, as an added benefit, the resulting equations of motion may be more efficiently integrated due to the absence of any required transcendental function evaluation (on their RHS).

Furthermore, the Cartesian form of Eq. (5.12) illustrates that the MM model is a mapping of a set of F electronic states onto a set of F coupled "electronic" oscillators, and from the canonical transformation given by Eqs. (5.10) and (5.11a), one has $\frac{1}{2}p_k^2+\frac{1}{2}x_k^2 = n_k+\gamma$, showing that the γ-parameter represents the amount of zero-point energy (ZPE) injected into these oscillators when they are initialized. Moreover, if γ is taken to be $\frac{1}{2}$, Stock and Thoss have shown [26] that replacing the classical coordinates and momentum (x,p) in Eq. (5.12) by their quantum mechanical operators $(\hat{x},\hat{p})$ yields an exact representation of the full nuclear-electronic quantum system.[1]

Finally, one further transformation has generally been applied to the MM Hamiltonian to put it into its final form for implementation (as it has been employed in most of this work). That is, the diagonal elements—i.e., the electronic PESs—are generally expressed relative to some reference potential function, $\bar{H}(\mathbf{R})$, i.e.,

$$\sum_{k=1}^{F} n_k H_{kk}(\mathbf{R}) \rightarrow \bar{H}(\mathbf{R}) + \sum_{k=1}^{F} n_k \left(H_{kk}(\mathbf{R}) - \bar{H}(\mathbf{R})\right) \tag{5.13}$$

with the reference potential $\bar{H}(\mathbf{R})$ generally taken to be the average of all the

[1] While this fact is not utilized in the present work, it is important in a broader context because it provides a justification for using Eq. (5.12) in more rigorous (and computationally intensive) semiclassical treatments.

PESs, $\sum_k^F H_{k,k}(\mathbf{R})$. After re-expressing the summation[2] in Eq. (5.13) to give

$$\sum_{k=1}^{F} n_k H_{kk}(\mathbf{R}) \to \bar{H}(\mathbf{R}) + \frac{1}{F} \sum_{k<k'=1}^{F} (n_k - n_{k'}) \cdot (H_{kk}(\mathbf{R}) - H_{k'k'}(\mathbf{R})), \quad (5.14)$$

this transformation, along with Eq. (5.11a), may be applied to Eq. (5.12) yielding

$$\begin{aligned} H(\mathbf{P},\mathbf{R},\mathbf{p},\mathbf{x}) = \frac{|\mathbf{P}|^2}{2\mu} + \bar{H}(\mathbf{R}) \\ + \sum_{k<k'=1}^{F} \left\{ \begin{array}{r} \frac{1}{F}\left(\frac{1}{2}p_k^2 + \frac{1}{2}x_k^2 - \frac{1}{2}p_{k'}^2 - \frac{1}{2}x_{k'}2\right) \cdot (H_{kk}(\mathbf{R}) - H_{k'k'}(\mathbf{R})) \\ + (p_k p_{k'} + x_k x_{k'}) \cdot H_{kk'}(\mathbf{R}) \end{array} \right\} \end{aligned} \quad (5.15)$$

which is the final form used herein. Eq. (5.15) treats the general case of F electronic states. For the case of $F = 2$ electronic states, the MM Hamiltonian is thus

$$\begin{aligned} H(\mathbf{P},\mathbf{R},\mathbf{p},\mathbf{x}) = \frac{|\mathbf{P}|^2}{2\mu} + \bar{H}(\mathbf{R}) \\ + \frac{1}{2}\left(\frac{1}{2}p_1^2 + \frac{1}{2}x_1^2 - \frac{1}{2}p_2^2 - \frac{1}{2}x_2^2\right) \cdot \Delta H(\mathbf{R}) \\ + (p_1 p_2 + x_1 x_2) \cdot H_{12}(\mathbf{R}) \end{aligned} \quad (5.16)$$

[2]The second terms in Eq. (5.13) and Eq. (5.14) are equivalent since:

$$\begin{aligned} \sum_{k=1}^{F} n_k \left(H_{kk} - \bar{H}\right) &= \sum_{k=1}^{F} n_k \left(H_{kk}\left(\frac{1}{F}\sum_{k'=1}^{F}\right) - \frac{1}{F}\sum_{k'=1}^{F} H_{k'k'}\right) \\ &= \frac{1}{F}\sum_{k=1}^{F}\sum_{k'=1}^{F} n_k \cdot (H_{kk} - H_{k'k'}) \\ &= \frac{1}{F}\sum_{k<k'=1}^{F} n_k \cdot (H_{kk} - H_{k'k'}) + \frac{1}{F}\sum_{k>k'=1}^{F} n_k \cdot (H_{kk} - H_{k'k'}) \\ &= \frac{1}{F}\sum_{k<k'=1}^{F} (n_k - n_{k'}) \cdot (H_{kk} - H_{k'k'}) \end{aligned}$$

where in the last step the dummy-indices k and k' have been interchanged in the second summation.

where $\bar{H} = \frac{1}{2}(H_{11} + H_{22})$ and $\Delta H = H_{11} - H_{22}$. It is interesting to note that with the rewriting of the Hamiltonian in terms of an average potential $\bar{H}(\mathbf{R})$, the γ-parameter does not appear, however it does still play the role of setting the ZPE through its presence in the action-angle to Cartesian transformation of Eq. (5.10).

Time-evolution of the combined nuclear-electronic system is then typically done by generating classical trajectories in the Cartesian variables $\{p_k, x_k\}$ from the Hamiltonian of Eq. (5.15), which for 2 states is Eq. (5.16). When required by the SQC procedure, as explained below, the electronic actions $\{n_k\}$ may be computed via Eq. (5.11a), the inverse transformation from Cartesian coordinates.

5.2 Symmetrical Windowing of the Electronic States

In Part I, histogram and Gaussian window functions were applied symmetrically to the vibrational DOF of the H_2 molecule to compute state-to-state reaction probabilities in $H + H_2$ scattering, and in this work it was discovered, *inter alia*, that variation in the width of the window function had a much more pronounced effect on the computed results than the functional form of the window function—i.e., whether it was taken to be a histogram or Gaussian. From this perspective, it is seen that the important feature of the "Gaussian Binning" procedure of Bonnet and Rayez [5] is that the window functions are taken to be substantially less than unit-width (thereby imposing a narrowed quantization condition) rather than that the "Gaussian Binning" uses Gaussian functions *per se*. Thus, for sake of simplicity, and also for purposes of remedying ZPE leakage to be explained below, only histogram window functions were employed in the SQC procedure as applied to the treatment of electronic DOFs in this Part II.

Accordingly, similar to the window function of Eq. (2.1) (employed in Part I for the treatment of vibrational DOFs), a variable width normalized histogram window function for binning the action n_k corresponding to electronic state k may be written as

$$w_{N_k}(n_k) = \frac{1}{2\gamma} h\left(\gamma - |n_k - N_k|\right), \tag{5.17}$$

where N_k is a quantum number corresponding to the occupation of the kth

state, i.e.

$$N_k = \begin{cases} 1 & \text{occupied} \\ 0 & \text{unoccupied} \end{cases},$$

γ is the allowed deviation from the quantum value—i.e., half the width of window function, and

$$h(x) = \begin{cases} 0 & x < 0 \\ 1 & x \geq 0 \end{cases}$$

is the Heaviside function. The only difference between this window function and that of Eq. (2.1) from Part I is that the width of the window function Δn has been set equal to 2γ, where γ is the ZPE parameter of Eqs. (5.10) and (5.11a) (and appearing in the Hamiltonian of Eq. (5.12)). This is a key choice, as it was discovered that tying the γ-parameter to the width of the action window function exactly balances the symmetric windowing constraints (applied to the initial and final states) against the amount of ZPE put into the model via Eq. (5.10), essentially remedying the ZPE-leakage problem which has troubled and been worked on by others [27, 28].

For the case of a system consisting of two energetically accessible electronic states, there is a pair of electronic action-angle variables (n, q) which correspond to each state, and thus the window functions for use in the SQC procedure are functions of the two action variables (n_1, n_2) associated with the two states, parametrized by the two quantum numbers (N_1, N_2). Electronic state 1 has quantum numbers $(N_1, N_2) = (1, 0)$ associated with it—corresponding to state 1 being occupied and state 2 being unoccupied—and likewise, electronic state 2 has quantum numbers $(N_1, N_2) = (0, 1)$. The joint window function for the complete electronic configuration corresponding to state 1 is thus the product of two one-dimensional window functions of the form of Eq. (5.17) and given by

$$W_1(n_1, n_2) = w_1(n_1) \cdot w_0(n_2), \tag{5.18a}$$

and the joint window function for the complete electronic configuration corresponding to state 2 is

$$W_2(n_1, n_2) = w_0(n_1) \cdot w_1(n_2). \tag{5.18b}$$

Similarly, for a system having an arbitrary number of electronic states F, the window function for the complete electronic configuration of the kth electronic state is given by

$$W_k(\mathbf{n}) = w_1(n_k) \cdot \prod_{\substack{k'=1, \\ k' \neq k}}^{F} w_0(n_{k'}) \tag{5.19}$$

These window functions may then be used in the SQC approach to compute the transition probability from initial electronic state i to final electronic state f at time t, $P_{f\leftarrow i}(t)$. For the general case of F electronic states and G nuclear DOFs having an initial distribution of nuclear coordinates $\mathbf{R}$ and momentum $\mathbf{P}$ given by $\rho(\mathbf{P}_0, \mathbf{R}_0)$, this is done by evaluating

$$\tilde{P}_{f\leftarrow i}(t) = \frac{1}{(2\pi\hbar)^{G+F}} \int \mathbf{dP_0}\, \mathbf{dR_0}\, \mathbf{dn_0}\, \mathbf{dq_0}\, \rho\left(\mathbf{P_0}, \mathbf{R_0}\right) \cdot W_f(\mathbf{n}(t)) \cdot W_i(\mathbf{n}_0) \tag{5.20}$$

The phase space average of Eq. (5.20) is evaluated by Monte Carlo using $\rho(\mathbf{P}_0, \mathbf{R}_0) \cdot W_i(\mathbf{n_0})$ as the sampling function, integrating trajectories (nuclear and electronic DOFs) using the Hamiltonian of Eq. (5.15), and finally "projecting" the time-evolved ensemble onto the specified final state f by evaluating the window function $W_f(\mathbf{n}(t))$. Regarding the initial sampling of electronic actions, it is done according to Eq. (5.19): the action variable n_i corresponding to the initial electronic state i is sampled uniformly from the interval $[1-\gamma, 1+\gamma]$ and the other action variables $\{n_k, \forall\, k \neq i\}$ are sampled uniformly from the interval $[-\gamma, \gamma]$. As for the angle variables $\{q_k\}$, they are sampled uniformly over the interval $[0, 2\pi]$.[3]

It turns out that a transition probability $\tilde{P}_{f\leftarrow i}(t)$ computed with Eq. (5.20) is generally unnormalized over the array of F possible final electronic states. Thus, to complete the SQC procedure, a renormalized transition probability $P_{f\leftarrow i}(t)$ is given by

$$P_{f\leftarrow i}(t) = \frac{\tilde{P}_{f\leftarrow i}(t)}{\sum_{k=1}^{F} \tilde{P}_{k\leftarrow i}(t)}. \tag{5.21}$$

which is evaluated by calculating a $\tilde{P}_{f\leftarrow i}(t)$ via Eq. (5.20) for each combination of initial state i and possible final state f. This can be done efficiently with a single ensemble of trajectories sampled according to $\rho(\mathbf{P}_0, \mathbf{R}_0) \cdot W_i(\mathbf{n}_0)$ by simply accumulating the time-evolved electronic actions $\{n_k(t)\}$ into the various "bins" given by Eq. (5.19) at the final time t.

For example, for the most common case of $F = 2$ electronic states, the transition probability from initial state $i = 1$ to final state $f = 2$ is simply

$$P_{2\leftarrow 1}(t) = \frac{\tilde{P}_{2\leftarrow 1}(t)}{\tilde{P}_{2\leftarrow 1}(t) + \tilde{P}_{1\leftarrow 1}(t)} \tag{5.22}$$

[3]The integrand doesn't explicitly depend on $\mathbf{q}_0$ and so the angle variables are sample uniformly, however the electronic actions $\mathbf{n}(t)$ will generally depend on $\mathbf{q}_0$ through the Hamiltonian of Eq. (5.15) and Hamilton's equations, Eq. (5.3).

where $\tilde{P}_{2\leftarrow 1}(t)$ and $\tilde{P}_{1\leftarrow 1}(t)$ are evaluated according to Eq. (5.20) using the 2-state window functions of Eq. (5.18).

5.3 The Adiabatic Version of the Meyer-Miller Classical Electronic Hamiltonian

Although a diabatic representation of the multi-state electronic Hamiltonian is frequently used for the treatment of model non-adiabatic problems, for the study of real chemical systems, one would generally employ the potential energy surfaces (PESs) that come from "quantum chemistry" electronic structure calculations, and these PESs are typically expressed in the adiabatic representation—i.e., they are the Born-Oppenheimer (BO) PESs computed by diagonalizing the electronic Hamiltonian at each configuration of the nuclear coordinates. Thus, "real" applications of the SQC/MM approach would typically more easily be accomplished directly in the adiabatic representation, though in principle they should be equivalent.[4]

As developed in Section 5.1, in a diabatic representation, the electronic Hamiltonian is generally not diagonal, and the off-diagonal elements represent non-adiabatic couplings (possibly dependent on the nuclear coordinates) between what may be viewed as the diabatic PESs which are represented by the diagonal elements. Hence, for the case of 2 electronic states in the diabatic representation:

$$\hat{H}_{el}(\mathbf{R}) \xrightarrow{\text{diabatic rep.}} \begin{pmatrix} H_{11}(\mathbf{R}) & H_{12}(\mathbf{R}) \\ H_{21}(\mathbf{R}) & H_{22}(\mathbf{R}) \end{pmatrix};$$

whereas in the adiabatic representation, the electronic Hamiltonian is diagonal with eigenvalues representing the BO PESs:

$$\hat{H}_{el}(\mathbf{R}) \xrightarrow{\text{adiabatic rep.}} \begin{pmatrix} E_1(\mathbf{R}) & \emptyset \\ \emptyset & E_2(\mathbf{R}) \end{pmatrix}.$$

Thus, for two electronic states, the adiabatic version of the Meyer-Miller Hamiltonian [18] is expressed in terms of the Born-Oppenheimer PESs $E_1(\mathbf{R})$

[4]Though, they obviously *cannot* be equivalent if the transition probability being computed is between initial and final states which are not equivalent to each other in their respective representations—i.e., they are not transformations of one another.

and $E_2(\mathbf{R})$, and takes the form

$$H(\mathbf{P},\mathbf{R},\mathbf{p},\mathbf{x}) = \frac{|\mathbf{P}+\mathbf{\Delta P}|^2}{2\mu} + \bar{E}(\mathbf{R}) + \frac{1}{2}\left(\frac{1}{2}p_1^2 + \frac{1}{2}x_1^2 - \frac{1}{2}p_2^2 - \frac{1}{2}x_2^2\right)\cdot\Delta E(\mathbf{R}), \tag{5.23}$$

where , $\bar{E} = \frac{1}{2}(E_1+E_2)$, $\Delta E = E_1 - E_2$, and

$$\mathbf{\Delta P} = (p_1x_2 - p_2x_1)\cdot\left\langle\psi_2\middle|\frac{\partial\psi_1(\mathbf{R})}{\partial\mathbf{R}}\right\rangle. \tag{5.24}$$

From this expression, it is seen that while the electronic Hamiltonian provides no coupling between electronic states in the adiabatic representation, the electronic states *are* coupled through the addition of $\mathbf{\Delta P}$ to the vector of nuclear momenta $\mathbf{P}$ in the nuclear kinetic energy term, and $\mathbf{\Delta P}$ is a function of the non-adiabatic coupling $\left\langle\psi_2\middle|\frac{\partial\psi_1(\mathbf{R})}{\partial\mathbf{R}}\right\rangle$. The wavefunctions $\psi_1(\mathbf{R})$ and $\psi_2(\mathbf{R})$ are the adiabatic eigenvectors corresponding to the Born-Oppenheimer PESs, and these and their non-adiabatic coupling $\left\langle\psi_2\middle|\frac{\partial\psi_1(\mathbf{R})}{\partial\mathbf{R}}\right\rangle$, along with the adiabatic BO PESs, are typically obtained from an electronic structure calculation.

If instead, one begins with the non-adiabatic coupling of the diabatic electronic Hamiltonian matrix, $H_{12}(\mathbf{R}) = H_{21}(\mathbf{R})$, one can compute the non-adiabatic coupling from

$$\left\langle\psi_2\middle|\frac{\partial\psi_1(\mathbf{R})}{\partial\mathbf{R}}\right\rangle = \frac{\partial\omega(\mathbf{R})}{\partial\mathbf{R}} \tag{5.25}$$

where the so-called "mixing angle" $\omega(\mathbf{R})$ is given by

$$\omega(\mathbf{R}) = \frac{1}{2}\tan^{-1}\left(\frac{2H_{12}(\mathbf{R})}{H_{11}(\mathbf{R}) - H_{22}(\mathbf{R})}\right). \tag{5.26}$$

There are model problems treated in this work which, although written in a diabatic representation, have non-adiabatic couplings that do not vanish asymptotically. As as a result, only the electronic states of the adiabatic representation constitute physically meaningful initial and final states between which a transition probability can be sensibly defined. For these problems, the work presented here employed the adiabatic representation of Eq. (5.23).[5]

[5] An alternative approach would have been to (i) sample initial conditions in the adiabatic

5.4 Alternative Representations and an Interpretation of the γ-Parameter

5.4.1 The Miller-McCurdy Representation

Most of the calculations presented herein employed the Cartesian version of the Meyer-Miller Hamiltonian given in Eq. (5.15), or more specifically, for two states, Eq. (5.16). This particular classical representation of the electronic degrees of freedom (DOFs) is advantageous because (i) the equations of motion are simple, containing no singularities nor requiring the evaluation of square roots or transcendental functions, and (ii) because the general case of F electronic states is elegantly handled with no additional complexity beyond requiring additional pairs of action-angle variables.

However, for just $F = 2$ electronic states, the Cartesian representation of Eq. (5.16) does involve twice as many electronic DOFs as are really required. This can be seen by going back to the MM Hamiltonian written in terms of action-angle variables $(\mathbf{n}, \mathbf{q})$—i.e, Eq. (5.8)—which for two states is

$$\begin{aligned} H(\mathbf{P}, \mathbf{R}, n_1, n_2, q_1, q_2) = \frac{|\mathbf{P}|^2}{2\mu} \; + \; n_1 \, H_{11}(\mathbf{R}) \; + \; n_2 \, H_{22}(\mathbf{R}) \\ + \; 2\sqrt{(n_1+\gamma)(n_2+\gamma)} \, \cos(q_1 - q_2) \, H_{12}(\mathbf{R}). \end{aligned} \tag{5.27}$$

Due to conservation of probability, i.e., since $n_1 + n_2 = 1$, clearly one of the electronic action variables can be rewritten in terms of the other; and because the Hamiltonian only depends on the difference between the angles, $q_1 - q_2$ can also be replaced by a single angle variable.

The formal theory of canonical transformations can be used to show this systematically. Specifically, one seeks two new pairs of action-angle variables (N_1, Q_1) and (N_2, Q_2) which are functions of the old variables (n_1, q_1) and (n_2, q_2) and which maintain the symplectic form of the Hamiltonian Eq. (5.27) written in terms of the new variables. One of the new action variables is selected to remain unchanged,

$$N_1(n_1, n_2) = n_1 \tag{5.28a}$$

representation, (ii) make a canonical transformation to the diabatic representation, (iii) do the dynamics to time t using the diabatic Meyer-Miller Hamiltonian of Eq. (5.16), and (iv) at time t make the inverse canonical transformation back to the adiabatic representation to "bin" the trajectories via the SQC approach.

and the other is selected to be the sum of the probabilities,

$$N_2(n_1, n_2) = n_1 + n_2 \tag{5.28b}$$

(and then since $N_2 = 1$ this variable can be eliminated in the transformed Hamiltonian). The so-called F_3-type[6] generating function

$$F_3 \equiv F_3(n_1, n_2, Q_1, Q_2) \tag{5.29}$$

along with its associated relations[7]

$$N_i = -\frac{\partial F_3}{\partial Q_i} \tag{5.30a}$$

$$q_i = -\frac{\partial F_3}{\partial n_i} \tag{5.30b}$$

can then be used to find the correct new angle variables (Q_1, Q_2) which maintain the symplectic form of the transformed Hamiltonian. In particular, satisfaction of Eq. (5.30a) leads to the immediate identification of the proper F_3 generating function as

$$F_3(n_1, n_2, Q_1, Q_2) = -N_1(n_1, n_2) \cdot Q_1 - N_2(n_1, n_2) \cdot Q_2, \tag{5.31}$$

which can be used with the other F_3-relation, Eq. (5.30b), and the transformation equations for the new actions $\{N_i\}$, Eq. (5.28), to give

$$q_1 = \frac{\partial N_1}{\partial n_1} \cdot Q_1 + \frac{\partial N_2}{\partial n_1} \cdot Q_2 = Q_1 + Q_2 \tag{5.32a}$$

$$q_2 = \frac{\partial N_1}{\partial n_2} \cdot Q_1 + \frac{\partial N_2}{\partial n_2} \cdot Q_2 = Q_2 \tag{5.32b}$$

whose inversion gives the new angle variables $\{Q_i\}$ in terms of the originals:

$$Q_1 = q_1 - q_2, \qquad Q_2 = q_2. \tag{5.33}$$

Likewise, inverting Eq. (5.28) gives

$$n_1 = N_1, \qquad n_2 = N_2 - N_1, \tag{5.34}$$

[6]See Goldstein [29], p. 384, Eq. (9-18).
[7]See Goldstein [29], p. 384, Eq. (9-20a).

and substituting into the Hamiltonian Eq. (5.27) gives

$$H(\mathbf{P},\mathbf{R},N_1,N_2,Q_1,Q_2) = \frac{|\mathbf{P}|^2}{2\mu} \;+\; N_1\, H_{11}(\mathbf{R}) \;+\; (N_2-N_1)\, H_{22}(\mathbf{R}) \\ +\; 2\sqrt{(N_1+\gamma)(N_2-N_1+\gamma)}\,\cos(Q_1)\, H_{12}(\mathbf{R}). \tag{5.35}$$

As expected, the transformed Hamiltonian is independent of Q_2, and hence $\dot{N}_2 = -\frac{\partial H}{\partial Q_2} = 0$ and N_2 can be set to its quantum value of 1. Doing this, and defining $q \equiv Q_1$ and $n \equiv N_1$ then gives

$$H(\mathbf{P},\mathbf{R},n,q) = \frac{|\mathbf{P}|^2}{2\mu} \;+\; n\, H_{11}(\mathbf{R}) \;+\; (1-n)\, H_{22}(\mathbf{R}) \\ +\; 2\sqrt{(n+\gamma)(1-n+\gamma)}\,\cos(q)\, H_{12}(\mathbf{R}), \tag{5.36}$$

which, other than the presence of γ, is the expression given by Miller and McCurdy [21].

The Miller-McCurdy (MMc) Hamiltonian of Eq. (5.36) was used in the SQC approach to treat several of the 2-state examples below along with the Cartesian MM version. It was seen to give comparable results in these cases, though more difficult to apply because care must be taken to handle the singularities in the equations of motion.

Strictly speaking, when used in the SQC approach, the MMc Hamiltonian of Eq. (5.36) does not yield exactly the same results as the Cartesian MM Hamiltonian of Eq. (5.16) because though the sum of the probabilities, $n_1 + n_2$, is dynamically conserved by both Hamiltonians, its conserved value is determined by how one sets the initial conditions, and in the SQC approach, due to the symmetric windowing functions having finite width 2γ, initialization of n_1 and n_2 does not force their sum to unity. In contrast, it is implicit in the construction of the MMc Hamiltonian in terms of a single action variable n that the probabilities sum to unity. Nevertheless, the results were seen to be basically equivalent.

As far as efficiency is concerned, any gains from integrating one pair of action-angle variables (n, q) versus two pairs of Cartesian coordinates and conjugate momenta (p_1, x_1, p_2, x_2) are likely offset by the square roots, singularities, and transcendental function evaluations appearing in the equations of motion for n and q. Likewise, although one might expect improved convergence of the Monte Carlo integration using the MMc Hamiltonian due to the reduced dimensionality of the phase space, in practice, both methods converge without difficulty for the systems treated in this work.

5.4.2 A 2-State Spin-Representation

Another version of the MMc representation that is basically equivalent to that given in Eq. (5.36) is a re-writing in terms of the action-angle variables for a classical angular momentum of a spin-$\frac{1}{2}$ system. To see this, one may again begin with the MM Hamiltonian for 2 electronic states written in terms of action-angle variables, Eq. (5.27), but in this case re-express it in terms of sum and difference potential functions

$$\bar{H}(\mathbf{R}) = \frac{1}{2}\left(H_{11}(\mathbf{R}) + H_{22}(\mathbf{R})\right) \tag{5.37a}$$

$$\Delta H(\mathbf{R}) = H_{11}(\mathbf{R}) - H_{22}(\mathbf{R}) \tag{5.37b}$$

which gives

$$\begin{aligned} H(\mathbf{P},\mathbf{R},n_1,n_2,q_1,q_2) = \frac{|\mathbf{P}|^2}{2\mu} \;+\; (n_1+n_2)\;\bar{H}(\mathbf{R}) \;+\; \frac{1}{2}(n_1-n_2)\;\Delta H(\mathbf{R}) \\ +\; 2\sqrt{(n_1+\gamma)(n_2+\gamma)}\;\cos(q_1-q_2)\;H_{12}(\mathbf{R}). \end{aligned} \tag{5.38}$$

Here—in order to reduce the Hamiltonian to depend on one action variable, and again recognizing that the sum of the probabilities, n_1+n_2, is conserved—one seeks a canonical transformation to the new action variables

$$N(n_1,n_2) = n_1 + n_2, \tag{5.39a}$$

$$m(n_1,n_2) = \frac{1}{2}(n_1 - n_2), \tag{5.39b}$$

or inversely

$$n_1 = \frac{1}{2}N + m \tag{5.40a}$$

$$n_2 = \frac{1}{2}N - m. \tag{5.40b}$$

To find the appropriate angle variables (Q,q), one can again resort to the appropriate F_3-type generating function, satisfying Eq. (5.30a),

$$F_3(n_1,n_2,Q,q) = -N(n_1,n_2)\cdot Q - m(n_1,n_2)\cdot q, \tag{5.41}$$

for use in Eq. (5.30b), which yields

$$q_1 = Q + \frac{1}{2}q \tag{5.42a}$$

$$q_2 = Q - \frac{1}{2}q, \tag{5.42b}$$

or inversely

$$Q = \frac{1}{2}(q_1 + q_2) \tag{5.43a}$$

$$q = q_1 - q_2. \tag{5.43b}$$

In terms of (N, Q) and (m, q), the Hamiltonian of Eq. (5.38) is then

$$\begin{aligned} H(\mathbf{P}, \mathbf{R}, N, m, q) &= \frac{|\mathbf{P}|^2}{2\mu} + \bar{H}(\mathbf{R}) \ + \ m \cdot \Delta H(\mathbf{R}) \\ &\qquad + \ 2\sqrt{\left(\frac{N}{2} + m + \gamma\right)\left(\frac{N}{2} - m + \gamma\right)}\,\cos(q) \cdot H_{12}(\mathbf{R}) \\ &= \frac{|\mathbf{P}|^2}{2\mu} + \bar{H}(\mathbf{R}) \ + \ m \cdot \Delta H(\mathbf{R}) \\ &\qquad + \ 2\sqrt{\left(\frac{N}{2} + \gamma\right)^2 - m^2}\,\cos(q) \cdot H_{12}(\mathbf{R}). \end{aligned} \tag{5.44}$$

Since the quantum values of the original action variables are given by

$$(n_1, n_2) = \begin{cases} (1, 0) & \text{State 1} \\ (0, 1) & \text{State 2} \end{cases} \tag{5.45}$$

the corresponding quantum values of (N, m) from Eqs. (5.39a) and (5.39b) are given by

$$(N, m) = \begin{cases} (1, +\frac{1}{2}) & \text{State 1} \\ (1, -\frac{1}{2}) & \text{State 2} \end{cases} \tag{5.46}$$

which suggests that Eq. (5.44) is the Hamiltonian for a spin-$\frac{1}{2}$ system in spin action-angle variables (m, q) where m is the classical analogue of the spin-projection quantum number (and q its conjugate angle), and that $\left(\frac{N}{2} + \gamma\right)^2$

may be identified as S^2, the square of the total spin angular momentum:

$$H(\mathbf{P},\mathbf{R},S,m,q) = \frac{|\mathbf{P}|^2}{2\mu} + \bar{H}(\mathbf{R}) \; + \; m\cdot\Delta H(\mathbf{R}) \\ + \; 2\sqrt{S^2-m^2}\,\cos(q)\cdot H_{12}(\mathbf{R}). \tag{5.47}$$

Of course, if one sets $N = 1$, Eq. (5.44) is algebraically equivalent to the MMc Hamiltonian of Eq. (5.36) with the identification that $m = n - \frac{1}{2}$.

An alternative (and distinctly different) derivation of the spin-$\frac{1}{2}$ Hamiltonian of Eq. (5.47) was given in a later paper by Meyer and Miller [19]. In this latter work, first it was appreciated that any Hermitian quantum operator $\hat{A}$ in a 2-state basis may be written as some linear combination of the 3 Pauli spin operators (or matrices) $\hat{\sigma}_x$, $\hat{\sigma}_y$, $\hat{\sigma}_z$ along with the identify operator (matrix) $\hat{I}$, i.e.

$$\hat{A} = a_0\hat{I} + a_x\hat{\sigma}_x + a_y\hat{\sigma}_y + a_z\hat{,}\sigma_z, \tag{5.48}$$

because, collectively, the 3 Pauli matrices plus the identity are linearly independent and thus span the space of all possible Hermitian[8] quantum operators in 2 dimensions. On this basis, $\hat{A}$ may be taken in Eq. (5.48) to be a 2-state diabatic electronic Hamiltonian

$$\hat{H}_{el} \rightarrow \begin{bmatrix} H_{11} & H_{21} \\ H_{12} & H_{22} \end{bmatrix} \tag{5.49}$$

and, after inserting the Pauli spin matrices

$$\hat{\sigma}_x \rightarrow \frac{1}{2}\begin{bmatrix} 0 & 1 \\ 1 & 0 \end{bmatrix} \qquad \hat{\sigma}_y \rightarrow \frac{1}{2}\begin{bmatrix} 0 & i \\ -i & 0 \end{bmatrix} \qquad \hat{\sigma}_z \rightarrow \frac{1}{2}\begin{bmatrix} -1 & 0 \\ 0 & 1 \end{bmatrix} \tag{5.50}$$

(and the identify $\hat{I}$), the expression in Eq. (5.48) may be inverted to give the a-coefficients (a_0, a_x, a_y, a_z) in terms of the matrix elements $\{H_{k,k'}\}$, thus providing an expansion of an arbitrary 2-state electron Hamiltonian $\hat{H}_{el}$ in terms of spin-$\frac{1}{2}$ operators. Doing this for an arbitrary real-symmetric 2-state diabatic electronic Hamiltonian (parametrically dependent on nuclear coordinates $\mathbf{R}$) results in

$$\hat{H}_{el}(\mathbf{R}) = \bar{H}(\mathbf{R})\cdot\hat{I} + \Delta H(\mathbf{R})\cdot\hat{\sigma}_z + 2H_{-\frac{1}{2},\frac{1}{2}}(\mathbf{R})\cdot\hat{\sigma}_x, \tag{5.51}$$

[8]The "Hermitian"-qualfier is applied because an arbitrary 2×2 complex matrix has 8 independent elements and so would not be generally representable as a linear combination of only 4 2×2 matrices.

where the electronic states "1" and "2" have been relabeled "$-\frac{1}{2}$" and "$\frac{1}{2}$" (to correspond to the values of the projection spin quantum number $m = \pm\frac{1}{2}$); $H_{12} \rightarrow H_{-\frac{1}{2},\frac{1}{2}}$ and similarly for the matrix elements defining $\bar{H}$ and ΔH. It is interesting to note that if the parameters $\mathbf{R}$ representing the nuclear coordinates were replaced by their position-space quantum operators $\hat{\mathbf{R}}$, then this—with the addition of the nuclear kinetic energy operator—is an *exact* representation of the full coupled nuclear-electronic Hamiltonian quantum operator for this 2-state system. In other words, no approximation has been made by re-expressing the electronic Hamiltonian operator in terms of the Cartesian spin-operators.

Where the classical approximation does come into play is with the replacement of the quantum Cartesian spin-operators by their classical analogues. The Cartesian components of a classical angular momentum vector in free-space may be written in terms of action-angle variables (m, q) as

$$\begin{bmatrix} S_x \\ S_y \\ S_z \end{bmatrix} = \begin{bmatrix} \sqrt{S^2 - m^2}\ \cos(q) \\ \sqrt{S^2 - m^2}\ \sin(q) \\ m \end{bmatrix}. \tag{5.52}$$

Replacing $\hat{\sigma}_x$, $\hat{\sigma}_y$, $\hat{\sigma}_z$ in Eq. (5.51) with S_x, S_y, S_z written in terms of (m, q) (and dropping the identity $\hat{I}$) then—with the addition of the nuclear kinetic energy term $\frac{|\mathbf{P}|^2}{2\mu}$—yields the same expression given in Eq. (5.47) above. This spin-operator analysis is extended to 3 electronic states below as presented in the same work by Meyer and Miller [19].

5.4.3 An Interpreation of γ

As noted in Ref. [2], interpreting the rewritten Miller-McCurdy (MMc) 2-state Hamiltonian of Eq. (5.47) as being that of a spin-$\frac{1}{2}$ system, suggests a potentially preferred choice for the γ-parameter. If

$$S^2 \equiv \left(\frac{N}{2} + \gamma\right)^2 = \left(\frac{1}{2} + \gamma\right)^2$$

is identified as the square of the total spin angular momentum for a spin-$\frac{1}{2}$ system, then possible choices for S^2 and that of $\gamma = \sqrt{S^2} - \frac{1}{2}$ are:

$$S^2_{\text{Classical}} = s^2 = \left(\frac{1}{2}\right)^2 = \frac{1}{4} \qquad \Longrightarrow \quad \gamma = 0, \tag{5.53a}$$

i.e., the classical value for a spin-s system, and that implicitly used originally by Miller and McCurdy [21]; and

$$S^2_{\text{Langer}} = \left(s + \frac{1}{2}\right)^2 = \left(\frac{1}{2} + \frac{1}{2}\right)^2 = 1 \quad \Longrightarrow \quad \gamma = \frac{1}{2}, \tag{5.53b}$$

i.e., the classical value with the Langer-correction of $\frac{1}{2}$ which was chosen by Meyer and Miller [18];

$$S^2_{\text{Quantum}} = s(s+1) = \frac{1}{2}\left(\frac{1}{2} + 1\right) = \frac{3}{4} \quad \Longrightarrow \quad \gamma = \frac{\sqrt{3}-1}{2} \approx 0.366, \tag{5.53c}$$

i.e., the quantum value.

As it turns out, the quantum value of $\gamma = 0.366$ was seen to be an effective choice for every example described herein involving the treatment of 2 electronic states; and moreover, for the particular 2-state examples where other values of γ were explicitly tested, 0.366 was determined to be the optimal choice over the tested range of γ values. Thus, no problem-specific tuning of the γ-parameter was used to generate the results reported in this work.[9]

5.4.4 Direct Utilization of the the Spin-Vector Representation for the Electronic DOF

As indicated, a problem with the MMc Hamiltonian, written either as Eq. (5.36) or Eq. (5.47), is that singularities, square roots, and transcendental function evaluations occur in the equations of motion. However, each of these problems may be eliminated by working directly in terms of the Cartesian spin-vector representation of the electronic DOF—i.e., by integrating the equations of motion in terms of S_x, S_y, and S_z as given by Eq. (5.52) instead of m and q.

To see this, it is noted that if a Hamiltonian which depends on S, m, and q (e.g., Eq. (5.47)) may be re-written so that it's dependence on S, m, and q is solely through the Cartesian components of the spin-vector given by

[9]The exemption being that for 3 electronic states, a similar justification (see Section 5.4.5) can be made for choosing $\gamma = 0.414$, which was thus used for each of the 3-state examples treated herein.

Eq. (5.52), i.e. if

$$\begin{aligned} H(m,q) &\equiv G(\sqrt{S^2-m^2}\ \cos(q), \sqrt{S^2-m^2}\ \sin(q), m) \\ &= G(S_x, S_y, S_z), \end{aligned} \tag{5.54}$$

then the time-evolution of $m(t)$ and $q(t)$ according to Hamilton's equations

$$\dot{m} = -\frac{\partial H(m,q)}{\partial q} \tag{5.55a}$$

$$\dot{q} = \frac{\partial H(m,q)}{\partial m} \tag{5.55b}$$

is equivalent to the time-evolution of the Cartesian spin-components according to

$$\dot{\vec{S}}(t) = \frac{\partial G(\vec{S}(t))}{\partial \vec{S}} \times \vec{S}(t). \tag{5.56}$$

The Hamiltonian of Eq. (5.47) in terms of the Cartesian spin components is

$$\begin{aligned} H(\mathbf{P},\mathbf{R},S_x,S_y,S_z) = \frac{|\mathbf{P}|^2}{2\mu} + \bar{H}(\mathbf{R}) \ + \ S_z \cdot \Delta H(\mathbf{R}) \\ + \ 2\, S_x \cdot H_{-\frac{1}{2},\frac{1}{2}}(\mathbf{R}), \end{aligned} \tag{5.57}$$

and, from Eq. (5.56), the corresponding equations of motion for $\dot{\vec{S}}(t)$ are

$$\dot{S}_x(t) = -\Delta H(t)\, S_y(t) \tag{5.58a}$$

$$\dot{S}_y(t) = -2H_{-\frac{1}{2},\frac{1}{2}}(t)\, S_z(t) + \Delta H(t)\, S_x(t) \tag{5.58b}$$

$$\dot{S}_z(t) = 2H_{-\frac{1}{2},\frac{1}{2}}(t)\, S_y(t) \tag{5.58c}$$

which are integrated simultaneously with the equations of motion for the nuclear DOF generated from Hamilton's equations and Eq. (5.57):

$$\dot{R}_i(t) = \ \frac{\partial H}{\partial P_i} = \frac{P_i}{\mu} \tag{5.59a}$$

$$\dot{P}_i(t) = -\frac{\partial H}{\partial R_i} = -\frac{\partial \bar{H}}{\partial R_i} \ - \ S_z \cdot \frac{\partial \Delta H}{\partial R_i} \ - \ 2\, S_x \cdot \frac{\partial H_{-\frac{1}{2},\frac{1}{2}}}{\partial R_i}; \tag{5.59b}$$

which, as usual, gives the nuclear DOFs moving on an effective electronic PES

which is a weighted-average of the two diabatic PESs, but here the weighting is specified by the electronic spin-components as they evolve according to Eq. (5.58). From Eqs. (5.58) and (5.59) it is seen that the equations of motion in the spin-vector representation are linear in the spin components, and free of singularities, square roots, and transcendental functions. In other words, for the case of $F = 2$ electronic states, integration in terms of the spin vector $\vec{S}$ provides all the advantages of the Cartesian representation.

The spin-vector representation is implemented within the SQC approach in much the same way as the action-angle and Cartesian representations presented above. The SQC phase space average over initial conditions is still evaluated according to Eq. (5.20) and the results renormalized according to Eq. (5.22), except that the 2 action variables (n_1, n_2) sampled and "binned" in the Cartesian representation are replaced by the single action variable $m = S_z$, and likewise, the joint 2-dimensional histogram window functions of Eqs. (5.18a) and (5.18b) are replaced by single-variable histogram window functions analogous to Eq. (5.17) corresponding to the two possible spin states:

$$W_{-\frac{1}{2}}(m) = \frac{1}{2\gamma} h\left(\gamma - \left|m + \tfrac{1}{2}\right|\right) \tag{5.60a}$$

$$W_{\frac{1}{2}}(m) = \frac{1}{2\gamma} h\left(\gamma - \left|m - \tfrac{1}{2}\right|\right). \tag{5.60b}$$

Thus, if the initial electronic state is assigned to the quantum value of $m = -\frac{1}{2}$, Eq. (5.20) is evaluated via Monte Carlo by uniformly sampling the initial actions m and conjugate angles q from the intervals $[-\frac{1}{2} - \gamma, -\frac{1}{2} + \gamma]$ and $[0, 2\pi]$, respectively, computing initial values for S_x, S_y, and S_z from Eq. (5.52), propagating the spin-components and nuclear DOFs to the final time by integrating Eqs. (5.58) and (5.59), and finally "projecting" onto the final spin states $-\frac{1}{2}$ and $\frac{1}{2}$ using the the value of $m = S_z$ for each trajectory with the window functions of Eq. (5.60). This approach was verified numerically for several examples below and, as expected, found to be essentially equivalent to the MMc approach done in terms of action-angle variables, and also quite similar to the Cartesian MM approach—though not exactly the same for the same reasons (stated in Section 5.4.1) that the MMc approach is not exactly equivalent to the Cartesian MM approach.

5.4.5 A 3-State Spin-Representation

For a 2-state electronic system, the MM and MMc Hamiltonians are analytically very similar and, in practice, have been verified to generate very similar results—the primary difference being, as noted earlier, whether each trajectory is initialized exactly on the $n_1 + n_2 = 1$ polyad (as is implicit in the MMc Hamiltonian), or whether there is some variation about the $n_1 + n_2 = 1$ polyad (as in the Cartesian SQC/MM approach). However, a 3-state version of the MMc Hamiltonian may also be constructed in terms of the Cartesian components of the spin vector $\vec{S}$, and this model *is* analytically quite different from the 3-state model given by the Cartesian MM Hamiltonian.

To construct the 3-state model, Meyer and Miller [19] analogized a system of 3 electronic states to the spin states of a spin-1 quantum system ($m \in \{-1, 0, 1\}$), and proceeded—in the spirit of the expansion given above for a spin-$\frac{1}{2}$ operator in terms of the Pauli matrices (Eq. (5.48))—to write an arbitrary quantum operator $\hat{A}$ expressed in a 3-state basis in terms of the spin-1 quantum operators $\hat{S}_x$, $\hat{S}_y$, and $\hat{S}_z$. However, the linear expansion in the spin operators (and the identify) given in Eq. (5.48) doesn't work for more than 2 states because, e.g., a complex 3×3 Hermitian matrix has 9 independent elements[10] and so 4 operators (including the identity $\hat{I}$) cannot span the full space of possible Hermitian operators in 3 dimensions. Recognizing this, Meyer and Miller sought an expansion of an arbitrary[11] Hermitian operator in terms of *products* of the quantum spin-operators, with the realization that once this was done, each quantum spin operator could still be replaced by its classical analogue—the appropriate Cartesian component of the classical spin-vector in terms of action-angle variables (S, m, q) as given in Eq. (5.52).

For the 3-state case, only quadratic terms in the spin-operators are needed to achieve this, and as shown in Ref. [19] in similar fashion to Eq. (5.48) for the 2-state case, an arbitrary 3-state symmetric diabatic electronic Hamiltonian operator may be expanded in terms of its matrix elements and the quantum

[10] That is, 3 real diagonal elements and 3 complex lower off-diagonal elements.

[11] Ref. [19] did this for an arbitrary Hermitian operator in a basis of F-states, but here just the 3-state case is considered.

spin-1 operators as

$$\begin{aligned}\hat{H}_{el}(\hat{S}_x,\hat{S}_y,\hat{S}_z) = H_{0,0} &+ \frac{1}{2}\left(H_{1,1}-H_{-1,-1}\right)\cdot\hat{S}_z \\ &+ \frac{1}{\sqrt{2}}\left(H_{0,1}+H_{-1,0}\right)\cdot\hat{S}_x + \sqrt{2}\left(H_{0,1}-H_{-1,0}\right)\cdot\hat{S}_x\,\hat{S}_z \\ &+ H_{-1,1}\left(\hat{S}_x^2-\hat{S}_y^2\right) + \left(\frac{H_{1,1}+H_{-1,-1}}{2}-H_{0,0}\right)\cdot\hat{S}_z^2.\end{aligned} \tag{5.61}$$

Once again, it is interesting to note that this representation of $\hat{H}_{el}$ in terms of the spin-operators $\hat{S}_x$, $\hat{S}_y$, and $\hat{S}_z$ is exact.

To obtain the classical analogue model, one replaces the the $\hat{S}_x$, $\hat{S}_y$, and $\hat{S}_z$ spin operators with the classical S_x, S_y, and S_z spin components, and then applies Eq. (5.56) to obtain the equations of motion for the spin components:

$$\dot{S}_x = \frac{\partial H}{\partial S_y}\cdot S_z - \frac{\partial H}{\partial S_z}\cdot S_y \tag{5.62a}$$

$$\dot{S}_y = \frac{\partial H}{\partial S_z}\cdot S_x - \frac{\partial H}{\partial S_x}\cdot S_z \tag{5.62b}$$

$$\dot{S}_z = \frac{\partial H}{\partial S_x}\cdot S_y - \frac{\partial H}{\partial S_y}\cdot S_x, \tag{5.62c}$$

where

$$\frac{\partial H}{\partial S_x} = \frac{1}{\sqrt{2}}(H_{0,1}+H_{-1,0}) + \sqrt{2}(H_{0,1}-H_{-1,0})\cdot S_z + 2H_{-1,1}\cdot S_x \tag{5.62d}$$

$$\frac{\partial H}{\partial S_y} = -2H_{-1,1}\cdot S_y \tag{5.62e}$$

$$\begin{aligned}\frac{\partial H}{\partial S_z} = \frac{1}{2}(H_{1,1}-H_{-1,-1}) &+ \sqrt{2}(H_{0,1}-H_{-1,0})\cdot S_x \\ &+ (H_{1,1}+H_{-1,-1}-2H_{0,0})\cdot S_z.\end{aligned} \tag{5.62f}$$

What is most interesting about the spin vector approach is that a single spin DOF is used to represent the occupations of an arbitrary number of electronic states. In other words, for F electronic states, what was represented in the Cartesian MM model as F harmonic oscillators with 1 quantum of excitation shared between them, is represented in the MM spin model as a single spin-$\frac{F-1}{2}$ DOF which evolves between the integer or half-integer spin states ranging from

$-\frac{F-1}{2} \cdots \frac{F-1}{2}$. For the case of 2 electronic states, these two different views are essentially equivalent due to the fact that conservation of probability can be used to eliminate one DOF from the MM model yielding the MMc model or the MM spin model (the latter two being equivalent with the identification of $n = m + \frac{1}{2}$). However, because conservation of probability can only be used to eliminate 1 DOF, this restraint cannot recreate the 1 DOF spin-model from the MM Hamiltonian for $F = 3$ or more electronic states. Thus, for the case of 3 (or more) electronic states, due to the Cartesian MM model and MM spin model employing different numbers of DOFs, they are not necessarily expected to give equivalent results.

However, there is an elegance and simplicity to the mapping of an arbitrary number of electronic states to a single spin DOF (with the different electronic states represented by the single spin-DOF being within γ of the quantum spin values). Thus, the results in Section 9.3 begin to investigate whether such a simple model, for the case of 3 electronic DOFs, provides the same level of accuracy seen with the Cartesian SQC/MM approach. In this regard, rigorous quantum path integral calculations for several 3-state non-adiabatic spin-boson systems are provided in Refs. [30] and [31], and these serve as good benchmarks for evaluating the 3-state spin-vector model.

Chapter 6

Applications to Simple Scattering Problems

Application of the SQC approach to the treatment of non-adiabatic dynamics was first developed in the context of several simple scattering problems involving 1 nuclear DOF and 2 electronic states/DOFs. For each of these problems, the nuclear DOF begins in the asymptotic region of one of the potential energy surfaces (PESs), enters a region of non-adiabatic coupling, and then emerges—either through reflection or transmission—on the same or the other PES with some branching probability.

The benchmark problems chosen were the three well-studied non-adiabatic models originally used by Tully [16] to test his "fewest switches" surface hopping (FSSH) approach—specifically single and dual avoided crossings models and a model of extended non-adiabatic coupling. For both the avoided crossing problems, and to a certain extent the extended coupling problem, the SQC/MM approach is seen to give good quantitative agreement with the quantum results. In addition, these benchmark problems provided a proving ground for making valuable adjustments to the initial SQC model which have been utilized throughout all subsequent work.

6.1 The Tully Models

Each of the Tully models were written in terms of a real-symmetric diabatic electronic Hamiltonian matrix:

$$\hat{H}_{el}(R) \xrightarrow[\text{rep.}]{\text{diabatic}} \begin{bmatrix} H_{11}(R) & H_{12}(R) \\ H_{12}(R) & H_{22}(R) \end{bmatrix}. \tag{6.1}$$

The diagonal elements of this matrix may be referred to as the "diabatic" PESs representing the different electronic "states," while the off-diagonal elements are the non-adiabatic couplings which, for these models, generally depend on the nuclear coordinate R. Diagonalization of this matrix for each nuclear configuration (R) yields the adiabatic PESs, $E_1(R)$ and $E_2(R)$. The diabatic and adiabatic PESs (but not the couplings) are plotted in Fig. 6.1 for each of the 3 models detailed below. For all three test problems, the mass associated with nuclear coordinate R was taken to be 2000 (in atomic units) as was done in Tully's original paper.

6.1.1 Avoided Crossing

The one-dimensional single avoided crossing of two PESs is the most elementary (and common) non-adiabatic scenario, and the test problem used by Tully is given by:

$$\begin{aligned} H_{11}(R) &= \begin{cases} A(1-e^{-BR}) & R \geq 0 \\ -A(1-e^{BR}) & R < 0 \end{cases} \\ H_{22}(R) &= -H_{11}(R) \\ H_{12}(R) &= Ce^{-DR^2} \end{aligned} \tag{6.2}$$

where $A = 0.01$, $B = 1.6$, $C = 0.005$, and $D = 1$ (all expressed in atomic units). Again, the off-diagonal element $H_{12}(R)$ represents nuclear coordinate-dependent couplings between the diabatic PESs of the two electronic states, $H_{11}(R)$ and $H_{22}(R)$. See Fig. 6.1a.

6.1.2 Dual Avoided Crossing

The dual avoided crossing model used by Tully presents a somewhat more complicated problem, exhibiting what are often referred to as Stückelberg oscillations in the transmission probability curves. The model is given by

$$\begin{aligned} H_{11}(R) &= 0 \\ H_{22}(R) &= -Ae^{-Bx^2} + E_0 \\ H_{12}(R) &= Ce^{-DR^2} \end{aligned} \tag{6.3}$$

where $A = 0.1$, $B = 0.28$, $C = 0.015$, $D = 0.06$, and $E_0 = 0.05$. See Fig. 6.1b.

6.1.3 Model of Extended Coupling

The last of Tully's three test problems is a model of extended coupling given by:

$$\begin{aligned} H_{11}(R) &= -A \\ H_{22}(R) &= \quad A \\ H_{12}(R) &= \begin{cases} Be^{CR}) & R < 0 \\ B(2 - e^{-CR}) & R \geq 0 \end{cases} \end{aligned} \tag{6.4}$$

where $A = 6 \times 10^{-4}$, $B = 0.1$, and $C = 0.9$. See Fig. 6.1c. Note that this extended coupling model does not present a non-adiabatic curve-crossing problem in the same sense as the first two problems.

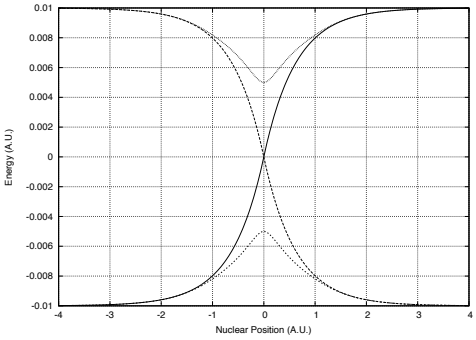

(a) Single avoided crossing

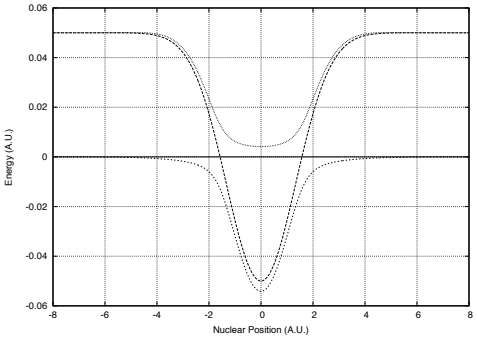

(b) Dual avoided crossing

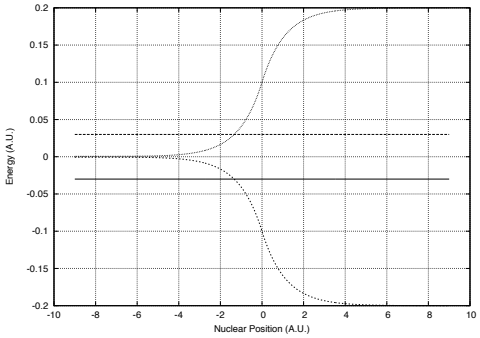

(c) Extended coupling; flat lines are $50 \times H_{11}(R)$ and $50 \times H_{22}(R)$

Figure 6.1: Diabatic and adiabatic potential energy surfaces for the 3 Tully models

6.2 Initial Results for the Single Avoided Crossing

When the SQC approach was first applied to the treatment of non-adiabatic dynamics, it was initially assumed that the γ-parameter in the MM Hamiltonian of Eq. (5.16) had the value of $\frac{1}{2}$, since that was the value used in Meyer and Miller's original work [18] and also in more recent work applying various semiclassical approximations to Eq. (5.16). In other words, originally, the so-called γ-parameter was not a parameter of the model at all, and the selection of a width for the symmetric window functions used in the SQC approach was not thought to relate to it. Accordingly, the first non-adiabatic calculations—which applied the SQC approach to the single and dual avoided crossing models—assumed a value of $\gamma = \frac{1}{2}$ in Eq. (5.16) and proceeded to vary the width parameter Δn of the symmetric window functions without any corresponding modification to the γ-parameter.[1]

The results of this γ-less approach are shown in Fig. 6.2. Specifically, Fig. 6.2a shows the SQC-calculated probabilities of transmission onto the lower surface, $T_{2\leftarrow 1}$, as a function of initial nuclear momentum, calculated using window functions of different widths $\Delta n = \{1.0, 0.7, 0.5\}$, along with the exact quantum result;[2] likewise Fig. 6.2b shows corresponding results for transmission onto the upper surface, $T_{1\leftarrow 1}$.[3]

For transmission onto either surface, the $\Delta n = 1$ result shows reasonable agreement with the quantum result, at least qualitatively, throughout the calculated momenta range. However, with regards to the SQC results calculated using $\Delta n < 1$: the $\Delta n = 0.5$ result exhibits improved quantitative agreement with the quantum result for low values of initial momenta, i.e., in the threshold energy region, but unfortunately exhibits an unphysical oscillation or dip in the transmission probabilities beyond the threshold region, becoming most severe when the initial nuclear momentum is about 15 A.U. The same is true

[1] Once again, although the γ-parameter does not appear in the Hamiltonian of Eq. (5.16) used for these calcuations, it still has an effect through the action-angle to Cartesian transformation of Eq. (5.10)

[2] QM resuts were obtained via two-surface wave-packet propagation using the FFT method of representing the kinetic energy operator in momentum-space—a generalization of the standard single-surface approach of Ref. [32].

[3] For the single avoided crossing model, although the nuclear DOF begins on the lower surface, the transmission probability $T_{2\leftarrow 1}$ (switching from state 1 to state 2) corresponds to the nuclear DOF emerging on the lower surface because the PESs cross and reverse energies in the diabatic representation. Likewise, $T_{1\leftarrow 1}$ (remaining in state 1) corresponds to the nuclear DOF emerging on the upper surface.

for the $\Delta n = 0.7$ curve, albeit to a lesser extent.

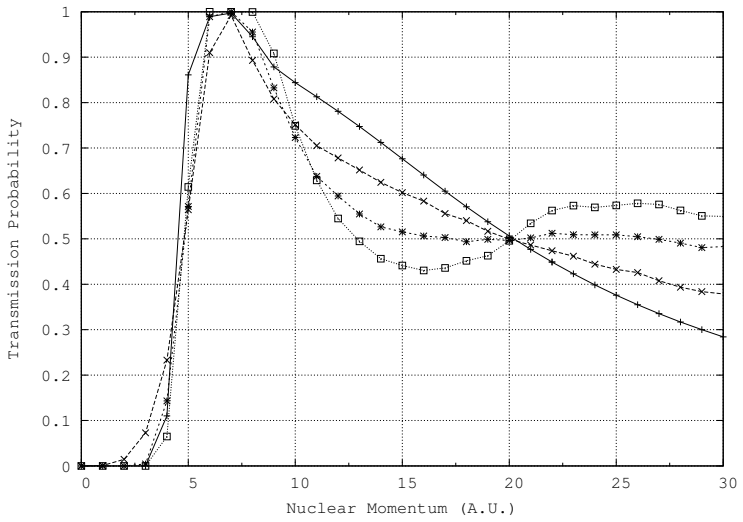

(a) Transmission to the lower surface, $T_{2\leftarrow 1}$

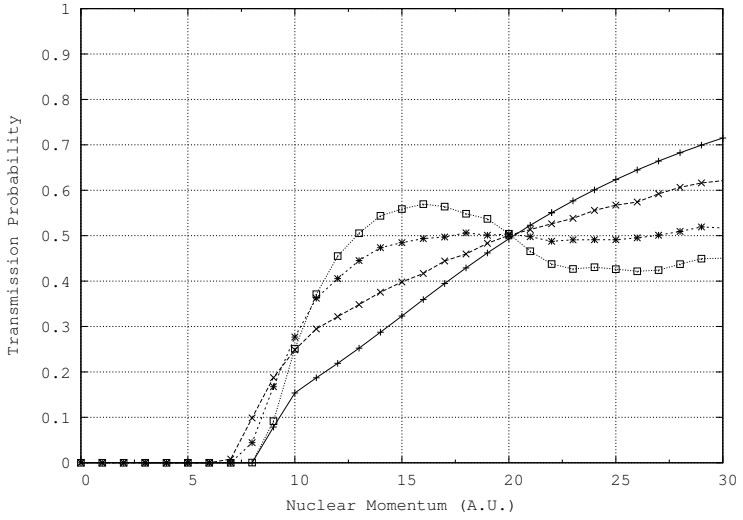

(b) Transmission to the upper surface, $T_{1\leftarrow 1}$

Figure 6.2: Transmission probabilities for the single avoided crossing calculated via the SQC approach without a γ-parameter: exact QM result (+); SQC with $\Delta n = 1$ ($\times$), $\Delta n = 0.7$ ($*$), and $\Delta n = 0.5$ ($\Box$)

6.3 Analyzing Zero-Point Energy (ZPE) Leakage

To understand what appeared to be a serious defect in the model, the oscillations in the transition probability curves were investigated, and it was discovered that these effects are just a consequence of the fact that a classical trajectory model will not generally maintain each electronic oscillator with an amount of energy at least equal to its quantum zero-point energy (ZPE). In this particular scattering example, an initial nuclear kinetic energy of around 15 A.U. is seen to cause a significant number of trajectories to end up with too much electronic "action" localized in one oscillator at the expense of the other. As a result, if the action window functions are contracted such that $\Delta n < 1$, these trajectories tend to be excluded—despite their final actions (n_1, n_2) not representing a configuration intermediate between electronic states 1 and 2.

To illustrate this in detail, Fig. 6.3 presents scatter plots of the electronic action variables n_2 versus n_1 for an ensemble of trajectories as they are initialized in the SQC approach, and after they reach their final electronic configuration once the scattering process is complete (i.e., as $t \to \infty$). Fig. 6.3a corresponds to an initial nuclear momentum of 15 A.U. and so corresponds to a data point in Fig. 6.2 where the unphysical oscillation in the transmission probabilities has a severe effect. The scatter plot in Fig. 6.3b corresponds to an initial nuclear momentum of 20 A.U., a particular value in Fig. 6.2 where the transmission probabilities aren't effected by the oscillation. Both plots correspond to calculations with $\Delta n = \frac{1}{2}$, as can be seen by the box-shaped cluster of points of width $\Delta n = \frac{1}{2}$ centered at $(n_1, n_2) = (1, 0)$—which are the initial actions of the trajectories since the trajectories begin in electronic state 1; and, electronic state 2 corresponds to a 2-D box of width $\Delta n = \frac{1}{2}$ centered at $(n_1, n_2) = (0, 1)$. The points scattered roughly along a diagonal line (joining the two "boxes") correspond to the final action distributions of the trajectories after each trajectory has exited the region of the avoided crossing.[4]

Fig. 6.3a shows that for the case of an initial nuclear momentum of 15 A.U. the final action distribution largely favors electronic state 2, but that a large number of the trajectories finish beyond the "box" representing electronic state 2, specifically, in the far upper left of the plot, in a vertical strip with n_1 in the range of $[-0.5, -0.25]$ and n_2 in the range of $[1, 2]$.[5] Since for a

[4]The trajectories move along this diagonal line because Hamilton's equations preserve the value of $n_1(t) + n_2(t)$ even if the sum isn't initialized exactly to 1.

[5]Recall that with the convention of having n corresponding to the vibrational quantum number, n_1 and n_2 can be negative, down to $-\frac{1}{2}$, since the actual classical actions of the

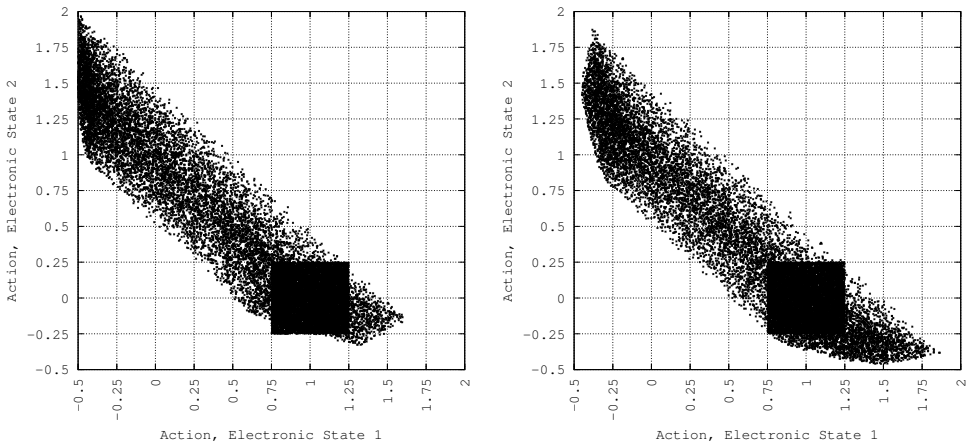

(a) Initial momentum of 15 A.U. (b) Initial momentum of 20 A.U.

Figure 6.3: Scatter plots of n_2 versus n_1 for both the initial and final conditions of the ensemble of trajectories used in the $\Delta n = \frac{1}{2}$ calculations for the single avoided crossing model

trajectory to be counted in calculating $P_{2\leftarrow 1}$ it must end up within the final action window function centered at $(0, 1)$, those finishing in this leftmost strip do not end up being counted when $\Delta n = \frac{1}{2}$—i.e., which would require n_1 to be in the range $[-0.25, 0.25]$. However, it can also be seen from the figure that if a wider window function with $\Delta n = 1$ had been used instead—allowing n_1 within the range $[-0.5, 0.5]$—many of these trajectories would be counted, explaining why the transmission curves corresponding to $\Delta n = 1$ shown in Fig. 6.2 do not exhibit the anomalous unphysical oscillation.

Fig. 6.3b confirms this analysis. For the case of an initial nuclear momentum of 20 A.U., the transmission probabilities ($P_{2\leftarrow 1}$ and $P_{1\leftarrow 1}$) plotted in Fig. 6.2 exactly match the true quantum transmission probabilities ("+" symbols in Fig. 6.2), and it is clearly seen that the oscillations in the transmission curves do not effect this particular data point. The scatter plot of Fig. 6.3b shows why. In comparison to Fig. 6.3a, Fig. 6.3b shows that at 20 A.U., a fair number of trajectories still land outside the $\Delta n = \frac{1}{2}$ box centered at $(n_1, n_2) = (0, 1)$, but the accumulation in the upper left of the figure is not nearly as severe, and is offset by a similar pattern in the lower right of the figure (which also affects the calculation of $P_{2\leftarrow 1}$ due to renormalization). Moreover, the distribution of final electronic actions displayed in 6.3b appears to be nearly symmetric if reflected about a line given by $n_2 = n_1$, and it is

oscillators are then obtained by adding $\frac{1}{2}$.

therefore nearly symmetric with respect to the windowing of the final electronic states, which explains why all the transmission curves in Fig. 6.2 (for all values of Δn) coincide at this point.

In sum, the spurious dips in the transmission curves shown in Fig. 6.2 are clearly a result of the fact that for some range of initial nuclear momenta, trajectories tend to overshoot the closest window function—whether it corresponds to state 1 or 2—ending up with all their "vibrational" action stored in either one electronic oscillator or the other; and that this problem stems from the simple fact that a classical trajectory model does not preserve the QM ZPE. However, what is immediately encouraging about this result is that despite the fact that these particular trajectories do not fit the criteria of either window function, they actually do finish much closer in action-space (n_1, n_2) to one or the other of the electronic states (see, e.g., Fig. 6.3a)—i.e., they are *not* being discarded for embodying a mixture of the two electronic states—suggesting that, at least for this particular problem, if there was some sensible way to include these trajectories in the statistics, the unphysical oscillations could be eliminated.

6.4 Initial Results for the Dual Avoided Crossing Model

Initial SQC results analogous to those presented for the single avoided crossing problem are shown for the dual avoided crossing problem in Fig. 6.4. These γ-less SQC results were again calculated using widths of $\Delta n = \{1, 0.7, 0.5\}$ and are plotted in Fig. 6.4 against the exact quantum result. Here, again, it is seen that the $\Delta n = 1$ result shows reasonable agreement with the quantum result for transmission on either surface, $T_{2\leftarrow 1}$ and $T_{1\leftarrow 1}$, throughout the displayed energy range. However, as was also seen in modeling the single avoided crossing, when $\Delta n < 1$, the transmission probability curves exhibit an anomalous oscillation, in this case becoming most severe in two regions of initial nuclear kinetic energy (E)—at about $\log(E) = -1.2$ and about $\log(E) = 0.4$.

Accordingly, as was done above for the single avoided crossing model, the cause of the oscillations was investigated and for this case too it was discovered that the oscillations were a consequence of the classical simulation's inability to maintain the QM ZPE of the oscillators corresponding to the two electronic states. And, this was again revealed by inspecting scatter plots of n_2 versus n_1, one corresponding to an initial energy where the oscillation had a severe effect ($\log(E) = -1.2$ in Fig. 6.4) and one corresponding to an energy region where the oscillation had no effect ($\log(E) = -2.8$ in Fig. 6.4). The former is

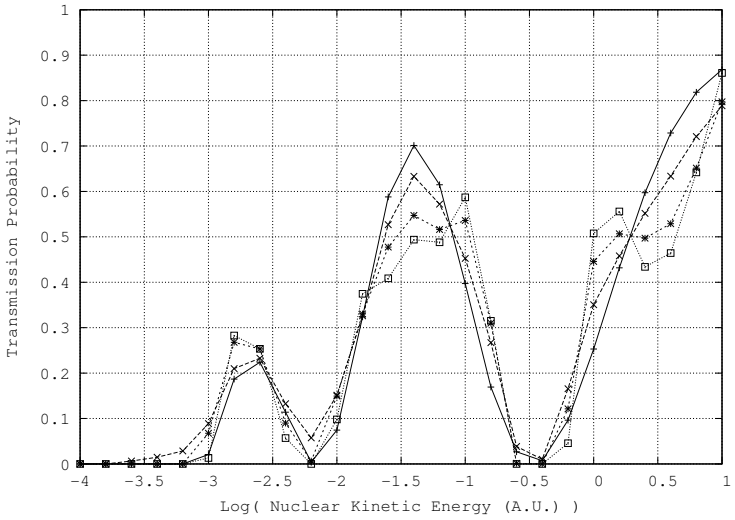

(a) Upper surface, $T_{2\leftarrow 1}$

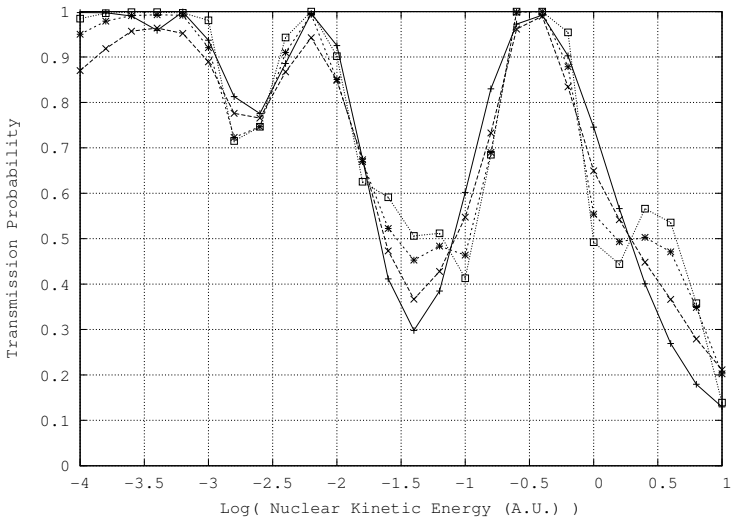

(b) Lower surface, $T_{1\leftarrow 1}$

Figure 6.4: Transmission probabilities for the dual avoided crossing calculated via the SQC approach without a γ-parameter: exact QM result (+); SQC with $\Delta n = 1$ ($\times$), $\Delta n = 0.7$ ($*$), and $\Delta n = 0.5$ ($\Box$)

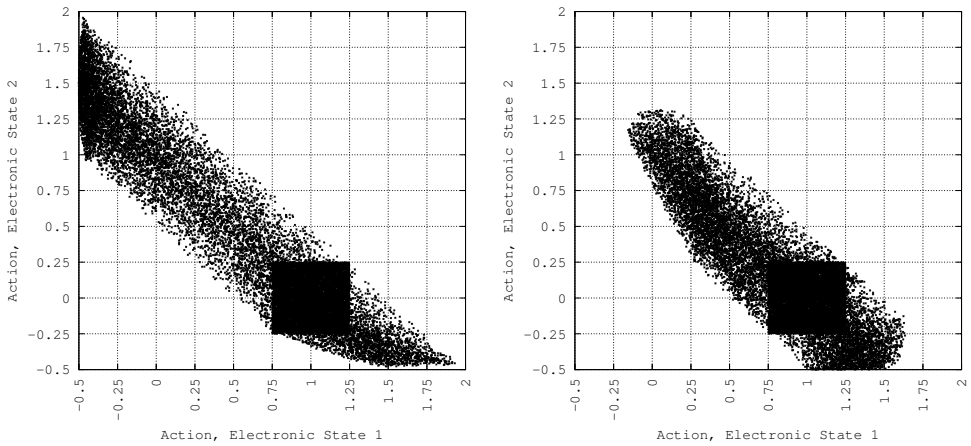

(a) Initial nuclear kinetic energy of $\log(E) = -1.2$

(b) Initial nuclear kinetic energy of $\log(E) = -2.8$

Figure 6.5: Scatter plots of n_2 versus n_1 for the dual avoided crossing problem; plotted are both initial and final conditions of the ensemble of trajectories used in the $\Delta n = \frac{1}{2}$ calculations; E in A.U.

shown in Fig. 6.5a and the latter in Fig. 6.5b, both for $\Delta n = \frac{1}{2}$, as done in the analysis of the single avoided crossing model. Comparing Fig. 6.5a to the result seen for the single avoided crossing model seen in Fig. 6.3a reveals that the results are analogous, with a large number of trajectories finishing beyond the $\Delta n = \frac{1}{2}$ window function for state 2. The similar scatter plot shown in Fig. 6.5b for $\log(E) = -2.8$ (where the oscillation isn't present), does not exhibit this effect.

Therefore, in sum, it was found that essentially the same defect was present in the SQC simulation of both model problems, and that in both cases the defects—the anomalous oscillations in the $P_{1\leftarrow 1}$ and $P_{2\leftarrow 1}$ transmission probabilities —were a direct consequence of ZPE leakage—an issue that would seem to intrinsically plague any simple model based on classical trajectory simulation.

6.5 Attempt to Cure ZPE Leakage with the Miller-McCurdy Model

One approach which was tried to deal with the ZPE leakage problem was to use the Miller-McCurdy (MMc) Hamiltonian. The scatter plots in Figs. 6.3 and 6.5 seem to suggest that ZPE leakage may be most severe for trajectories

initialized further from the $n_1+n_2 = 1$ polyad because in these regions the joint action windowing functions written in terms of n_1 and n_2 are more restrictive than right on the polyad. As explained in Section 5.4.1, in an SQC approach based on the Miller-McCurdy Hamiltonian, there is only one action variable—representing the fractional occupation of the 2 states—to be windowed, and it is implicit in the model that the sum of the probabilities for the 2 states is 1.

Accordingly, the Miller-McCurdy model[6] was employed in the SQC approach (using one-dimensional action window functions), and histograms describing the initial and final action distributions analogous to the scatter plots shown in Figs. 6.3 and 6.5 are shown in Figs. 6.6a and 6.6b. However, rather

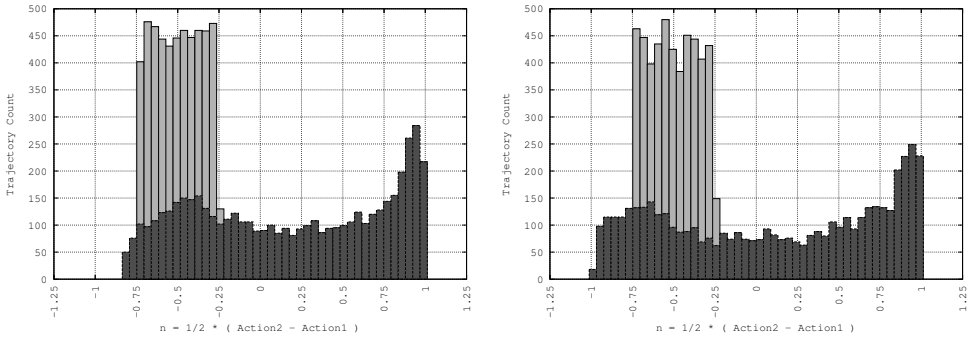

(a) Single avoided crossing; Initial nuclear momentum of 15 A.U.

(b) Dual avoided crossing; initial nuclear kinetic energy of $\log(E) = -1.2$; E in A.U.

Figure 6.6: Histogram plots of the MMc action variable $n = \frac{1}{2}(n_2 - n_1)$ for both the initial (light-colored bars) and final conditions (darkened bars) of the ensemble of trajectories used in the $\Delta n = \frac{1}{2}$ calculations with the MMc model

than the MMc Hamiltonian curing the problem, the results shown in Figs. 6.6a and 6.6b illustrate it even more clearly: It is seen that the *most probable* value of the action difference variable n after the scattering interaction is ≈ 1, which since $n = \frac{1}{2}(n_2 - n_1)$ and $n_1 + n_2 = 1$ (strictly, in the MMc model) corresponds to $(n_1, n_2) = \left(-\frac{1}{2}, \frac{3}{2}\right)$, which means that oscillator 1 is left with essentially

[6]Actually, an expression equivalent to the MMc Hamiltonian of Eq. (5.44) was used having $N = n_1 + n_2 = 1$, $\gamma = \frac{1}{2}$, and defining the action variable $n = \frac{1}{2}(n_2 - n_1)$, or equivalently $n = -m$ as defined in Eq. (5.39b). The actual version of the MMc Hamiltonian employed was thus

$$H(\mathbf{P}, \mathbf{R}, n, q) = \frac{P^2}{2\mu} + \bar{H}(R) \; - \; n \cdot \Delta H(R) + \; 2\sqrt{1-n^2}\,\cos(q) \cdot H_{12}(\mathbf{R}). \tag{6.5}$$

zero energy,[7] and that oscillator 2 has an action which is $\approx \frac{1}{4}$ too high to fall within the $\Delta n = \frac{1}{2}$ window function.

Therefore, it is seen that the MMc Hamiltonian doesn't provide the answer. Figs. 6.6a and 6.6b do show again that a $\Delta n = 1$ window function would solve the problem, but that would eliminate the constrained quantization condition which the SQC approach is supposed to provide.

6.6 SQC Results Obtained by Tying γ to Δn

Based on the foregoing analysis, it is now rather obvious that ideally the width of the widowing functions exactly match the amount of ZPE used to initialize the trajectories so that no trajectories are lost due to ZPE leakage. One way to do this is to set $\Delta n = 1$ to match the ZPE, but the other way to do this is to set the ZPE to match Δn. Hence, in the MM and MMc Hamiltonians given in Sections 5.1 and 5.4.1, the Langer modification of $\frac{1}{2}$ has been replaced by a variable γ-parameter, and the width of the window functions used in the SQC approach are also written in terms of γ where $\Delta n = 2\gamma$. Thus, the strictness of the "quantization" in the SQC approach is now expressed in terms of the γ-parameter, which also sets the amount of ZPE injected into the classical trajectory simulation, as discussed in Section 5.1 (see Eq. (5.11a)).

Results using this approach (specifically, Eqs. (5.16), (5.20), and (5.21) as described in Sections 5.1 and 5.2) for the single avoided crossing problem are displayed in Fig. 6.7 calculated for a range of values of the γ-parameter, specifically for $\gamma \in \left\{\frac{1}{2}, \frac{1}{3}, \frac{1}{4}, \frac{1}{5}\right\}$. Fig. 6.7a shows results for the probability of transmission onto the lower surface ($T_{2\leftarrow 1}$) as a function of initial nuclear momentum. Fig. 6.7b shows analogous results for the probability of transmission on the upper surface ($T_{1\leftarrow 1}$). Compared to the initial SQC results shown in Fig. 6.2, it is seen here that the unphysical oscillations in the transition probabilities for $\gamma < \frac{1}{2}$ (corresponding to $\Delta n < 1$) have been completely eliminated, allowing one to choose an optimal γ and thereby set the restrictiveness of the SQC "quantization." Figs. 6.7a and 6.7b show that the primary effect of varying γ is to adjust the sharpness of the transmission probabilities onto the lower and upper surfaces, and that a value for γ of about $\frac{1}{3}$ yields reasonable results. However, based on the interpretation of the 2-state MMc Hamiltonian as that of a classical spin-$\frac{1}{2}$ DOF, as discussed in Section 5.4.3, γ has been selected to have the value $0.366 \approx \frac{\sqrt{3}-1}{2}$ for all the 2-state calculations presented in this

[7] Again, the convention here is that n_1 and n_2 correspond to the quantum numbers, so the true classical actions are obtained by adding $\frac{1}{2}$.

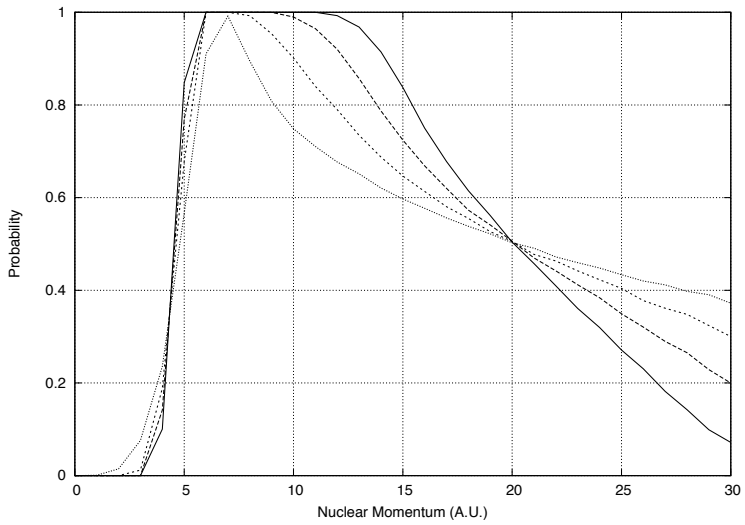

(a) Transmission to the lower surface, $T_{2\leftarrow 1}$

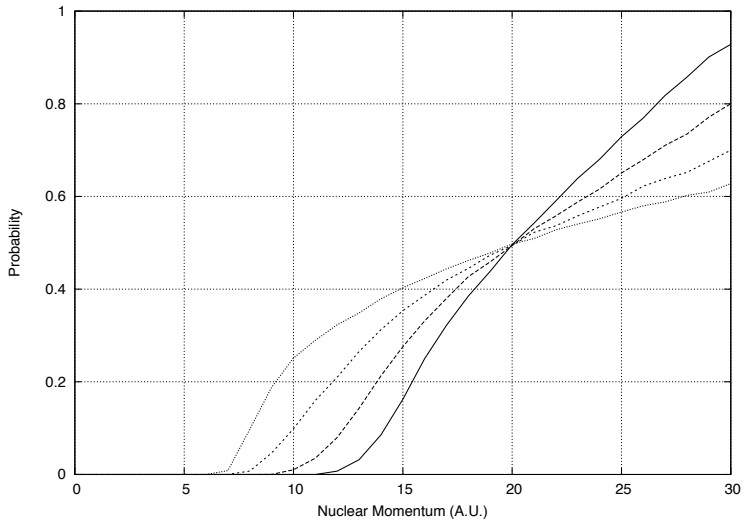

(b) Transmission to the upper surface, $T_{1\leftarrow 1}$

Figure 6.7: Transmission probabilities for the single avoided crossing problem calculated via the SQC approach for various values of $\gamma \in \left\{\frac{1}{2}, \frac{1}{3}, \frac{1}{4}, \frac{1}{5}\right\}$ with $\Delta n = 2\gamma$; the solid line (–) corresponds to $\gamma = \frac{1}{5}$, and so forth

work.[8]

Accordingly, for the single avoided crossing problem, Fig. 6.8a compares SQC computed results using $\gamma = 0.366$ to the exact quantum result, for both upper and lower surface transmission ($T_{1\leftarrow 1}$ and $T_{2\leftarrow 1}$), and the agreement is seen to be excellent. Likewise, Fig. 6.8b shows results for the dual avoided crossing problem, and again the SQC results using $\gamma = 0.366$ show excellent agreement with the quantum results. It is noted that the dual avoided crossing problem exhibits what are referred to as Stückelberg oscillations in the transmission probabilities, and despite the oscillations usually being attributed to quantum (or semiclassical) interference effects, they are well described in this purely classical model.[9]

The extended coupling model of Eq. (6.4) is different than the preceding two avoided crossing models in that the off-diagonal non-adiabatic coupling element $H_{12}(R)$ is not localized in a particular region of the nuclear DOF and instead is non-vanishing asymptotically in the product channel ($R > 0$). For this reason, rather than use the diabatic Cartesian representation of the MM Hamiltonian, the adiabatic Cartesian representation given by Eq. (5.23) was employed. The calculated transmission curves ($T_{1\leftarrow 1}$ and $T_{2\leftarrow 1}$) using $\gamma = 0.366$ versus the quantum results[10] are plotted in Fig. 6.9a, and likewise, the reflection curves ($R_{1\leftarrow 1}$ and $R_{2\leftarrow 1}$) are plotted in Fig. 6.9b. The calculated transmission on the lower surface ($T_{1\leftarrow 1}$) as a function of incoming nuclear momentum shows excellent agreement with the quantum result, however, for transmission on the upper surface ($T_{2\leftarrow 1}$), there is a discrete step structure in the quantum result which is not reproduced in these calculations.[11] The same step structure is also present in the quantum-calculated reflection curves, and again it is seen that this step structure is not reproduced in the SQC/MM results.

This is likely to be a limitation of the SQC/MM approach. Although it is seen to do an excellent job with the two avoided crossing problems, when there are sharp transmission and reflection features—sharps steps, sharp resonances, etc.—the windowing functions will tend to average them out of the results,

[8]Nevertheless, the feeling is that γ should still be viewed as a "parameter" of the SQC model, and that it is sensible to try different values for it depending on the system being modeled, if for no other reason than to assess its effect on the calculations and to gauge the sensitivity of the results to its value.

[9]It has been noted before that so-called "quantum coherence" may be well described by the classical MM model. [15, 33]

[10]Prof. John Tully provided the QM results.

[11]Though it is noted that different values of γ were tried and $\gamma = 0.366$ still turned out to be essentially optimal based on the $T_{1\leftarrow 1}$ curve.

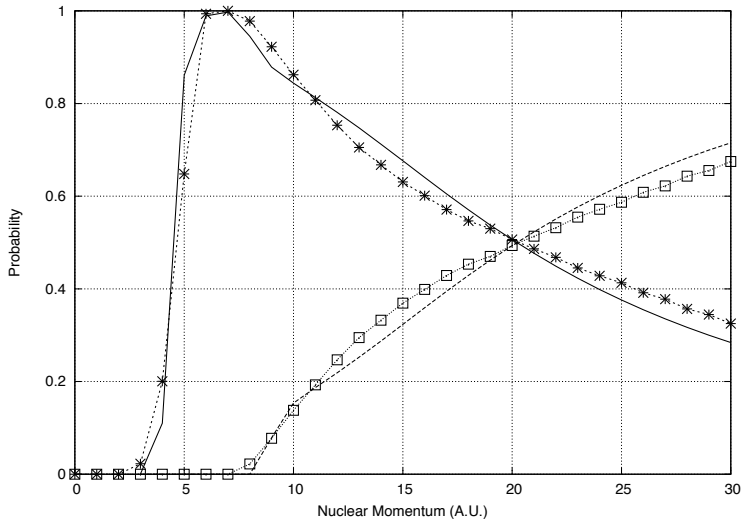

(a) Single avoided crossing: $T_{2\leftarrow 1}$: QM (–), SQC (∗); $T_{1\leftarrow 1}$: QM (···), SQC (□)

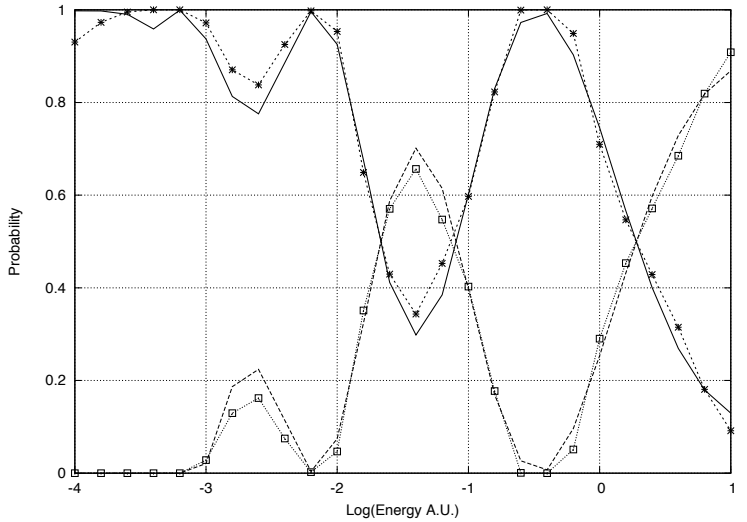

(b) Dual avoided crossing: $T_{1\leftarrow 1}$: QM (–), SQC (∗); $T_{2\leftarrow 1}$: QM (···), SQC (□)

Figure 6.8: Transmission probabilities for the single and dual avoided crossing problems calculated via the SQC approach employing $\gamma = 0.366$ and with $\Delta n = 2\gamma$ versus the exact QM results

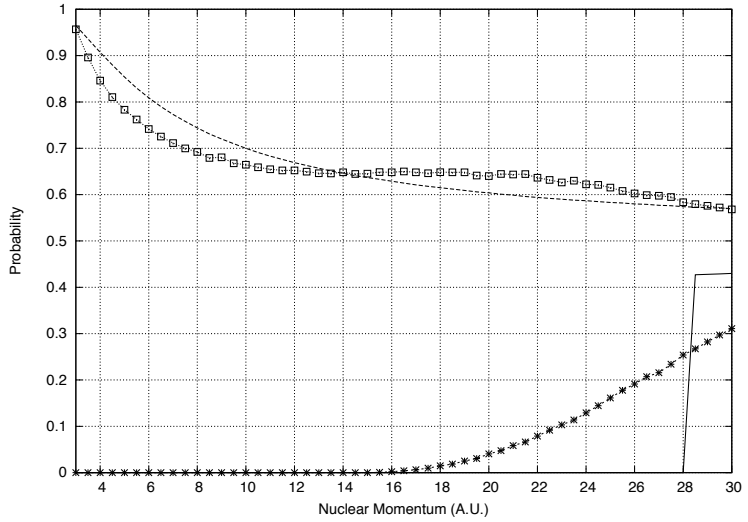

(a) $T_{2\leftarrow 1}$: QM (–), SQC (∗); $T_{1\leftarrow 1}$: QM (---), SQC (□)

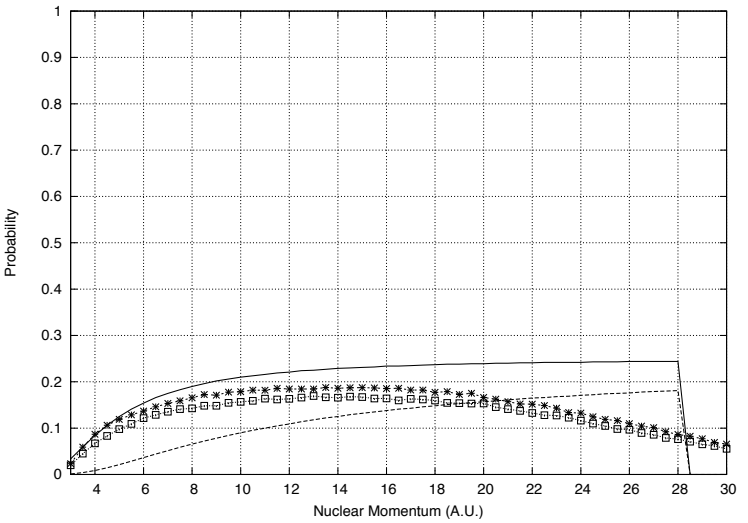

(b) $R_{2\leftarrow 1}$: QM (–), SQC (∗); $R_{1\leftarrow 1}$: QM (---), SQC (□)

Figure 6.9: Transmission and reflection probabilities for the extended coupling problem calculated via the SQC approach employing $\gamma = 0.366$ and with $\Delta n = 2\gamma$ versus the exact QM results

at least to a certain extent. Of course, real non-adiabatic systems having many interacting DOFs are less likely to show such sharp features.[12] However, even for this relatively strange model problem (with non-adiabatic coupling extending as $R \to \infty$), the SQC approach does a reasonable job of estimating the threshold energy for reflection off of both surfaces, as well as giving a reasonable estimate of the general magnitude of the reflection probabilities.

6.7 Conclusion

It has been shown that for this initial class of non-adiabatic models—scattering problems where the quantities of interest are the transmission and reflection probabilities into the different electronic states as a function of incident nuclear kinetic energy—that the SQC approach does a reasonable job of describing the dynamics, qualitatively in all cases and quantitatively in most cases (the exception being the rather odd extended coupling problem). These simple scattering problems served as an initial proving ground of the approach and, in particular, were useful for understanding that there needs to be a relationship between the width of the SQC windowing functions and the zero-point energy parameter in the MM Hamiltonian. With the approach validated for these simple low-dimensional models, the logical next step is to tackle higher dimensional models which are more representative of the types of non-adiabatic dynamics seen in the condensed phase environment.

[12] For example, see the spin-boson problems presented in Section 7.1.

Chapter 7

Application to Electronic Transitions in the Condensed Phase

7.1 The Spin-Boson Model

The so-called "spin-boson" model provides a simple mathematical representation of the types of dissipative non-adiabatic dynamics seen in the condensed phase. The model is given by the following diabatic Hamiltonian matrix elements:

$$\begin{aligned} H_{11}(\mathbf{Q}) &= V_0(\mathbf{Q}) + V_1(\mathbf{Q}) + \epsilon \\ H_{22}(\mathbf{Q}) &= V_0(\mathbf{Q}) - V_1(\mathbf{Q}) - \epsilon \\ H_{12}(\mathbf{Q}) &= H_{21}(\mathbf{Q}) = \Delta \end{aligned} \tag{7.1}$$

where $V_0(\mathbf{Q})$ represents a bath of oscillators

$$V_0(\mathbf{Q}) = \sum_{k=1}^{F} \frac{1}{2}\omega_k^2 Q_k^2 \tag{7.2}$$

shifted by $V_1(\mathbf{Q})$

$$V_1(\mathbf{Q}) = \sum_{k=1}^{F} c_k Q_k. \tag{7.3}$$

The model is therefore mathematically just a pair of spatially offset and energetically displaced multi-dimensional harmonic oscillators coupled together

by a constant non-adiabatic coupling Δ, but the notion is that the oscillators model the effect of the condensed phase environment on the energetics of the two electronic states which are separated in energy by some fixed bias, in this case 2ϵ. The bias (here 2ϵ, but often just ϵ) distinguishes between two classes of spin-boson problems: a symmetric variety where $\epsilon = 0$, and an asymmetric variety where there is a non-vanishing bias $\epsilon \neq 0$. Furthermore, it is to be noted that the asymmetric variant is generally viewed as being far more challenging for simple methods to "get right."

To make the modeling of the condensed phase environment more realistic, a spectral density is chosen to provide an appropriate distribution of bath frequencies $\{\omega_k\}$ in Eq. (7.2) (e.g., to match a particular solvent's characteristic distribution of vibrational frequencies), and the so-called coupling parameters $\{c_k\}$ in Eq. (7.3) are chosen by the relationship

$$J(\omega) = \frac{\pi}{2} \sum_{k=1}^{K} \frac{c_k^2}{w_k} \, \delta(\omega - \omega_k). \tag{7.4}$$

Often the spectral density $J(\omega)$ is chosen to be an Ohmic distribution,

$$J(\omega) = \eta \, \omega e^{-\omega/\omega_c}, \tag{7.5}$$

having characteristic frequency ω_c and coupling (or friction) parameter η, sometimes (as here) given in terms of the so-called Kondo parameter α by $\eta = \frac{\pi}{2}\alpha$. Representing the Ohmic distribution of Eq. (7.5) in the discrete form of Eq. (7.4) implies that in this case the $\{c_k\}$'s are given by

$$c_k = \sqrt{(2/\pi)\Delta\omega \; \omega_k \; J(\omega_k)}, \tag{7.6}$$

where $\Delta\omega$ is the spacing between the bath frequencies $\{\omega_k\}$. All calculations employed a bath of 100 nuclear DOFs—so of a dimensionality on the order of what would be relevant to an electronic transition in the condensed phase.

This is also a sufficient enough number of interacting heavy-particle DOFs that it is meaningful to characterize the system in terms of a temperature. This is set within the model via selection of the initial momenta $\{P_k\}$ and positions $\{Q_k\}$ by Monte Carlo from the Wigner transform of the Boltzmann operator for the initial state [14] (assumed here to be state 1):

$$e^{-\beta\left(\frac{1}{2}|\mathbf{P}|^2 + H_{11}(\mathbf{Q})\right)};$$

which gives

$$\rho(\{P_k, Q_k\}) \propto \prod_{k=1}^{F} \exp\left(-\alpha_k \cdot \left[\frac{1}{2} P_k^2 + \frac{1}{2} \omega_k^2 \left(Q_k + \frac{c_k}{w_k^2} \right)^2 \right] \right), \tag{7.7a}$$

where

$$\alpha_k = \frac{2}{\omega_k} \tanh\left(\frac{\beta \omega_k}{2} \right). \tag{7.7b}$$

It is noted that the calculation of the partition function is unnecessary in view of the renormalization required by Eq. (5.21).

7.2 Results

The SQC approach employing $\gamma = 0.366$[1] was used to treat the symmetric spin-boson problem (i.e., $\epsilon = 0$ in Eq. (7.1)) and the more challenging asymmetric version (i.e., $\epsilon \neq 0$), and in both high and low temperature regimes relative to the non-adiabatic coupling (expressed in terms of $\beta \cdot \Delta$). For each of the 4 cases, results are expressed in terms of the population difference between the upper (initial) state 1 and the lower state 2, i.e. as $D(t) = P_{1\leftarrow 1}(t) - P_{2\leftarrow 1}(t)$, and compared with the exact QM result. This highlights another difference between the calculations presented here for the spin-boson system versus those for the 1-dimensional scattering problems treated in Chapter 6: for the scattering problems the goal was to calculate the branching ratios between the 2 final states in reflection and transmission at long time (for various values of incident nuclear kinetic energy); here one wishes to calculate the detailed time-dependence of the population ratio between the two states (*as well as* the long-time limit of the population ratio, which should theoretically obey detailed balance).

Accordingly, Fig. 7.1a displays results for the symmetric ($\epsilon = 0$) spin-boson problem at high temperature relative to the non-adiabatic coupling, $\beta \cdot \Delta = 0.1$, with $\alpha = 0.09$ and $\omega_c/\Delta = 2.5$, a regime where the system exhibits incoherent relaxation dynamics. Fig. 7.1b displays corresponding results for the same symmetric ($\epsilon = 0$) system at low temperature relative to the non-adiabatic coupling, $\beta \cdot \Delta = 5$, where the relaxation dynamics over a longer time-scale manifests strong coherent oscillatory behavior. In both cases, the

[1] It should now be assumed implicit in the SQC model that $\Delta n = 2\gamma$.

result calculated using the SQC approach shows good agreement with the QM results [14, see Fig. 5].

Likewise, moving on to the asymmetric version (with $\epsilon = 1$), Fig. 7.2a provides results for the high temperature case, in this example with $\beta \cdot \Delta = 0.25$, $\alpha = 0.1$, and $\omega_c/\Delta = 1$.[2] As with the symmetric problem at high temperature, the SQC result here is seen to be in excellent agreement with the exact results [34, see Fig. 4].

Finally, Fig. 7.2b presents results for the asymmetric problem at low temperature, the most challenging of the 4 cases, with the parameters of the model (other than the bias ϵ) remaining virtually[3] the same as in Fig. 7.1b. Here, the population difference, $D(t) = P_{1\leftarrow 1}(t) - P_{2\leftarrow 1}(t)$, relaxes to an equilibrium value representing unequal population between the two electronic states (i.e., $\lim_{t\to\infty} D(t) \neq 0$). Fig. 7.2b shows that the SQC result for the asymmetric problem at low temperature reasonably replicates the oscillations, time-decay, and long-time limit of the electronic populations shown in the QM result [34, see Fig. 5.].

[2]Slightly different model parameters are used here relative to Fig. 7.1a simply due to the particular QM results which were readily available.

[3]$\alpha = 0.1$ in Fig. 7.2b, versus $\alpha = 0.09$ in Fig. 7.1b

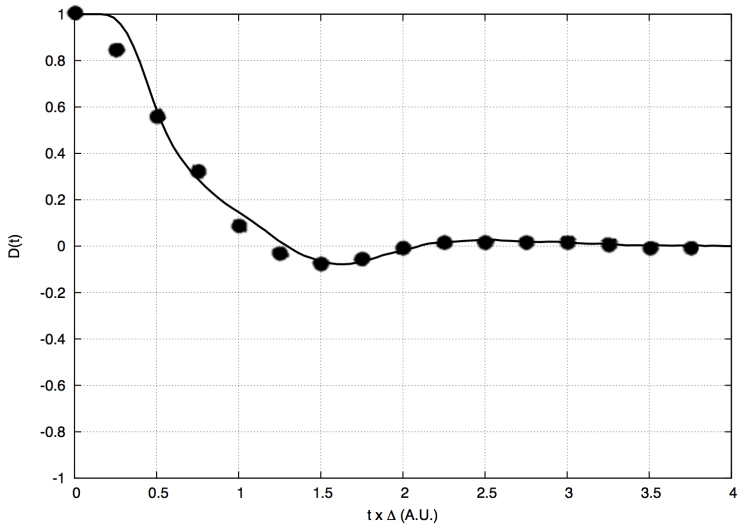

(a) High temperature: $\beta \cdot \Delta = 0.1$; $\alpha = 0.09$, $\omega_c/\Delta = 2.5$

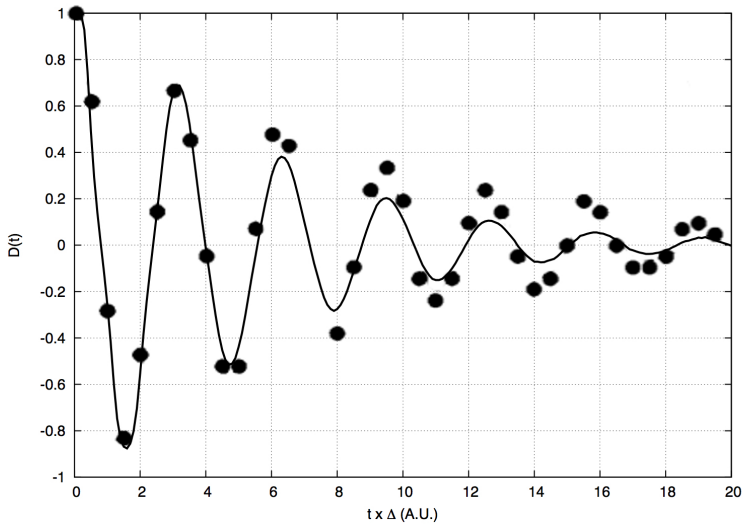

(b) Low temperature: $\beta \cdot \Delta = 5$; $\alpha = 0.09$, $\omega_c/\Delta = 2.5$

Figure 7.1: Symmetric spin-boson problem ($\epsilon = 0$): $D(t) = P_{1\leftarrow 1}(t) - P_{2\leftarrow 1}(t)$ calculated using the SQC approach (–) versus QM results (•) (The QM results are taken from Ref. [14].)

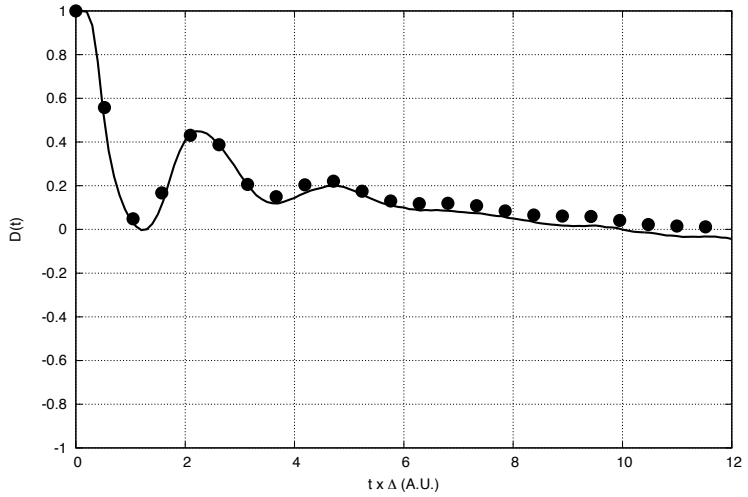

(a) High temperature, $\beta \cdot \Delta = 0.25$; $\alpha = 0.1$, $\omega_c/\Delta = 1$

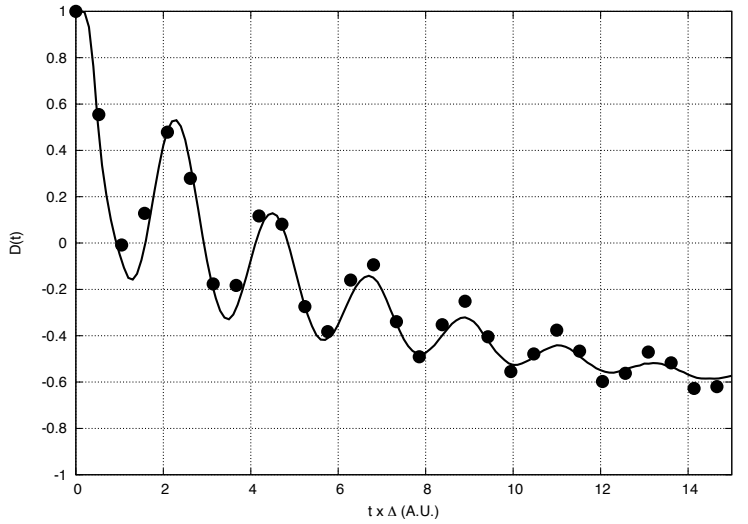

(b) Low temperature, $\beta \cdot \Delta = 5$; $\alpha = 0.1$, $\omega_c/\Delta = 2.5$

Figure 7.2: Asymmetric spin-boson problem, $\epsilon = 1$: $D(t) = P_{1\leftarrow 1}(t) - P_{2\leftarrow 1}(t)$ calculated using the SQC approach (–) versus QM results (•)

7.3 Conclusion

Thus, for each of the symmetric and asymmetric spin-boson problems presented here, results calculated via the SQC methodology show excellent agreement with QM results. It is noted that both the symmetric and asymmetric spin-boson systems addressed here exhibit strong coherence effects at low temperature (relative to the non-adiabatic coupling), and that the detailed time-dependence of these effects are accurately reproduced in the SQC result, despite the SQC model being based purely on classical mechanics.

While a technique as simple as the SQC/MM approach obviously cannot hope to describe all condensed phase non-adiabatic problems as well as is shown in Figs. 7.1 and 7.2, the successful treatment of the spin-boson model in these examples does suggest that the approach may provide a way to handle certain broad classes of these problems with great efficiency. The scattering results discussed in Chapter 6 only involved a single nuclear DOF, but the calculations presented here for the spin-boson problem treated the dynamics of a dissipative bath having 100 nuclear DOF. Nevertheless, despite the higher dimensionality needed for modeling the condensed phase, since the inputs to the SQC approach are still just ordinary classical trajectories, these systems may still be handled with great efficiency. It is noted that although most of the definitive results presented here were computed using in the range of 50,000-100,000 trajectories, even just 1,000 trajectories are sufficient to provide reasonable results, and this may be done in seconds on a current 4-core consumer-grade microprocessor.

Chapter 8

Electron Transfer Reactions

8.1 Marcus Theory and Related Electron Transfer Models

Electron transfer (ET) reactions in the condensed phase represent a particular class of non-adiabatic processes which play a key role in many important chemical and biological systems. It is well understood that when electron transfer occurs in the condensed phase, solvent molecules reorient so as to stabilize the charge distribution of the new electronic state. In Marcus Theory [35, 36, 37], this solvent reorganization (occurring in concert with the electron's motion) is represented by way of a "solvent coordinate," and the donor and acceptor electronic states which characterize the transferring of the electron are then represented as intersecting potential energy surfaces (PESs) expressed in terms of this solvent coordinate. Marcus Theory further assumes that these donor and acceptor diabatic PESs are of a simple quadratic form, and the famous Marcus Rate equation is arrived at by applying the Golden Rule to the crossing point of these surfaces:

$$k_{ET}(\beta) = \frac{1}{\hbar}\Delta^2\sqrt{\frac{\beta\pi}{\lambda}}\exp\left[-\beta\frac{(\epsilon-\lambda)^2}{4\lambda}\right] \tag{8.1}$$

where Δ is the non-adiabatic coupling constant between the donor (initial) and acceptor (final) electronic states, ϵ is the difference in energy between the electronic states, and λ is the "reorganization energy"—equal to the difference in energy between initial and final electronic states with the solvent coordinate fixed at its minimum value in the final electronic state.

While Marcus Theory has proved to be quite successful in a variety of

contexts, there is of course great interest in developing trajectory-based approaches which can be accurately applied to non-adiabatically coupled PESs of arbitrary form—i.e., generated from *ab initio* or semi-empirical electronic structure theory—and seamlessly incorporated into what are nowadays routine classical molecular dynamics (MD) simulations. In the spirit of developing such approaches, several recent studies have adopted the Marcus Theory scheme of characterizing the collective orientation of the solvent in terms of a "solvent coordinate" (and representing the donor and acceptor electronic states as intersecting quadratic PESs in the solvent coordinate), but then additionally coupling these surfaces to a dissipative harmonic bath so that trajectory-based approaches may be applied.

For example, Huo, Miller, and Coker [38] have proposed such a model and treated it with a mixed approach combining the linearized semiclassical (LSC) initial value representation (IVR) for the nuclear DOFs, and the full semiclassical (SC) IVR for the electronic DOFs, the latter represented in terms of the Cartesian version of the MM Hamiltonian as described herein. In so doing, these investigators demonstrated that this PLDM methodology ("partial linearized" semiclassical "density matrix" propagation) can accurately recover Marcus Theory electron transfer rates varying by 5 orders of magnitude as a function of the non-adiabatic coupling strength Δ, and by 3 orders of magnitude as a function of the energetic bias ϵ, with accuracy extending into the inverted rate regime known from Marcus Theory.[1]

A bit earlier, a similar "solvent coordinate" model was treated by Menzeleev, Ananth, and Miller [39] using the RPMD ("ring polymer molecular dynamics") approach, and these investigators found that reasonable results (i.e., in accordance with Marcus Theory) could be obtained in the normal to barrier-less regime, but that the RPMD approach (at least in that formulation) was unable to describe rates in the inverted regime correctly.

The SQC/MM approach, of course, represents a much simpler (and more easily implementable) strategy for the general treatment of non-adiabatic dynamics than either of these approaches, and so the question is whether it can be as accurate as the more rigorous mixed classical/semiclassical PLDM technique applied by Coker *et al.*—for example, accurately handling the Marcus inverted regime which, in contrast, the RPMD technique applied by Miller *et al.* was unable to properly characterize. The encouraging results obtained using the SQC/MM approach, in particular, for the dual avoided crossing

[1] The dependence of the ET rate on the bias ϵ in Eq. (8.1) shows that when the bias ϵ is increased beyond the reorganization energy λ the ET rate will "invert" and decrease as a function of ϵ.

problem and the low-temperature spin-boson problem with their prominent "quantum coherence" effects, provide a reasonable basis for anticipating that this very simple SQC approach will likely be able to describe the Marcus inverted region correctly.

The calculations presented below show that this is so, and that the SQC/MM approach may be used to accurately calculate ET thermal rate constants over wide ranges of non-adiabatic couplings and exothermicities. However, before the SQC results for these ET problems are presented, a technique for the calculation of thermal rate constants must be introduced which involves a modification to the standard flux-side correlation function rate calculation framework which adapts it to the SQC approach.

8.2 An SQC-Adapted Flux-Side Correlation Function Framework for Calculating Thermal Rate Constants

It is possible to calculate the thermal rate constant for an electron transfer process simply by fitting the time decay of the donor state population with a decaying exponential function; i.e., with SQC calculations, to fit the results of evaluating Eqs. (5.20) and (5.21). However, a better (and less ambiguous[2]) approach is to formulate the calculation in terms of a modified flux-side correlation function and to initialize trajectories at the "transition state" of the non-adiabatic process.[3]

[2]Fitting the decay curves ends up being more difficult than one might think because it is difficult to concoct a systematic (and automatic) process for determining what part of the decay curve to fit. For decay from one bound state to another in a closed system, at long enough times the backward reaction becomes a factor, and at very short times the population decay is not exponential. Given the very large range of non-adiabatic couplings and thus decay time scales treated here, unabmigously fitting this data becomes a non-trivial task.

[3]This relates to another issue with the fitting of decay curves for these model problems. As stated, at long times, the back reaction begins to have an effect on the calculated decay curve, yet it is difficult to distinguish between what should be considered a back reaction and what should properly be considered to be the recrossing dynamics of the foward reaction. These issues become more problematic when determining a rate from the donor-state decay curve because the dynamics must be calculated out to times long enough for trajectories to reach the transition state from the donor state—which may be a very long time if reaction rates are very low (i.e., for weak non-adiabatic coupling). Accordingly, for each of these reasons, calculating a rate from trajectories initialized at the "transition state" of the non-adiabatic process may be done with much less ambiguity and much greater computational

Accordingly, all calculations of ET rates presented herein employed the standard expression for the thermal rate constant as the long-time limit of a flux-side correlation function [40]:

$$k_{2\leftarrow 1}(\beta) = \frac{1}{Q_r} \lim_{t\to\infty} C^{(fs)}_{2\leftarrow 1}(t) \tag{8.2}$$

where $C^{(fs)}_{2\leftarrow 1}(t)$ is a flux-side correlation function corresponding to a non-adiabatic transition from electronic state 1 to electronic state 2, and

$$Q_r = \frac{1}{(2\pi\hbar)^G} \int \mathbf{dP}\, \mathbf{dR}\; e^{-\beta\left(\frac{\mathbf{P}^2}{2\mu} + H_{11}(\mathbf{R})\right)} \tag{8.3}$$

is the reactant partition function for a system of G nuclear DOFs.

To use Eq. (8.2), it was discovered in the course of this work that several modifications to the standard expression for $C^{(fs)}_{2\leftarrow 1}(t)$ are required in order to extract thermal rate constants from trajectory calculations in a manner consistent with (and in the spirit of) the SQC approach. These modifications result in a SQC-modified flux-side correlation function calculated as a "renormalized" Boltzmann-weighted phase-space average of the classical reactive flux F multiplied by a time-evolved SQC projection factor $\wp_{2\leftarrow 1}$ (which is essentially the SQC equivalent of the "side"-operator):

$$C^{(fs)}_{2\leftarrow 1}(t) = \frac{1}{(2\pi\hbar)^{G+2}} \frac{1}{\tilde{P}_{tot}(t)} \int \mathbf{dP_0}\, \mathbf{dR_0}\, \mathbf{dn_0}\, \mathbf{dq_0} \left\{ \begin{array}{c} e^{-\beta\left(\frac{|\mathbf{P_0}|^2}{2\mu} + \bar{H}(\mathbf{R_0}) + \frac{1}{2}\Delta n_0\, \Delta H(\mathbf{R_0})\right)} \\ \times\; F_0 \;\times\; \wp_{2\leftarrow 1}(t) \end{array} \right\}. \tag{8.4}$$

The renormalization factor $\tilde{P}_{tot}(t)$ in Eq. (8.4) is given by $\tilde{P}_{2\leftarrow 1}(t) + \tilde{P}_{1\leftarrow 1}(t)$ (as in Eqs. (5.20) and (5.22) for population decay); $\Delta n_0 = n_1(0) - n_2(0)$; and $\bar{H}$ and ΔH are the average and differences of the diabatic PESs as appearing in the MM Hamiltonian of Eq. (5.16)—which is used for evolving the trajectory dynamics.

The reactive flux factor in Eq. (8.4) is defined as

$$F_0 = \delta(n_1(0) - n_2(0)) \cdot \left.\frac{dn_2}{dt}\right|_0, \tag{8.5}$$

efficiency.

which thereby sets the "dividing surface" between reactants and products to be the line ($n_1 = n_2$) evenly dividing the space of the electronic action variables midway between the SQC window functions defining electronic states 1 and 2. Thus, the reactive flux factor F_0 does, as required, properly define a surface in the electronic phase space through which all reactive trajectories must penetrate. Note that $\Delta n_0 = 0$ in Eq. (8.4) with this choice of dividing surface.

The SQC projection factor $\wp_{2\leftarrow 1}(t)$ is expressed in terms of the windowing functions of Eq. (5.18) as

$$\wp_{2\leftarrow 1}(t) = W_2(n_1(t), n_2(t)) \cdot W_1(n_1(-t), n_2(-t)) \tag{8.6}$$

which requires (as $t \to \infty$) that trajectories begin in state 1 (the donor electronic state) and finish in state 2 (the acceptor electronic state). Thus, in the usual fashion, the phase space average of Eq. (8.4) is evaluated by beginning trajectories at the dividing surface defined by the flux factor of Eq. (8.5), evolving the trajectories forward and backward in time via Hamilton's equations (via the MM Hamiltonian of Eq. (5.16)), and then applying the SQC projection factor of Eq. (8.6). Again, for all of the 2-state ET calculations presented here, the γ-parameter was kept fixed at $0.366 \approx \frac{\sqrt{3}-1}{2}$.

The flux factor in Eq. (8.5) is written in terms of the "dividing surface" $n_1 = n_2$. However, the crux of the SQC approach is to impose quantization by defining the reactant and product regions of the electronic phase space by the window functions of Eq. (5.18), and since these regions are disjoint from one another, there is actually a "dividing volume" between reactant and product regions of the electronic phase space. Based on this notion and, in addition, based on the observance that (in many parameter regimes) the typical reactive trajectory re-crosses the surface $n_1 = n_2$ many times, it was found that convergence of the integral in Eq. (8.4) could best be accomplished by modifying Eq. (8.5) such that:

$$\left.\frac{dn_2}{dt}\right|_0 \to \frac{\Delta n_2}{\Delta t} = \frac{n_2(t_{for}) - n_2(t_{back})}{t_{for} - t_{back}} \tag{8.7}$$

where t_{for} is the (positive) time when a trajectory *first* enters the *product* electronic space running in the *forward* time direction, and t_{back} is the (negative) time when a trajectory *first* enters the *reactant* electronic space running in the *backward* time direction.[4] In the same spirit, it is noted that the renormalization factor $\tilde{P}_{tot}(t)$ is present in Eq. (8.4) for the same reason it is present in

[4]Note that Eqs. (8.5) and (8.7) could equivalently be written in terms of $\frac{dn_1}{dt}$ since

Eqs. (5.20) and (5.22): to account for those times when a trajectory is in the intermediate region of the electronic phase space and thereby effectively not counted (at that time) towards the population of any electronic state.

In any event, this SQC-modified framework for the direct calculation of thermal rate constants—provide by Eq. (8.2) through Eq. (8.7)—was found to be effective and was used for all the ET rate calculations presented here.

8.3 SQC Thermal Rate Constants for Two "Solvent Coordinate" Models of Electron Transfer

With the rate calculation properly formulated in terms of an SQC-consistent version of the flux-side correlation function (Eq. (8.4)), presented here are the results of applying this SQC methodology to the "solvent coordinate" models of ET proposed by Coker *et al.* [38] and Miller *et al.* [39].

8.3.1 Treatment of the "Solvent Coordinate" Model of Coker *et al.*

The ET model employed by Huo, Miller, and Coker [38] to test the PLDM methodology ("partial linearized" semiclassical "density matrix" propagation) is defined by the following diabatic electronic matrix for which the diagonal elements (i.e., the donor and acceptor diabatic PESs) are shifted quadratic functions of the solvent coordinate R, with constant off-diagonal coupling Δ and energetic bias ϵ:

$$\begin{aligned} H_{11}(R) &= \frac{1}{2}\mu\,\Omega^2 R^2 + C_s R + \frac{\epsilon}{2} \\ H_{22}(R) &= \frac{1}{2}\mu\,\Omega^2 R^2 - C_s R - \frac{\epsilon}{2} \\ H_{12} &= H_{21} = \Delta, \end{aligned} \tag{8.8}$$

$\frac{dn_1}{dt} = -\frac{dn_2}{dt}$ and so, on the basis of symmetry, $\frac{\Delta n_2}{\Delta t}$ was actually calculated as

$$\frac{1}{2}\cdot\frac{n_2(t_{for}) - n_2(t_{back}) - n_1(t_{for}) + n_1(t_{back})}{t_{for} - t_{back}}.$$

where $\Omega = 3.5\times10^{-4}$, $\mu = 1$, $\lambda = 2.39\times10^{-2}$, and $C_s = \sqrt{\lambda/2}\,\Omega$ (all expressed in atomic units). In this model, the two diabatic PESs, $H_{11}(R)$ and $H_{22}(R)$, are coupled through the solvent coordinate R to a bath of oscillators:

$$H_{bath}(\mathbf{P},\mathbf{Q}) = \sum_{k=1}^{K}\left\{\frac{1}{2}P_k^2 + \frac{1}{2}\omega_k^2\left(Q_k + \frac{c_k}{\omega_k^2}R\right)^2\right\}, \tag{8.9}$$

and, as with the spin-boson problems presented in Chapter 7, an Ohmic distribution—i.e., Eq. (7.5)—was chosen for spectral density of the bath, here with coupling/friction parameter $\eta = 1.49\times10^{-5}$ and characteristic frequency $\omega_c = \Omega$. The bath frequencies $\{\omega_k\}$ and coupling constants $\{c_k\}$ are therefore chosen as in Eqs. (7.4) and (7.6), as done with the spin-boson problems. Likewise, the bath DOFs were thermally initialized by Monte Carlo from the Wigner transform of the Boltzmann operator for the bath, $e^{-\beta H_{bath}(\mathbf{P},\mathbf{Q})}$, which gives a distribution function of the same form as in Eq. (7.7). All thermal rate calculations employed a discretization of 100 bath modes (except where noted below), also as done in Chapter 7.

Accordingly, thermal rate constants at 300 K for the ET model of Coker *et al.* in Eq. (8.8) were computed via the SQC approach as outline in Section 8.2. These SQC rate constants were then compared against the rates given by Marcus Theory from Eq. (8.1). The comparison is shown in Fig. 8.1. Fig. 8.1a shows the variation in thermal rates as a function of the non-adiabatic coupling Δ, and the agreement with Marcus Theory is excellent—over about 3 orders of magnitude in coupling strength and 5 orders of magnitude in ET rate. Fig. 8.1a also shows that for strong coupling, $\beta\cdot\Delta \approx 1$ or greater, the SQC-calculated ET rates are lower than those of Marcus Theory. Nevertheless, they are in good agreement with the PLDM results shown in Fig. 8.1a which also deviate from Marcus Theory in the strong-coupling regime.

Fig. 8.1a corresponds to the symmetric case where the energetic bias $\epsilon = 0$. In Fig. 8.1b the non-adiabatic coupling is held fixed at $\Delta = 5\times10^{-5}$ (at the lower end in Fig. 8.1a), and the energetic bias ϵ is varied in order to illustrate the ET rate dependence on exothermicity/bias and the inverted regime known from Marcus Theory. Once again, the SQC calculations show excellent agreement with MT—here, over about 3 orders of magnitude variation in ET rates. It is noted that these figures are analogous to those prepared by Coker *et al.* [38, see Figs. 1 and 2(a)] for illustrating the excellent accuracy of the PLDM technique, but again, because that technique treats the electronic DOF semiclassically, it presumably represents a substantially higher computational effort than the simple SQC binning approach applied here.

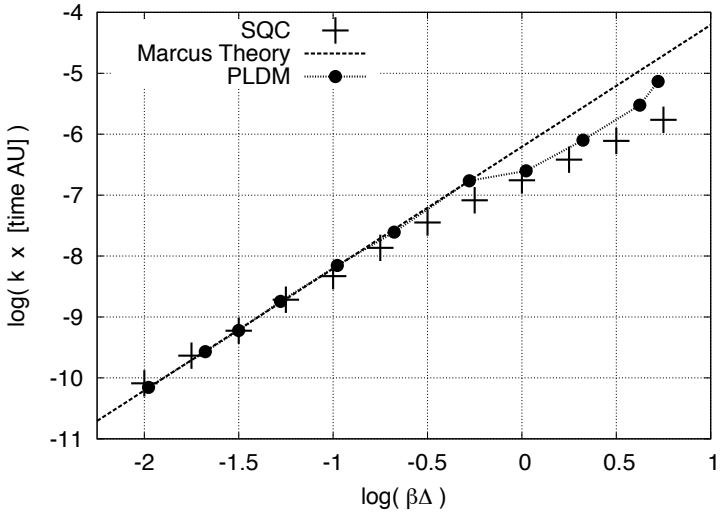

(a) Varying Δ (with $\epsilon = 0$)

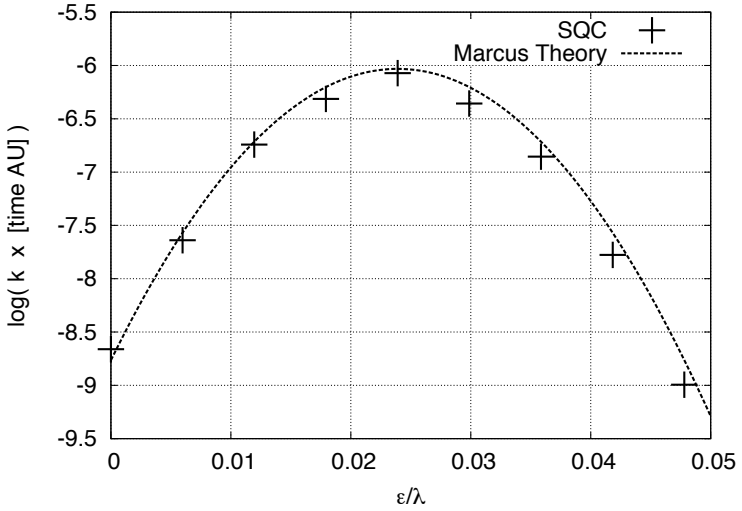

(b) Varying ϵ (with $\Delta = 5 \times 10^{-5}$)

Figure 8.1: SQC-calculated electron transfer (ET) thermal rate constants versus Marcus Theory for the "solvent coordinate" model of Coker *et al.* across widely varying regimes of non-adiabatic coupling Δ and energetic bias ϵ

The SQC results shown in Fig. 8.1 were calculated by evaluating the SQC-expression for the flux-side correlation function $C_{2\leftarrow 1}^{(fs)}(t)$ given in Eq. (8.4), dividing it by Q_r as calculated with Eq. (8.3), and doing this for a sufficient length of time t so as to estimate the long-time limit required by Eq. (8.2). Thus, presented in Figs. 8.2 and 8.3 is the explicit time-dependence of $Q_r^{-1}C_{2\leftarrow 1}^{(fs)}(t)$ corresponding to each of the thermal rate constants shown in Fig. 8.1. Figs. 8.2 and 8.3 illustrate that one consequence of the renormalization factor $\tilde{P}_{tot}(t)$ in Eq. (8.4) is that in the long-time limit $Q_r^{-1}C_{2\leftarrow 1}^{(fs)}(t)$ actually decays to the thermal rate constant. This is the reverse of the conventional property of the flux-side correlation function, but occurs because $\tilde{P}_{tot}(t)$ in the denominator of Eq. (8.4) grows in value as time progresses along with the integral in the numerator. (In effect, the first trajectory to give a non-zero projection factor $\wp_{2\leftarrow 1}(t)$ typically has the highest microscopic "rate.")

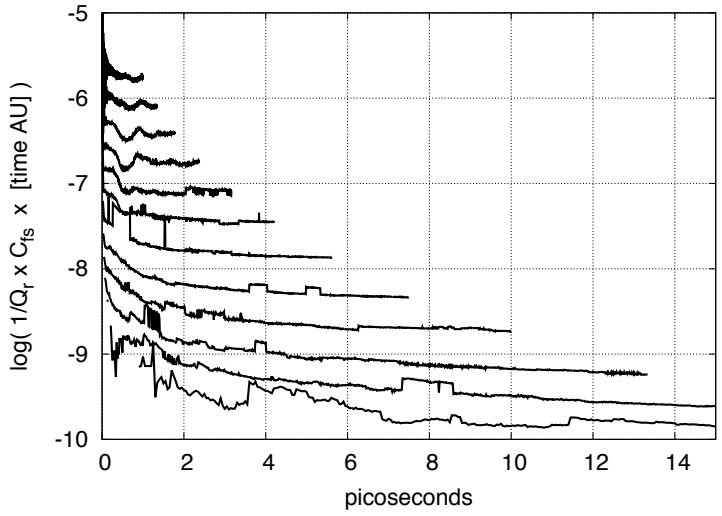

Figure 8.2: $Q_r^{-1}C_{2\leftarrow 1}^{(fs)}(t)$ corresponding to the thermal rate constants of Fig. 8.1a, showing the variation with the nonadiabatic coupling Δ

The correlation functions shown in Fig. 8.2 also illustrate the dependence of this system's relaxation dynamics on variation of the non-adiabatic coupling constant Δ. It is seen that Δ effectively sets the timescale of the relaxation dynamics, and it is for this reason that the time interval chosen for each dynamical calculation exhibited in Fig. 8.2 varies depending on the chosen value of Δ. (I.e., a longer time step is used for weaker coupling.) In contrast, Δ does not vary over the calculations presented in Fig. 8.3, and so each correlation function in this figure has been uniformly calculated out to 5 picoseconds.

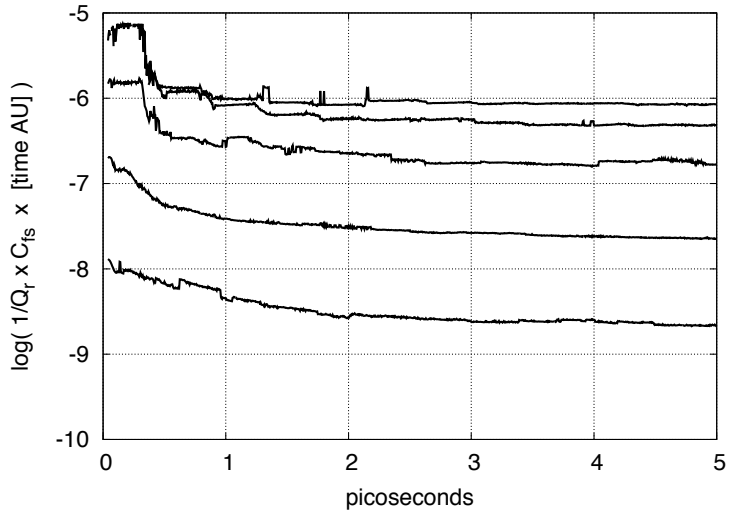

(a) Varying ϵ up to barrierless configuration

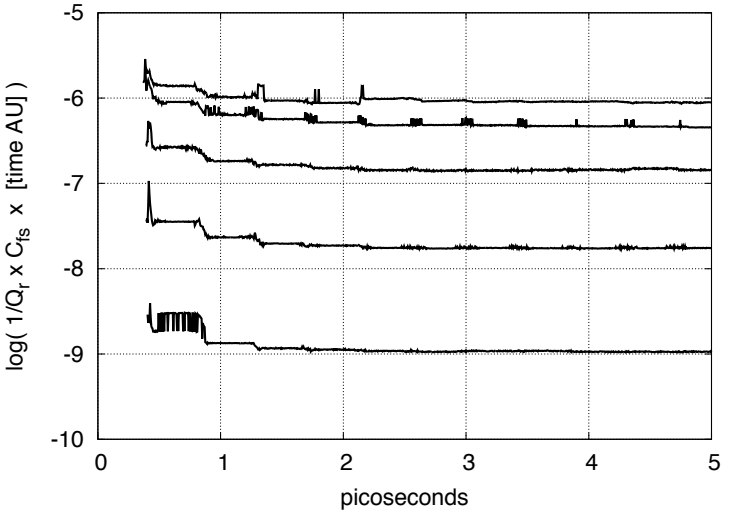

(b) Varying ϵ, Marcus inverted regime

Figure 8.3: $Q_r^{-1} C_{2\leftarrow 1}^{(fs)}(t)$ corresponding to the thermal rate constants of Fig. 8.1b, showing the variation with the energetic bias ϵ

Fig. 8.3a shows the manner in which $Q_r^{-1}C_{2\leftarrow 1}^{(fs)}(t)$ varies up to the barrierless rate, and Fig. 8.3b from the barrierless rate into the inverted regime. Thus the symmetry of the traces shown in Fig. 8.3a with those of Fig. 8.3b echoes the quadratic dependence of the ET rates shown in Fig. 8.1b.

One additional practical point concerns Monte Carlo sampling of the solvent coordinate R. In all calculations presented here, the solvent coordinate sampling function was chosen to be a Gaussian in R centered at the crossing point of $H_{11}(R)$ and $H_{22}(R)$. For the symmetric case ($\epsilon = 0$), this corresponds to $\bar{R} = 0$, which is the minimum of the effective potential felt by the solvent coordinate when the electronic DOFs are located at the dividing surface (i.e., where $n_1 = n_2$, and where they are initialized according to Eq. (8.5)). However, for the asymmetric cases ($\epsilon > 0$), the crossing point is located away from the minimum of the effective potential, and in the inverted region, high up on its repulsive wall. For this reason, it was found to be somewhat more challenging to obtain converged results in the inverted regime—which was also noted by Coker *et al.* with respect to their PLDM work. In these cases, initializing R using a relatively narrow Gaussian distribution was found to be helpful (and also in the spirit of Marcus Theory). Thus, for the calculations in Fig. 8.1b (varying ϵ), a choice of $\sigma_R = 10$ was employed (the standard deviation of the Gaussian distribution in atomic units). For Fig. 8.1a (varying Δ), the lack of energetic bias ($\epsilon = 0$) made a narrow distribution in R less important, however it was retained for consistency with Fig. 8.1b except in the strong coupling regime—i.e., for large values of Δ—where improved convergence was found by a slight scaling of σ_R with increased coupling. Thus, to summarize, for both Figs. 8.1a and 8.1b, the width of the solvent coordinate's sampling function was chosen such that:

$$\sigma_R = \begin{cases} \sigma_0 & \Delta \leq \Delta_0 \\ \sigma_0 \cdot \log_{10}\left(\frac{\Delta}{\Delta_0}\right) & \Delta > \Delta_0 \end{cases} \tag{8.10}$$

where $\sigma_0 = 10$, and $\Delta_0 = 5 \times 10^{-5}$ (i.e., the constant value of the non-adiabatic coupling from Fig. 8.1b). The larger value of σ_R used in the strong non-adiabatic coupling regime (far right of Fig. 8.1a) can be understood on the basis that strong non-adiabatic coupling allows electronic transitions to occur further from the crossing point of the PESs.

Finally, we note that while it may be instructive to analyze and understand where the most reactive regions of the solvent DOF are located, employing more sophisticated importance sampling techniques in a more general MD simulation would likely make this exercise unnecessary. Likewise, no attempt was made to minimize the number of trajectories used to generate the definitive

results shown here, using on the order of 10^6 trajectories to generate Fig. 8.1b, for instance. However, one again assumes that clever importance sampling would typically reduce this number by several orders of magnitude when called for. In fact, a very reasonable (similar) version of Fig. 8.1b can be obtained with an ensemble of just 10^4 trajectories sampled according to Eq. (8.10). See, e.g., Fig. 8.4.

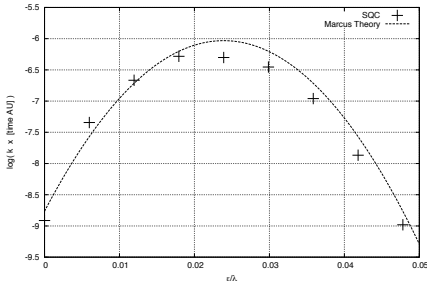

Figure 8.4: Same as Fig. 8.1b but using just 10^4 trajectories

8.3.2 Treatment of the "Solvent Coordinate" Model of Miller *et al.*

The second "solvent coordinate" ET model considered was that to which Menzeleev, Ananth, and Miller [39] applied the RPMD ("ring polymer molecular dynamics") method. Similar to Eq. (8.8) (of Coker *et al.* treated in Section 8.3.1), a quadratic Hamiltonian having constant non-adiabatic coupling was employed,

$$\begin{aligned} H_{11}(R) &= a_1\, R^2 + b_1\, R + c_1 \\ H_{22}(R) &= a_2\, R^2 + b_2\, R + c_2 \\ H_{12} &= H_{21} = \Delta, \end{aligned} \tag{8.11}$$

coupled to a harmonic bath of form equivalent to Eq. (8.9), with $\eta = 4.19$, $\omega_c = 2.28 \times 10^{-3}$, and $\mu = 1836$ (in Eq. (5.16)). The coefficients a_1, b_1, c_1, a_2, b_2, c_2 of Eq. (8.11) are listed in Table 8.1 for 4 different cases (I-IV) of energetic bias ϵ between the electronic states and slight variations in non-adiabatic coupling Δ.

Table 8.2 gives the ET rates reported in Miller *et al.*'s prior work calculated according to Marcus Theory (MT), the ring polymer molecular dynamics (RPMD) method, semiclassical instanton theory (SCI), and full quantum dynamics (QM), along with the present results calculated here using the SQC approach. The results show that the SQC approach very closely reproduces

Table 8.1: Diabatic electronic PES parmeters and non-adiabatic coupling parameters for the ET model of Miller *et al.* in Eq. (8.11)

(a) PES paramters for State 1

Case	$a_1 \times 10^3$	$b_1 \times 10^2$	c_1
I	4.7722	1.1308	-2.1576
II	4.7722	1.1308	-2.1477
III	4.7722	1.1308	-2.1411
IV	4.7720	1.1307	-2.1245

[All parameters are given in atomic units.]

(b) PES paramters for State 2

Case	$a_2 \times 10^3$	$b_2 \times 10^2$	c_2
I	4.7722	-1.1308	-2.1576
II	4.7722	-1.1308	-2.1561
III	4.7721	-1.1308	-2.1551
IV	4.7720	-1.1308	-2.1526

[All parameters are given in atomic units.]

(c) Bias and coupling between State 1 and State 2

Case	ϵ	$\Delta \times 10^5$
I	0.0	2.0662
II	-0.015	2.0916
III	-0.025	2.1088
IV	-0.050	2.1524

[All parameters are given in atomic units.]

Table 8.2: Comparison of thermal rate constants computed for the ET model of Miller *et al.* in Eq. (8.11) using various approaches; MT, RPMD, SCI, and QM results taken from Ref. [39]

Case	MT	RPMD	SCI	QM	SQC
I	6.7	6.05	5.1	6.7 ± 0.1	6.92
II	8.3	7.73	6.6	8.5 ± 0.1	8.43
III	9.1	8.54	7.4	9.0 ± 0.3	9.17
IV	9.8	9.27	8.6	10.8 ± 0.9	9.38

[values are $\log_{10}(k_{ET} \times \text{sec})$]

the QM results for 3 of the 4 cases, doing a notably better job than the other methods listed with the exception of Marcus Theory (MT) which also does quite well. Fig. 8.5a plots these SQC rates for Cases I-IV along with Miller *et al.*'s QM results, again showing good agreement within the QM result's reported error bars. Fig. 8.5b shows the time-dependence of $Q_r^{-1} C_{2\leftarrow 1}^{(fs)}(t)$ for each of the 4 cases.[5]

As before, it was important to center the solvent coordinate sampling function about the crossing point between the electronic PESs in order to generate reasonable results, and in addition, it was again helpful to choose the width of the sampling function σ_R to be relatively narrow. The length scale implied by Eq. (8.11) and Table 8.1 is much smaller than that given by Eq. (8.8) above, and so here the variation in R was set to $\sigma_R = 0.1$ in order to generate the results shown in Fig. 8.5a (and σ_R was kept at that value despite Eq. (8.10) since Δ varies only slightly between Cases I-IV as shown in Table 8.1).

The final case, Case IV, nearly corresponds to the barrierless configuration of the two electronic states, and for this set of parameters, the calculation did not seem to converge with any reliability (as shown by the noisy correlation function in Fig. 8.5b for Case IV) while producing the least accurate result (see Table 8.2 and Fig. 8.5a). However, one should also note that the QM rate for Case IV is reported in Ref. [39] with a much larger uncertainty than that for Cases I-III, and nor do the other approximate methods whose results are reported in Ref. [39] do a better job of hitting either the MT result or the QM result (which for Case IV seems to possibly be fairly different from the MT result). In any event, one notes that difficulty with Case IV may not be unique to the SQC approach.

It should also be noted that the harmonic bath of Eq. (8.9) (coupled to the Hamiltonian of Eq. (8.11)) was discretized in Ref. [39] using only 12 bath

[5] Again, per Eq. (8.2), equal to the rate constant as $t \to \infty$.

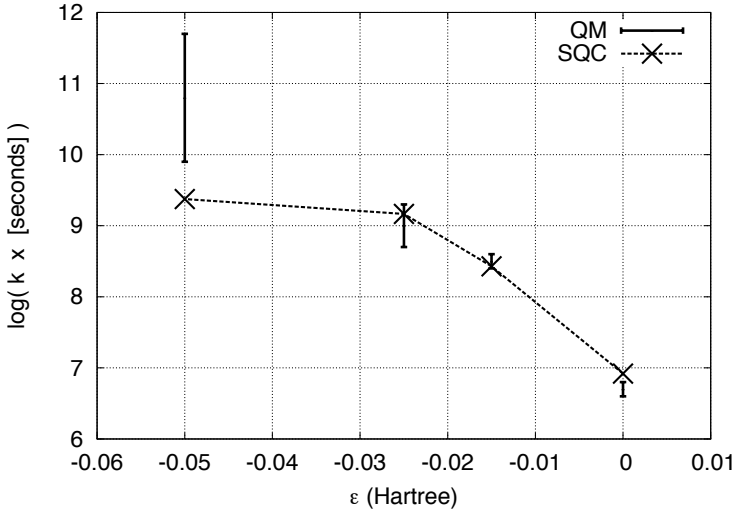

(a) SQC-calculated electron transfer (ET) thermal rate constants versus quantum results

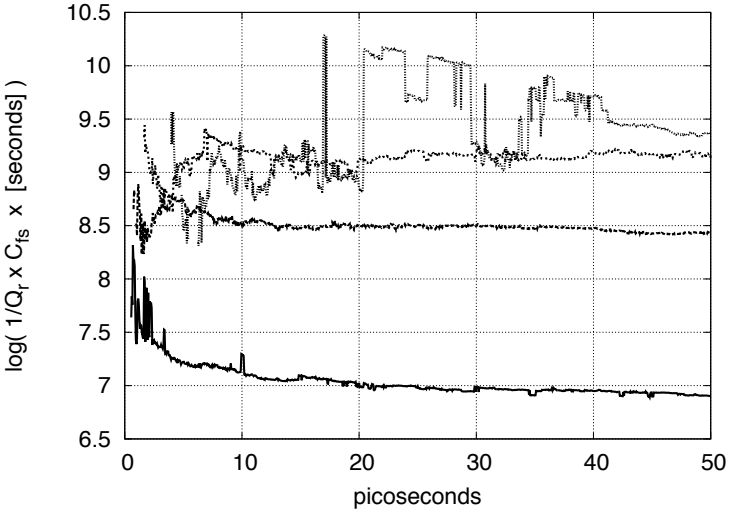

(b) $Q_r^{-1} C_{2\leftarrow 1}^{(fs)}(t)$ corresponding to the SQC-calculated thermal rate constants in (a)

Figure 8.5: SQC results for the "solvent coordinate" model of Miller *et al.* for Cases I-IV shown in Table 8.1

modes, and so for purposes of comparison the same has been done here. However, increasing the number of bath modes (to say 100, as used in the other calculations presented here) does affect the results—particularly for Case IV where it was found that a more finely discretized bath caused the system to relax so quickly that virtually no electronic transitions were found to occur. Possibly, this provides a clue as to why Case IV was difficult for the various approaches to handle. Nevertheless, one concludes that within the constraints and limitations of this prior ET model, it has been shown that the SQC approach produces quite reasonable results overall.

8.4 Modeling of Photoinduced Proton Coupled Electron Transfer

Another recent analytical model of a condensed phase ET processes is the simple model of photoinduced proton coupled electron transfer (PCET) suggested by Venkataraman, Soudackov, and Hammes-Schiffer [41]. Their proposed diabatic Hamiltonian matrix is very similar to those of Eqs. (8.8) and (8.11), except that in the PCET context, instead of a solvent coordinate, the key DOF (coupled to a harmonic bath) is the coordinate R of the proton which facilitates the ET process. Furthermore, since the electron transfer process from donor electronic state $H_{11}(R)$ to acceptor electronic state $H_{22}(R)$ is being modeled as photoinduced, the donor state $H_{11}(R)$ is assumed populated via instantaneous photoexcitation from a ground electronic state $H_0(R)$. Each of these electronic states is given a quadratic form in the model, and thus the ground, donor, and acceptor states, and the non-adiabatic coupling are as follows:

$$\begin{aligned} H_0(R) &= \frac{1}{2}\, m_p\, \omega_0^2\, (R - R_0)^2 \\ H_{11}(R) &= \frac{1}{2}\, m_p\, \omega_1^2\, (R - R_1)^2 + \epsilon_1 \\ H_{22}(R) &= \frac{1}{2}\, m_p\, \omega_2^2\, (R - R_2)^2 + \epsilon_2 \\ H_{12} &= H_{21} = \Delta \end{aligned} \tag{8.12}$$

where m_p is taken to be 1836 A.U. so that the coordinate R depicts the dynamics of a proton-mediated ET process.

Similar to the collective solvent coordinate models treated in Sections 8.3.1 and 8.3.2, interaction with the condensed phase is modeled by coupling the

PCET system to a dissipative harmonic bath of nearly the same form as Eq. (8.9)—including a spectral density given by Eq. (7.4) and initialized via Eq. (7.6)—the difference being here that instead of coupling to the nuclear coordinate R, the bath is coupled to n_1, the electronic population of the donor state (in the Meyer-Miller framework, the action of the electronic oscillator DOF associated with state 1):

$$H_{bath}(P,Q) = \sum_{k=1}^{K} \left\{ \frac{1}{2}P_k^2 + \frac{1}{2}\omega_k^2 \left(Q_k + \frac{c_k}{\omega_k^2} n_1 \right)^2 \right\}. \tag{8.13}$$

The parameters used here and in the prior work of Hammes-Schiffer *et al.* for each of the four Models A-D are given in Table 8.3. As above, 100 modes were used in the discretized bath of Eq. (8.13).

Table 8.3: Parameters for the donor and acceptor diabatic electronic states, and ground electronic state, of the photoinduced PCET model of Hammes-Schiffer *et al.* in Eq. (8.12)

Model	$\epsilon_1 - \epsilon_2$	R_0	R_1	R_2	ω_0	ω_1	ω_3
A	1	-0.5	0	-0.5	3000	3000	3000
B	0	-0.5	0	-0.5	3000	3000	3000
C	0	-0.5	0	-0.5	2500	3000	2500
D	0	-0.15	0	-0.5	3000	3000	3000

[Energies are in eV, lengths in Å, and frequencies in cm^{-1}]

Within this model, photoinduced proton coupled electron transfer (PCET) from donor state H_{11} to acceptor state H_{22} is simulated by setting the initial electronic state to H_{11}, and initializing the proton coordinate R and its conjugate momentum from the Wigner distribution associated with the Boltzmann operator for the *ground state* H_0—thus modeling instantaneous photoexcitation from H_0 to the donor electronic state H_{11}. In the SQC approach, of course, setting the initial electronic state to 1 amounts to choosing the action variables (n_1, n_2) from the window function of Eq. (5.18a). Donor state H_{11} is then allowed to decay to acceptor state H_{22} by time-evolving the electronic DOFs and proton DOF according to the MM Hamiltonian of Eq. (5.16) in the usual manner and applying the windowing functions associated with the donor and acceptor states Eqs. (5.18a) and (5.18b), respectively, at each desired time.

SQC results for the survival probability $P_{1\leftarrow 1}(t)$ of the donor state for each of the 4 Models A-D given in Table 8.3 are shown in Fig. 8.6 plotted against the results given by reduced density matrix (RDM) theory as calculated by

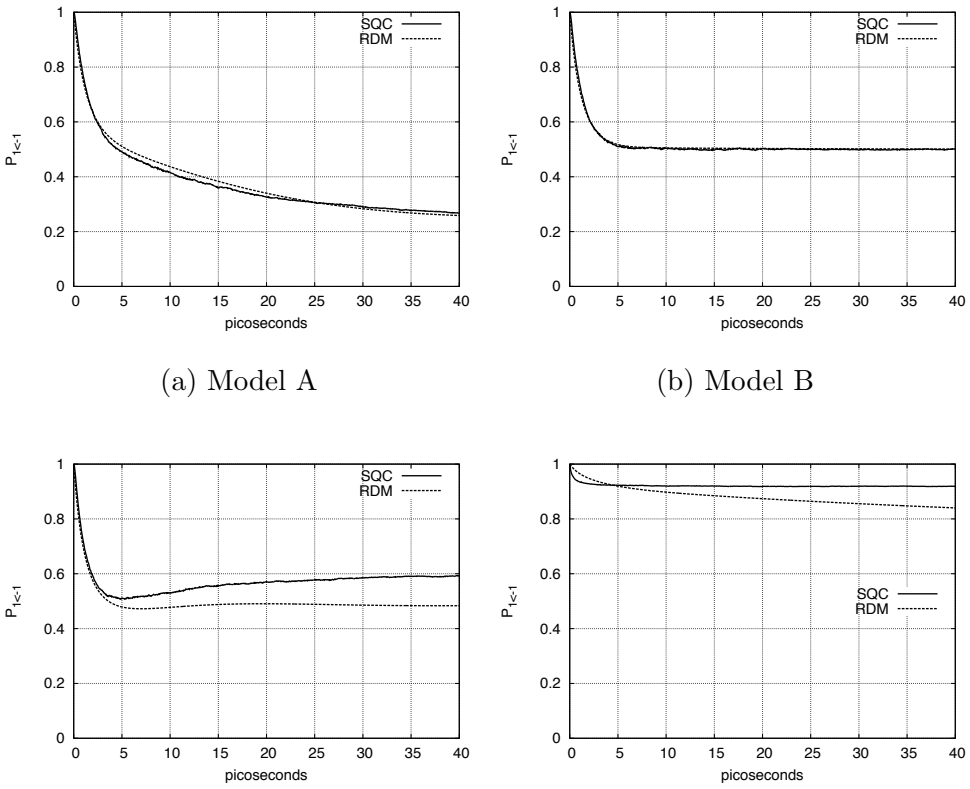

(a) Model A

(b) Model B

(c) Model C

(d) Model D

Figure 8.6: Electronic state population dynamics calculated with the SQC approach versus RDM theory for the PCET model of Hammes-Schiffer *et al.*, specifically for the 4 sets of parameters given in in Table 8.3 as Models A-D

Hammes-Schiffer *et al.* in Ref. [41]. The SQC results shown in Figs. 8.6a and 8.6b (for Models A and B) show nearly perfect agreement with Hammes-Schiffer *et al.*'s prior RDM results. The SQC results shown in Figs. 8.6c and 8.6d exhibit some deviation from the RDM results, but are still fairly reasonable, being off by a population difference of about 10%. One has to assume that these deviations are due to the limitations of the SQC approach, but since the RDM methodology is also not exact, one cannot necessarily rule out the possibility that part of the discrepancy is attributable to the limitations of the RDM technique. In any event, overall the SQC approach does a commendable job of capturing the varying characteristics of the PCET dynamics exhibited by these different models.

8.5 Conclusion Regarding Electron Transfer Results

Condensed phase electron transfer represents an important class of non-adiabatic processes, and the examples treated and discussed in this chapter have shown that the SQC/MM approach can successfully be applied to a variety of condensed phase ET models over a variety of parameter regimes.

In particular, it was shown that with a suitably modified flux-side correlation function framework adapted for consistency with the SQC approach, thermal rate constants for ET may be directly calculated in very good agreement with Marcus Theory over 5 orders of magnitude as a function of the non-adiabatic coupling strength and over 3 orders of magnitude as a function of the energetic bias between the electronic states, including a correct description of the Marcus inverted regime. Moreover, similar to what was shown for the spin-boson problems treated in Chapter 7, the explicit time-dependence of donor and acceptor electronic state populations for a non-equilibrium PCET process was also considered, and it was seen that the population decay from the photoexcited donor electronic state was handled very reasonably (relative to results from reduced density matrix theory) with the SQC/MM approach.

Finally, it is worth emphasizing that no problem-specific tuning of parameters was done to achieve these results. The only parameter of the SQC/MM model is the γ-parameter, and its value was held fixed $0.366 \approx \frac{\sqrt{3}-1}{2}$ throughout these calculations—the same value used for the spin-boson problems treated in Chapter 7 and for the 3 Tully problems treated in Chapter 6.

Chapter 9

Treatment of 3-State Non-Adiabatic Systems

Non-adiabatic systems having 3 energetically viable electronic PESs present a progressively more challenging problem for simple methods to handle properly. Results for the treatment of such systems with the SQC/MM approach are shown below, though it should be noted that these are not the first SQC results to be generated for systems having 3 or more coupled electronic states. Specifically, Tao (of Peking University) has already successfully applied the SQC approach to the treatment of 3- and 5-state models of singlet fission in polyacene dimers. [42]

9.1 A 3-Oscillator Cartesian Hamiltonian Versus a Spin-1 Hamiltonian with 1 DOF

The MM Hamiltonian may be easily written in terms of F electronic states as shown in Eq. (5.15). In this representation, a pair of action-angle variables (n, q) is assigned to each of the F electronic states, and F-dimensional window functions are applied symmetrically both initially and finally to the F classical action variables (possibly converted to-and-from a (p, x)-pair if the Cartesian version is employed).

The MMc spin-representation, however—although more complicated to discover for 3 or more states—provides an even simpler representation involving only a single pair of spin angular momentum action-angle variables for an F-state system. As discussed in Section 5.4.5, for 2 electronic states this spin-representation is nearly equivalent to the MM Hamiltonian, but for 3 or more electronic states it is not. Thus, in this chapter, the first question

to be addressed is how well the 3-state Cartesian MM Hamiltonian treats a model 3-state system following the SQC approach, and if it works well, the second question to be addressed is whether the 3-state MMc spin-representation performs equivalently well.

9.2 Choice of γ for 3 Electronic States

In order to employ the SQC approach, one must choose a value for the γ-parameter. In this regard, it seems appropriate to adapt the interpretation of γ given in Section 5.4.3 to the case of 3 electronic states. For the case of 2 electronic states, the rationalization of Section 5.4.3 lead to an identification of $\gamma = 0.366$. This was based on viewing Eq. (5.44) as a Hamiltonian for a spin-$\frac{1}{2}$ DOF, identifying $\left(\frac{1}{2}+\gamma\right)^2$ as S^2 in Eq. (5.44), choosing $S^2 = s(s+1)$, the *quantum* value for the square of the total spin angular momentum, and then calculating $\gamma = \sqrt{S^2} - \frac{1}{2}$.

For the case of $F = 3$ or more electronic states, one again may choose γ in a manner consistent with the quantum value of the square of the total spin angular momentum. As explained in Section 5.4.5, a system of F electronic states may be mapped within the MMc spin model to a system of spin $s = \frac{F-1}{2}$ having integer or half-integer quantum values of the spin projection quantum number m ranging from $-s$ to s which correspond to the different electronic states (for 3 states $m \in \{-1, 0, 1\}$). These values serve as the centers of the SQC windowing functions in the MMc spin model, their width being 2γ, and so for each of the quantum values of m there is a windowing function covering the interval $[m-\gamma, m+\gamma]$.

The idea then is that one chooses γ so that if all the angular momentum associated with a given quantum value of $S^2 = s(s+1)$ ends up in S_z—which can happen because the classical trajectory simulation does not preserve the uncertainty principle[1]—then these extreme values of $S_z = \pm\sqrt{S^2}$ still fall within the range of the windowing functions corresponding to the highest and lowest spin states whose centers are at $\pm s$. For either extremum, this amounts to choosing γ such that

$$\sqrt{S^2} = s + \gamma \tag{9.1}$$

which for the quantum value of $S^2 = s(s+1)$ gives

$$\gamma = \sqrt{s(s+1)} - s, \tag{9.2}$$

[1] This is really just the angular version of the zero-point energy leakage problem associated with oscillator model analyzed in detail in Section 6.6.

where $s = \frac{F-1}{2}$ for F electronic states. For $F = 2$ electronic states and $s = \frac{1}{2}$, this gives (as before) $\gamma = 0.366$. However, for $F = 3$ electronic states and $s = 1$, the chosen value of γ is $\sqrt{2} - 1 \approx 0.414$ (just slightly larger), and this value was used for all the 3-state calculations presented in Section 9.3, though it is noted that the value is close enough to the 2-state value that it was seen to make little difference. Finally, in the continuum limit, $\gamma \to \frac{1}{2}$ as $s \to \infty$.[2]

9.3 Results for Benchmark 3-State Spin-Boson Problems

Two papers by Sim and Makri, Refs. [30] and [31], provide rigorous quantum path integral calculations for 3-state spin-boson systems. Ref. [31] provides rigorous quantum results for a variety of spin-boson parameters regimes which model the dynamics of charge-transfer in a photosynthetic reaction center, specifically for various mutant and wild-type reaction center configurations.

Fig. 9.1 provides the results of treating the model 3-state spin-boson problem from Ref. [30] with the SQC approach—Fig. 9.1a showing the results of using the Cartesian MM Hamiltonian of Eq. (5.15), and Fig. 9.1b the results of using the spin-1 MMc Hamiltonian of Eq. (5.61). Both calculations employed $\gamma = 0.414$, as explained in Section 9.2. It is seen that the results are very similar (albeit not quite identical), despite the spin-Hamiltonian modeling the entire 3-state electronic configuration with only a single DOF treated within the SQC framework. Moreover, if one compares these two plots with those shown in Ref. [30, see, e.g., Fig. 8], it is seen that the populations of all 3 states shown in Fig. 9.1 are in quite reasonable quantitative agreement with Ref. [30]'s quantum path integral results over the full time interval simulated.

Likewise, Fig. 9.2 provides analogous SQC results for one of the benchmark 3-state spin-boson photosynthetic charge transfer models presented in Ref. [31], specifically, for the wild-type "C2" configuration at 280 K whose population dynamics are presented in Ref. [31]'s Fig. 13(a). Here, the pop-

[2] I.e.,

$$\lim_{s\to\infty} \gamma(s) = \lim_{s\to\infty} \left\{ \sqrt{s(s+1)} - s = s\left(\sqrt{1+\frac{1}{s}} - 1\right) = s\left(1 + \frac{1}{2s} - \frac{1}{8s^2} + \cdots - 1\right) \right\}$$
$$= \lim_{s\to\infty} \left\{ \frac{1}{2} + \frac{1}{8s} + \cdots \right\} = \frac{1}{2}.$$

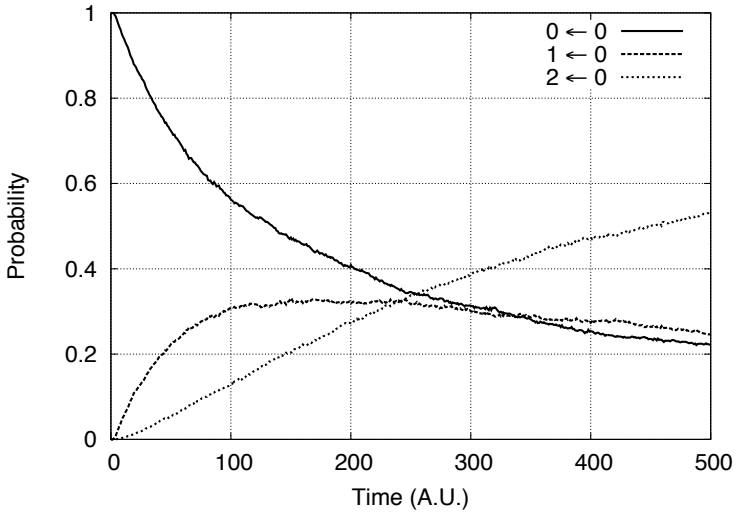

(a) Results using the Cartesian MM Hamiltonian of Eq. (5.15)

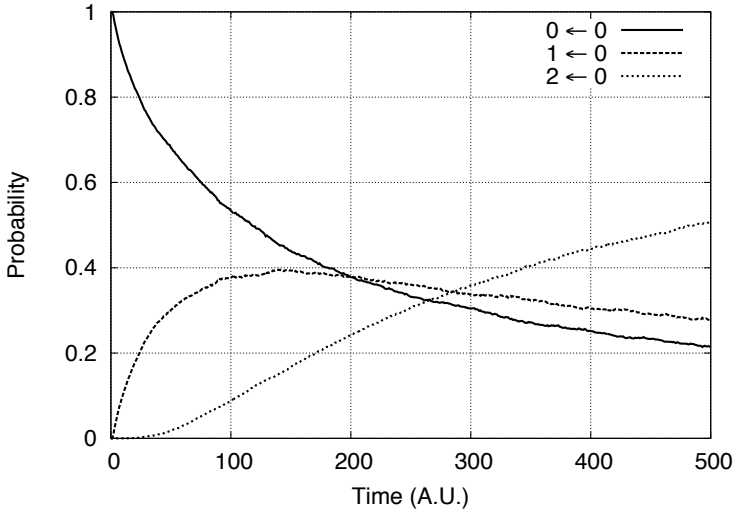

(b) Results using the spin-1 MMc Hamiltonian of Eq. (5.61)

Figure 9.1: Electronic state population dynamics calculated with the SQC approach for the benchmark 3-state spin-boson problem presented in Ref. [30, see, e.g., Fig. 8 for comparison]

ulation dynamics shown in Fig. 9.2a—calculated using the Cartesian MM Hamiltonian—exhibit some notable discrepancies with Makri *et al.*'s quantum path integral results, but the general characteristics of these SQC results are qualitatively reasonable. However, the SQC results shown in Fig. 9.2b—calculated using the spin-1 MMc Hamiltonian—are in complete disagreement with both the QM and Cartesian MM results, representing what appears to be a significant breakdown in the spin-1 MMc model. In particular, Fig. 9.2b shows almost no decay from the initial donor state 0, and thus no transfer of probability density to the acceptor state 2, in complete disagreement with what is seen in Fig. 9.2a for the Cartesian MM model (and in Ref. [30]'s QM results).

This was surprising in view of the reasonable results obtained for the treatment of the model from Ref. [30] (shown in Fig. 9.1b), and so the cause of the failure was investigated further. State 1 in this photosynthetic charge transfer model, the "bridge state," is intermediate in energy between the initial donor state 0, and acceptor state 2, and must play a role in the charge transfer process because both state 0 and state 2 are coupled to it (to state 1) but not to each other. The same is true for the spin-boson model of Ref. [30] shown in Fig. 9.1. However, in the wild-type "C2" configuration of the model from Ref. [31], the coupling between the initial donor state 0 and bridge state 1 is very weak (being only 22 cm^{-1})—making this $0 \rightarrow 1$ transition the rate-limiting step—and it turns out that this weak coupling is what somehow causes the spin-model to fail. While the mechanism of the failure is still not completely understood, it was verified that the spin-1 MMc Hamiltonian *would* give the same results as the Cartesian MM Hamiltonian if one simply increases the coupling constant between states 0 and 1 by about 50 cm^{-1}. In any event, one must conclude that while the MMc spin model may be appealing in many respects, at this point, it unfortunately does not seen to do a reasonable job of treating coupled 3-state dynamics over the same parameter regime well-handled by the Cartesian MM model—and, in particular, seems unable to properly handle the weak-coupling regime.

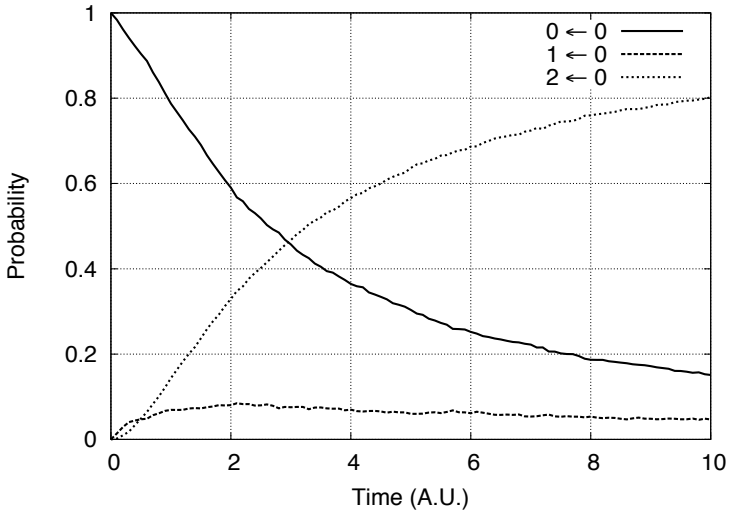

(a) Results using the Cartesian MM Hamiltonian of Eq. (5.15)

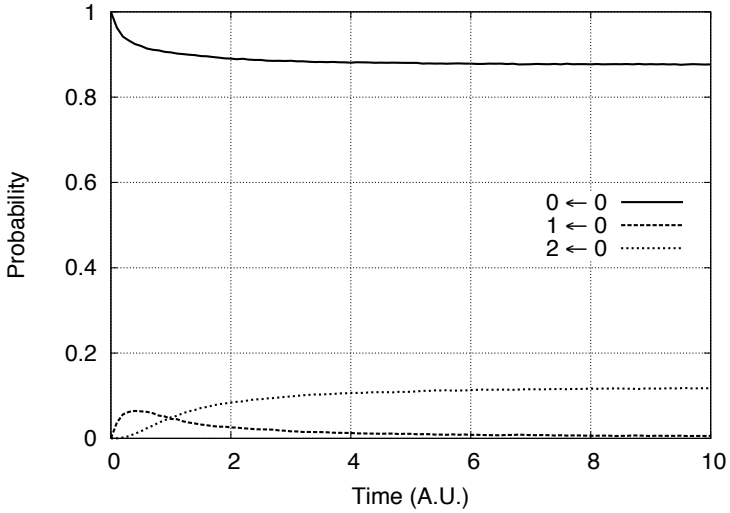

(b) Results using the spin-1 MMc Hamiltonian of Eq. (5.61)

Figure 9.2: Electronic state population dynamics calculated with the SQC approach for one of the benchmark 3-state spin-boson photosynthetic charge transfer models presented in Ref. [31, see results for wild-type configuration C2 at 280 K presented in Fig. 13(a) for comparison]

Chapter 10

Concluding Remarks

10.1 Significance of the SQC/MM Approach for the Treatment of Non-Adiabatic Processes

The SQC approach for incorporating non-adiabatic effects into classical trajectory simulations via the Meyer-Miller (MM) Hamiltonian is stunningly simple, but therein lies its potential strength. In short, within the SQC/MM framework, non-adiabatic effects may be straightforwardly incorporated into realistic simulations of complicated (high-dimensional) molecular processes simply by introducing an auxiliary pair of "electronic" action-angle variables for each energetically viable PES, and time-evolving these auxiliary variables via Hamilton's equations (using the MM electronic Hamiltonian) in the same manner that the other classical variables—i.e., the coordinates of the nuclei—are propagated forward in time.

Accordingly, it is noted that in a complex molecular system where the electronic energy is a function of a great many nuclear DOF, the propagation of these extra "electronic" variables represents a very modest increase in computational effort over a standard molecular dynamics (MD) approach. Furthermore, in view of its potential viability as demonstrated by the calculations presented in this work, the pedagogical and theoretical "advantages" of the SQC/MM approach should also be noted: e.g., that electronic and nuclear DOF are treated in a uniform dynamically consistent fashion—via the MM Hamiltonian—and in a manner that preserves microscopic time-reversal symmetry—via the SQC approach.

10.2 General Remarks Regarding the Incorporation of Quantum Mechanical Effects Via the SQC Approach

With regards generally to the incorporation of quantum effects, it has been shown that although the SQC approach is strictly-speaking purely classical—i.e., it uses classical trajectories as its inputs without any corresponding semiclassical phase calculation—it does provide a simple mechanism for incorporating a variety of quantum effects into chemical dynamics simulations.

Electronically non-adiabatic effects are generally perceived as being a purely quantum mechanical phenomena, yet the preceding work in Part II has demonstrated how these effects may be incorporated (quite accurately, in many cases) into purely classical simulations. Interestingly, quantum coherence between different electronic PESs—i.e., nuclear DOFs moving in quantum superposition on multiple electronic PESs—is well-described in the SQC/MM approach by the classical nuclear DOFs experiencing a mean-field effective potential due to contributions from *all* the relevant accessible electronic PESs. In this manner, the SQC/MM approach provides a more realistic model of multi-surface quantum coherence effects than what is provided by the standard surface-hopping approaches to non-adiabatic dynamics where the nuclear DOFs "hop" from one PES to another but at any one time only experience the forces exerted by a *single* electronic PES.

With respect to other classes of quantum effects, it was shown in Part I how nuclear motion—specifically nuclear vibration, but rotational motion could be handled analogously—may be quantized in the SQC approach through the application of symmetric windowing functions, in this case in the context of state-to-state reactive scattering calculations. From a semiclassical perspective, such quantization occurs through phase interference between trajectories taking different classical paths. In the SQC approach, instead of explicitly calculating the phase interference, it is mimicked through application of the symmetric windowing functions. If the incorporation of additional phase interference and quantization effects is desired—e.g., there are important quantized intermediate states—this could presumably additionally be incorporated through the use of windowing functions for the intermediate states.

In addition to coherence, interference, and quantization effects, tunneling (of course) represents an important class of quantum phenomena. In this regard, it was found in the context of reactive scattering that the SQC approach may be employed to usefully approximate the onset of tunneling in the reaction threshold energy region, although clearly, since the approach is purely

classical, individual trajectories do not "tunnel" per se. Rather, it is the distribution of initial coordinates and momenta given by an initial state windowing function of finite but constrained width which is able to mimic (but usefully) the true quantum tunneling effect. However, one does note the obvious limitation that this approach is not going to accurately reproduce the very low magnitude reaction probabilities characteristic of the deep tunneling regime.

10.3 Future Work

The most immediate task at hand is to investigate whether there is any way to "patch" the 3-state spin-1 MMc model (where the 3 quantum values of the projection quantum number $m \in \{-1, 0, 1\}$ represent the 3 electronic states) to properly handle the weak-coupling limit where it seems to fail in comparison to calculations done with the Cartesian MM model. It was noted that the (poor) results obtained in the weak coupling limit depended on which of the 3 electronic states was mapped to the middle spin-0 state of the spin model (the assignment of electronic states to spin states being arbitrary). This is obviously unsatisfactory—the results should be the same regardless of the chosen mapping (as it is in the Cartesian MM model)—and it is thought that this asymmetry may somehow be related to the root of the problem. It is true that the spin model is inherently asymmetric with respect to the treatment of the 3 electronic states, and so if this is the root of the issue, it may be impossible to correct in a reasonable way; though, oddly, it does not seem to be an issue outside of the weak coupling regime because, there, the spin MMc and Cartesian MM Hamiltonians give equivalent results as shown in Fig. 9.1. However, none of these issues have been studied in detail, and the spin-1 model, being such an elegant (and efficient) mapping of a 3-state non-adiabatic system onto just 1 DOF, seems to warrant further investigation.

Assuming no "patch" for the MMc 3-state spin-1 Hamiltonian can be discovered, another option to be explored involving the concept of a spin-Hamiltonian is to attempt to map N electronic states onto N spin-$\frac{1}{2}$ DOFs. In some respects, since there would be N spin DOFs the model could be viewed as a pedagogical hybrid between the N-DOF MM oscillator model and the 1-DOF MMc spin model. Such an approach may be based on the approach Miller and White took [43] for constructing a multi-fermion spin-Hamiltonian.

An avenue for future work in an entirely different direction is an investigation into whether (and how) the MM Hamiltonian treats so-called geometric phase effects. Recently, Ryabinkin, Joubert-Doriol, and Izmaylov studied [44] the role of the geometric phase in radiationless electronic state transitions in

the bis(methylene) adamantyl cation, the butatriene cation, and pyrazine in its neutral state by solving the time-dependent Schrödinger equation for different (reduced dimensional) versions of the Hamiltonians for the three systems which include and exclude (to different extents) geometric phase effects. In future studies, one would like to determine the extent to which this class of quantum effects is properly included in the purely classical models presented in this work.

Finally, the hope and goal is that the SQC/MM approach will find good use treating non-adiabatic effects in "real" chemical systems where adiabatic PESs and non-adiabatic couplings are computed via rigorous "quantum chemistry" electronic structure calculations. The Martinez Research Group at Stanford University is in the process of applying the SQC/MM approach to the non-adiabatic dynamics of ethylene—likely doing the quantum chemistry on the fly; see, e.g., Ref. [45]. Likewise, the Head-Gordon Research Group at U.C. Berkeley—specialists in electronic structure theory— have expressed interest in applying these techniques in their work with realistic systems. It will be interesting to see the SQC/MM approach scaled-up, and to determine whether any additional theoretical "tweaks" to the model will be required.

Bibliography

[1] Stephen J. Cotton and William H. Miller. Symmetrical windowing for quantum states in quasi-classical trajectory simulations. *The Journal of Physical Chemistry A*, 117(32):7190–7194, 2013.

[2] Stephen J. Cotton and William H. Miller. Symmetrical windowing for quantum states in quasi-classical trajectory simulations: Application to electronically non-adiabatic processes. *The Journal of Chemical Physics*, 139(23):234112, 2013.

[3] Stephen J. Cotton, Kirill Igumenshchev, and William H. Miller. Symmetrical windowing for quantum states in quasi-classical trajectory simulations: Application to electron transfer. *The Journal of Chemical Physics*, 141(8):084104, 2014.

[4] M. Karplus, R. N. Porter, and R. D. Sharma. Exchange reactions with activation energy. I. Simple barrier potential for (H, H_2). *The Journal of Chemical Physics*, 43(9):3259–3287, 1965.

[5] L. Bonnet and J. C. Rayez. Quasiclassical trajectory method for molecular scattering processes: Necessity of a weighted binning approach. *Chemical Physics Letters*, 277(1-3):183–190, 1997.

[6] Gábor Czakó and Joel M. Bowman. Quasiclassical trajectory calculations of correlated product distributions for the $F + CHD_3(v_1 = 0, 1)$ reactions using an ab initio potential energy surface. *The Journal of Chemical Physics*, 131(24):244302, 2009.

[7] W. H. Miller and A. W. Raczkowski. Partial averaging in classical S-matrix theory. Vibrational excitation of H_2 by He. *Faraday Discuss. Chem. Soc.*, 55:45–50, 1973.

[8] William H. Miller. Classical S matrix: Numerical application to inelastic collisions. *The Journal of Chemical Physics*, 53(9):3578–3587, 1970.

[9] William H. Miller. The semiclassical initial value representation: A potentially practical way for adding quantum effects to classical molecular dynamics simulations. *The Journal of Physical Chemistry A*, 105(13):2942–2955, 2001.

[10] Arnold I. Boothroyd, William J. Keogh, Peter G. Martin, and Michael R. Peterson. A refined H_3 potential energy surface. *The Journal of Chemical Physics*, 104(18):7139–7152, 1996.

[11] Tamar Seideman and William H. Miller. Quantum mechanical reaction probabilities via a discrete variable representation-absorbing boundary condition Green's function. *The Journal of Chemical Physics*, 97(4):2499–2514, 1992.

[12] Daniel T. Colbert and William H. Miller. A novel discrete variable representation for quantum mechanical reactive scattering via the S-matrix Kohn method. *The Journal of Chemical Physics*, 96(3):1982–1991, 1992.

[13] Uwe Manthe and William H. Miller. The cumulative reaction probability as eigenvalue problem. *The Journal of Chemical Physics*, 99(5):3411–3419, 1993.

[14] Xiong Sun, Haobin Wang, and William H. Miller. Semiclassical theory of electronically nonadiabatic dynamics: Results of a linearized approximation to the initial value representation. *The Journal of Chemical Physics*, 109(17):7064–7074, 1998.

[15] Guohua Tao and William H. Miller. Semiclassical description of electronic excitation population transfer in a model photosynthetic system. *The Journal of Physical Chemistry Letters*, 1(6):891–894, 2010.

[16] John C. Tully. Molecular dynamics with electronic transitions. *The Journal of Chemical Physics*, 93(2):1061–1071, 1990.

[17] Xiong Sun and William H. Miller. Semiclassical initial value representation for electronically nonadiabatic molecular dynamics. *The Journal of Chemical Physics*, 106(15):6346–6353, 1997.

[18] Hans-Dieter Meyer and William H. Miller. A classical analog for electronic degrees of freedom in nonadiabatic collision processes. *The Journal of Chemical Physics*, 70(7):3214–3223, 1979.

[19] Hans-Dieter Meyer and William H. Miller. Classical models for electronic degrees of freedom: Derivation via spin analogy and application to $F^* + H_2 \rightarrow F + H_2$. *The Journal of Chemical Physics*, 71(5):2156–2169, 1979.

[20] Hans-Dieter Meyer and William H. Miller. Analysis and extension of some recently proposed classical models for electronic degrees of freedom. *The Journal of Chemical Physics*, 72(4):2272–2281, 1980.

[21] W. H. Miller and C. W. McCurdy. Classical trajectory model for electronically nonadiabatic collision phenomena. A classical analog for electronic degrees of freedom. *The Journal of Chemical Physics*, 69(11):5163–5173, 1978.

[22] Nandini Ananth, Charulatha Venkataraman, and William H. Miller. Semiclassical description of electronically nonadiabatic dynamics via the initial value representation. *The Journal of Chemical Physics*, 127(8):084114, 2007.

[23] William H. Miller. Electronically nonadiabatic dynamics via semiclassical initial value methods. *The Journal of Physical Chemistry A*, 113(8):1405–1415, 2009.

[24] Gerhard Stock. Classical description of nonadiabatic photoisomerization processes and their realtime detection via femtosecond spectroscopy. *The Journal of Chemical Physics*, 103(23):10015–10029, 1995.

[25] Gerhard Stock. A semiclassical self-consistent-field approach to dissipative dynamics. II. Internal conversion processes. *The Journal of Chemical Physics*, 103(8):2888–2902, 1995.

[26] Gerhard Stock and Michael Thoss. Semiclassical description of nonadiabatic quantum dynamics. *Physical Review Letters*, 78:578–581, Jan 1997.

[27] Gerhard Stock and Uwe Müller. Flow of zero-point energy and exploration of phase space in classical simulations of quantum relaxation dynamics. *The Journal of Chemical Physics*, 111(1):65–76, 1999.

[28] Uwe Müller and Gerhard Stock. Flow of zero-point energy and exploration of phase space in classical simulations of quantum relaxation dynamics. II. Application to nonadiabatic processes. *The Journal of Chemical Physics*, 111(1):77–88, 1999.

[29] Herbert Goldstein. *Classical Mechanics*. Addison-Wesley, second edition edition, 1980.

[30] Eunji Sim and Nancy Makri. Filtered propagator functional for iterative dynamics of quantum dissipative systems. *Computer Physics Communications*, 99:335–354, 1997.

[31] Eunji Sim and Nancy Makri. Path integral simulation of charge transfer dynamics in photosynthetic reaction centers. *Journal of Physical Chemistry B*, 101:5446–5458, 1997.

[32] D. Kosloff and R. Kosloff. A Fourier method solution for the time dependent Schrödinger equation as a tool in molecular dynamics. *Journal of Computational Physics*, 52(1):35–53, 1983.

[33] William H. Miller. Perspective: Quantum or classical coherence? *The Journal of Chemical Physics*, 136(21):210901, 2012.

[34] Haobin Wang, Michael Thoss, and William H. Miller. Systematic convergence in the dynamical hybrid approach for complex systems: A numerically exact methodology. *The Journal of Chemical Physics*, 115(7):2979–2990, 2001.

[35] R. A. Marcus. On the theory of oxidation-reduction reactions involving electron transfer. I. *The Journal of Chemical Physics*, 24(5):966–978, 1956.

[36] R. A. Marcus. Chemical and electrochemical electron-transfer theory. *Annual Review of Physical Chemistry*, 15(1):155–196, 1964.

[37] R. A. Marcus and Norman Sutin. Electron transfers in chemistry and biology. *Biochimica et Biophysica Acta (BBA) - Reviews on Bioenergetics*, 811(3):265–322, 1985.

[38] Pengfei Huo, Thomas F. Miller, and David F. Coker. Communication: Predictive partial linearized path integral simulation of condensed phase electron transfer dynamics. *The Journal of Chemical Physics*, 139(15):151103, 2013.

[39] Artur R. Menzeleev, Nandini Ananth, and Thomas F. Miller. Direct simulation of electron transfer using ring polymer molecular dynamics: Comparison with semiclassical instanton theory and exact quantum methods. *The Journal of Chemical Physics*, 135(7):074106, 2011.

[40] William H. Miller, Steven D. Schwartz, and John W. Tromp. Quantum mechanical rate constants for bimolecular reactions. *The Journal of Chemical Physics*, 79(10):4889–4898, 1983.

[41] Charulatha Venkataraman, Alexander V. Soudackov, and Sharon Hammes-Schiffer. Photoinduced homogeneous proton-coupled electron transfer: Model study of isotope effects on reaction dynamics. *The Journal of Chemical Physics*, 131(15):154502, 2009.

[42] Guohua Tao. Electronically nonadiabatic dynamics in singlet fission: A quasi-classical trajectory simulation. *The Journal of Physical Chemistry C*, 118(31):17299–17305, 2014.

[43] William H. Miller and Kim A. White. Classical models for electronic degrees of freedom: The second-quantized many-electron Hamiltonian. *The Journal of Chemical Physics*, 84(9):5059–5066, 1986.

[44] Ilya G. Ryabinkin, Loïc Joubert-Doriol, and Artur F. Izmaylov. When do we need to account for the geometric phase in excited state dynamics? *The Journal of Chemical Physics*, 140(21):214116, 2014.

[45] Dmitry V. Makhov, William J. Glover, Todd J. Martinez, and Dmitrii V. Shalashilin. Ab initio multiple cloning algorithm for quantum nonadiabatic molecular dynamics. *The Journal of Chemical Physics*, 141(5):054110, 2014.